UNIVERSIDADE FEDERAL DO CEARÁ
CENTRO DE TECNOLOGIA
DEPARTAMENTO DE ENGENHARIA DE TELEINFORMÁTICA
PROGRAMA DE PÓS-GRADUAÇÃO EM ENGENHARIA DE TELEINFORMÁTICA

LÁSZLON RODRIGUES DA COSTA

SPATIAL COMPATIBILITY METRICS APPLIED IN 5G C-RAN NETWORKS

FORTALEZA
2020

LÁSZLON RODRIGUES DA COSTA

SPATIAL COMPATIBILITY METRICS APPLIED IN 5G C-RAN NETWORKS

Tese apresentada ao Curso de Doutorado em Engenharia de Teleinformática da Universidade Federal do Ceará, como parte dos requisitos para obtenção do Título de Doutor em Engenharia de Teleinformática. Área de concentração: Sinais e Sistemas

Orientador: Prof. Dr.-Ing. Yuri Carvalho Barbosa Silva

Coorientador: Prof. Dr. Francisco Rafael Marques Lima

FORTALEZA
2020

Dados Internacionais de Catalogação na Publicação
Universidade Federal do Ceará
Biblioteca Universitária
Gerada automaticamente pelo módulo Catalog, mediante os dados fornecidos pelo(a) autor(a)

C873s Costa, Lászlon Rodrigues da.
Spatial Compatibility Metrics Applied in 5G C-RAN Networks / Lászlon Rodrigues da Costa. – 2020.
98 f. : il. color.

Tese (doutorado) – Universidade Federal do Ceará, Centro de Tecnologia, Programa de Pós-Graduação em Engenharia de Teleinformática, Fortaleza, 2020.
Orientação: Prof. Dr. Yuri Carvalho Barbosa Silva.
Coorientação: Prof. Dr. Francisco Rafael Marques Lima.

1. Spatial Compatibility. 2. Hybrid Beamforming. 3. DTDD. I. Título.
CDD 621.38

LÁSZLON RODRIGUES DA COSTA

SPATIAL COMPATIBILITY METRICS APPLIED IN 5G C-RAN NETWORKS

Tese apresentada ao Curso de Doutorado em Engenharia de Teleinformática da Universidade Federal do Ceará, como parte dos requisitos para obtenção do Título de Doutor em Engenharia de Teleinformática. Área de concentração: Sinais e Sistemas

Aprovado em: 22/12/2020.

BANCA EXAMINADORA

Prof. Dr.-Ing. Yuri Carvalho Barbosa Silva (Orientador)
Universidade Federal do Ceará

Prof. Dr. Francisco Rafael Marques Lima (Coorientador)
Universidade Federal do Ceará

Prof. Dr.-Ing. Anja Klein
Technische Universität Darmstadt

Prof. Dr. Wallace Alves Martins
Universidade Federal do Rio de Janeiro

Prof. Dr. Diego Aguiar Sousa
Instituto Federal do Ceará

Prof. Dr.-Ing. Tarcisio Ferreira Maciel
Universidade Federal do Ceará

ACKNOWLEDGEMENTS

Though only my name appears on the cover of this work as author, many people have contributed to its production. I would like to offer my sincere thanks to all of them.

First and above all, I thank my family: my parents (Juscelino and Lucielida) and my brother (Lucas). Each of them has contributed somehow to the accomplishment of this work. A special thanks to my parents, who always believed in me and have invested in my studies. I love you.

Special thanks go to my supervisor Prof. Dr.-Ing. Yuri Carvalho Barbosa Silva. I greatly appreciate the freedom you have given me to find my own path and the guidance and support you offered when needed. Your advice on both research as well as on my career has been invaluable. I would also like to thank my co-supervisor Prof. Dr. Francisco Rafael Marques Lima, who guided me through my master's degree, introduced me to the research world and advised me with insights.

My sincere thanks also go to my supervisor during the sandwich Ph.D. at the Technische Universität Darmstadt in Germany - Prof. Dr.-Ing. Anja Klein, for accepting to be my supervisor and for welcoming me. I would like to thank her for her immense knowledge and motivation. Her guidance helped me in the research and in finishing this thesis. Important discussions arose at our meetings.

I would also like to thank my colleagues at GTEL/UFC, mainly my Project team (Khaled, Eduardo, Darlan, Rafael, and Prof. Dr. Walter). I also thank my old friend Weskley, we shared nice and hard times together.

Finally, I acknowledge the technical and financial support from CAPES, CAPES/PROBRAL and Ericsson Innovation Center, Brazil, under UFC.45 Technical Cooperation Contract Ericsson/UFC.

'"There is always hope, my friend, though it often comes in forms not looked for. The key is knowing how to see it and seizing that opportunity.'

(Master Jedi Qui-Gon Jinn)

RESUMO

Densificação de rede, espectro de ondas milimétricas, e MIMO (do inglês, *multiple-input multiple-output*) massivo são três das tecnologias chave apontadas pela comunidade científica e pela indústria para atender aos requisitos de capacidade para a quinta geração (5G) das comunicações móveis e além da quinta geração (B5G). No entanto, alguns desafios surgem durante a aplicação destas tecnologias. Esta tese investiga estratégias para resolver alguns problemas inerentes destas tecnologias utilizando métricas de compatibilidade espacial que mapeiam propriedades dos canais MIMO para avaliar o quão eficientemente estes canais podem ser separados no espaço. Esta tese é dividida em duas partes. A primeira parte tem por objetivo controlar a interferência em uma rede de células pequenas utilizando MIMO convencional. A densificação de rede leva a uma rápida flutuação e ao desbalanceamento da demanda de tráfego entre *uplink* e *downlink* devido ao reduzido número de usuários em cada célula. A técnica DTDD (do inglês, *dynamic time division duplex*), em que cada estação rádio base escolhe a direção em que irá transmitir, vem sendo apontada como uma solução promissora. Nestes cenários, surge uma interferência cruzada entre estações rádio base e usuários. Para controlar esta interferência, propõe-se uma métrica de compatibilidade espacial baseada em dois parâmetros que controlam a relação entre atenuação do canal desejado, correlação do canal cruzado e correlação co-canal. A métrica proposta foi analisada em um problema de escalonamento multicelular, o qual foi resolvido utilizando diferentes técnicas de otimização. Na segunda parte, o foco é em HBF (do inglês, *hybrid beamforming*) em cenários multicelulares operando em frequências milimétricas. Nesta arquitetura, o *beamforming* é separado em *beamforming* analógico e precodificador digital. Neste contexto, propõe-se uma solução gulosa baseada em uma métrica de compatibilidade espacial para assinalamento de feixes analógicos. A última proposta desta tese é uma solução para associação de usuários e estações rádio base, bem como para calcular o *beamforming* analógico e precodificador digital. A associação usuário-base tem como referência a similaridade espacial dos canais com o objetivo de evitar interferência entre células. Também foram considerados problemas de otimização para maximização de taxa e minimização de potência. A solução proposta apresentou um bom custo-benefício entre eficiência energética e capacidade de encontrar soluções.

Palavras-chave: compatibilidade espacial, direcionamento de feixes híbrido, DTDD.

ABSTRACT

Network densification, millimiter wave (mmWave) spectrum frequencies, and massive multiple-input multiple-output (MIMO) are three key technologies pointed out by the research community and industry to meet the system capacity requirements for the fifth generation (5G) of wireless communications and beyond fifth generation (B5G). However, some challenges emerge during the application of these technologies. In this thesis, we investigate strategies to handle some problems inherent to these technologies by using spatial compatibility metrics that map properties of MIMO channels to evaluate how efficiently such channels can be separated in space. This thesis is divided into two parts. The first part aims to handle interference in a conventional MIMO small-cell network. The network densification leads to fast fluctuation and unbalanced traffic demand between uplink and downlink due to the small number of user equipments (UEs) in each cell. Dynamic time division duplex (DTDD), where each base station (BS) chooses its transmission direction, has been considered as a promising solution for this issue. In such scenario, cross-interference is created between BSs and UEs. To manage this interference, a spatial compatibility metric is proposed based on two parameters that control the trade-off between intended channel attenuation, cross-channel correlation, and co-channel correlation. The proposed spatial metric was evaluated in a multi-cell scheduling problem that was solved by using different optimization techniques.. In the second part, the focus is on hybrid beamforming (HBF) multi-cell scenario operating in mmWave frequencies. In such technology, the antenna array of BSs are connected to a smaller number of radio frequency (RF) chains to reduce costs and power consumption. In such architectures, the beamforming is separated into analog beamforming and a digital precoder. In this thesis, a greedy algorithm based on a spatial compatibility metric is proposed for analog-beam assignment. The last proposal of this thesis is a UE-BS association and HBF design framework. The UE-BS association is based on the spatial similarity of the channel to avoid inter-cell interference. The optimization problems for sum-rate maximization and power minimization have also been considered. The proposed framework is shown to achieve a good trade-off between energy efficiency (EE) and feasibility of solutions.

Keywords: spatial compatibility, hybrid beamforming, DTDD.

LIST OF FIGURES

LIST OF TABLES

LIST OF ABBREVIATIONS AND ACRONYMS

3GPP	third generation partnership project
4G	fourth generation
5G	fifth generation
AoA	angle of arrival
AWGN	additive white Gaussian noise
B5G	beyond fifth generation
BB	branch and bound
BBU	baseband unit
BS	base station
C-RAN	cloud radio access network
CAPEX	capital expenditure
CB	clustering based
CDF	cumulative distribution function
CLI	cross-link interference
cmWave	centimeter wave
CoMP	coordinated multi-point
CSI	channel state information
D2D	device-to-device
DFT	discrete Fourier transform
DTDD	dynamic time division duplex
EE	energy efficiency
eMBB	enhanced mobile broadband
EPA	equal power allocation
FDD	frequency division duplex
FJT	full joint transmission
GC	greedy correlation
GEC	greedy estimated capacity
HBF	hybrid beamforming
ICSI	instantaneous channel state information
ITU	International Telecommunication Union
JT	joint transmission
KPI	key peformance indicator
LOS	line-of-sight
LTE	long term evolution
MCP	mean channel power
MIMO	multiple-input multiple-output

MIQCP	mixed integer quadratically constrained program
MISO	multiple-input single-output
MMSE	minimum mean square error
mMTC	massive machine-type communication
mmWave	millimiter wave
MRC	maximum ratio combining
MRT	maximum ratio transmission
MU	multi-user
OFDMA	orthogonal frequency division multiple access
OPEX	operation expenditure
PRB	physical resource block
QoS	quality of service
QuaDRiGA	quasi deterministic radio channel generator
RA	resource allocation
RB	resource block
RF	radio frequency
RRH	remote radio head
RZF	regularized zero-forcing
SCA	sucessive convex approximation
SDMA	space division multiple access
SDP	semi-definite program
SDR	semi-definite relaxation
SE	spectral efficiency
SINR	signal-to-interference-plus-noise ratio
SISO	single input single output
SNR	signal-to-noise ratio
SRS	sounding reference signal
SVD	singular value decomposition
TDD	time division duplex
TTI	transmit time interval
UE	user equipment
ULA	uniform linear array
UMi	urban micro
UPA	uniform plannar array
URLLC	ultra-reliable and low latency communication
ZF	zero-forcing

LIST OF SYMBOLS

$(\cdot)^{\mathrm{H}}$	Complex conjugate tranpose
$(\cdot)^{\mathrm{T}}$	Transpose
$\mathcal{M}$	Set of BSs
B	Bandwidth in Hz
G	Number of UEs in the SDMA group
M_k	Number of BSs in $\mathcal{M}_k$
N	Number of antennas of each BS
Q	Number of codewords in the codebook $\mathcal{Q}$
R	Number of RF chains of each BS
T	Number of channel samples
α	Trade-off between correlation of BS-to-UE and BS-to-BS channels
β	Trade-off between channel correlation and channel gain
$\mathrm{blkdiag}(\mathbf{A}_1, \cdots, \mathbf{A}_A)$	Block-diagonal matrix whose main-diagonal blocks are the $\mathbf{A}_1, \cdots, \mathbf{A}_A$ matrices
$\mathrm{diag}(\mathbf{a})$	Diagonal matrix whose main diagonal entries are the elements of vector $\mathbf{a}$
γ_k	Downlink SINR of UE k
$(\mathscr{A})^{+}$	Vector whose entries are the elements of set $\mathscr{A}$ in ascending order
$[\cdot]_i$	The i-th entry of a vector
$[\cdot]_{i,j}$	The entry of a matrix in the i-th row and the j-th column
$\lVert\cdot\rVert_p$	p-norm operator
$\mathbf{0}_{A\times A}$	Matrix of zeros with dimension $A \times A$
$\mathbf{1}_{A\times A}$	Matrix of ones with dimension $A \times A$
$\mathbf{\Sigma}_{m,k}$	Interfering channel matrix regarding the downlink transmission from BS m to UE k
$\mathbf{h}_{m,k}^{(t)}$	Downlink channel between BS m and UE k at the t-th channel sample
$\mathcal{C}_{m,c}$	c-th cluster of UEs found by BS m
$\mathcal{F}$	Set of analog beamforming matrices
$\mathcal{Q}$	Set of codewords from an analog beamforming codebook
$\mathcal{W}$	Set of downlink digital precoders
$\mathbf{B}_{m,k}$	Auxiliary matrix used to isolate the digital precoder matrix $\mathbf{W}_{m,k}$ from $\mathbf{W}_k$
$\mathbf{C}$	Matrix with each column representing an analog beamforming vector of codebook $\mathcal{Q}$
$\mathbf{F}^{\mathrm{b}}$	Block-diagonal matrix whose main-diagonal blocks are the analog beamforming matrices $\mathbf{F}_m \quad \forall m \in \mathcal{M}$

$\mathbf{F}_m$	Analog beamforming matrix of BS m
$\mathbf{H}^{\text{eq}}$	Matrix whose columns are the $\mathbf{h}_k^{\text{eq}}$ vectors
$\mathbf{H}_{k,b}^{\text{eq}}$	Interfering equivalent channel matrix defined as $\left(\mathbf{h}_{k,b}^{\text{eq}}\right)^{\text{H}} \mathbf{h}_{k,b}^{\text{eq}}$
$\mathbf{H}_{m,p}$	Channel matrix between BSs m and p
$\mathbf{H}_m$	Channel matrix between BS m and all active UEs
$\mathbf{I}_A$	Identity matrix of dimension $A \times A$
$\mathbf{Q}_m$	Correlation matrix between BS-to-UE channels related to the BS m
$\mathbf{R}_m$	Correlation channel matrix of BS m
$\mathbf{V}_{m,k}^{(0)}$	Matrix whose columns are right singular vectors of matrix $\mathbf{\Sigma}_{m,k}$ corresponding to the zero singular values
$\mathbf{W}_k$	Digital precoder matrix of UE k defined as $\mathbf{W}_k = \mathbf{w}_k \mathbf{w}_k^{\text{H}}$
$\mathbf{W}_{m,k}$	Digital precoder matrix used by BS m to transmit signals to UE k defined as $\mathbf{W}_{m,k} = \mathbf{w}_{m,k} \mathbf{w}_{m,k}^{\text{H}}$
$\mathbf{Y}_k$	Block-diagonal matrix whose main-diagonal blocks are the analog beams associated with UE k
$\mathbf{Y}_{m,k}$	Binary matrix representing the beam allocation of BS m to UE k
$\mathbf{Y}$	Matrix whose columns are the analog beam vectors of BSs in the system
$\odot$	Element-wise multiplier operator
$\otimes$	Kronecker product
$\overline{\mathbf{F}}$	Block-diagonal matrix whose main-diagonal blocks are the codebook matrices of all BSs in $\mathcal{M}$
$\overline{\mathbf{Q}}_m$	Correlation matrix between BS-to-UE and BS-to-BS channels related to the BS m
$\overline{\mathbf{a}}_m$	Vector whose elements are the channel attenuation between BS m and the associated UEs
$\overline{\mathbf{d}}_m$	Binary vector where an element k assumes 1 if the UE k is operating in a link direction different from that of BS m
$\overline{\mathbf{h}}_{m,b}$	Equivalent channel between BS m and UE b
$\overleftarrow{\gamma}_{m,k}$	Uplink SINR of UE k served by BS m
$\overleftarrow{\mathbf{\Sigma}}_{m,k}$	Interfering channel matrix regarding the uplink transmission from a UE k to BS m
$\overleftarrow{\mathbf{U}}_{m,k}$	Matrix whose columns are left singular vectors of matrix $\overleftarrow{\mathbf{\Sigma}}_{m,k}$ corresponding to the zero singular values
$\overleftarrow{\overline{\mathbf{h}}}_{m,b}$	Equivalent uplink channel between BS m and UE b
$\overleftarrow{\mathbf{h}}_{m,k}$	Uplink channel vector between BS m and UE k
$\overleftarrow{\mathbf{w}}_{m,k}$	Digital uplink combiner vector used by BS m to transmit a signal to UE k
$\overleftarrow{\mathbf{y}}_m$	Signal received by a BS m in operating uplink direction
$\overleftarrow{i}_{m,k}$	Interference power perceived by BS m regarding the signal sent by UE k

ρ	Parameter to control the interference in the regularized zero-forcing (RZF) digital precoder design
$\mathcal{D}$	Set of BSs operating in downlink
$\mathcal{K}_m$	Set of UEs associated with BS m
$\mathcal{K}$	Set of UEs
$\mathcal{M}_k$	Set of BSs associated with UE k
$\mathcal{U}$	Set of BSs operating in uplink
$\tilde{\mathbf{R}}_{m,k}$	Covariance matrix of the channel between a BS m and UE k
$\mathbf{a}_m$	Vector whose elements are the channel attenuation between BS m and all UEs in the network
$\mathbf{d}_m$	Binary vector where an element $[\mathbf{d}_m]_k$ assumes 1 if the UE k is operating in the same link direction of BS m
$\mathbf{f}_{m,r}$	Analog beamforming vector of BS m and associated with RF chain r
$\mathbf{h}_k^{\text{eq}}$	Downlink equivalent channel created by analog beamformings used by all BSs in the network, and perceived by UE k
$\mathbf{h}_{k,b}^{\text{eq}}$	Interfering equivalent channel perceived by UE k and created by analog beamforming of BSs serving a UE b
$\mathbf{h}_k$	Concatenation of channel vectors between a UE k and all BSs
$\mathbf{h}_{m,k}$	Downlink channel vector between the BS m and the UE k
$\mathbf{n}_m$	Noise vector perceived by BS m during uplink reception
$\mathbf{o}_m$	Binary association vector of BS m composed by binary values $o_{m,k}$
$\mathbf{v}_{m,k}$	Dominant eigenvector of covariance matrix $\tilde{\mathbf{R}}_{m,k}$
$\mathbf{w}_k$	Concatenation of $\mathbf{w}_{m,k}$ downlink digital beamforming vector $\forall m \in \mathcal{M}$
$\mathbf{w}_{m,k}$	Digital downlink beamforming vector used by BS m to transmit a signal to UE k
$\mathbf{x}$	Binary variable that indicates if a UE has been chosen to the SDMA group
ζ	Parameter to perform the power allocation in the RZF digital precoder design
a_k	Weight priority of UE k defined by the system scheduler
$g_{m,c}$	Quality of c-th cluster found by BS m
$h_{k,b}$	Channel gain between UEs k and b
i_k	Interference power perceived by UE k in downlink
n_k	Additive noise with zero mean and variance σ^2 perceived by UE k during downlink reception
$o_{m,k}$	Binary value that assumes 1 if the UE k belongs to BS m
$p^{\max}$	Power budget of each BS
p^{BB}	Power consumed by the baseband processing
p^{DL}	Downlink transmission power

p^{PS}	Power consumed by phase-shift circuit associated with an RF chain
p^{RF}	Power consumed by an RF circuit
p_m^{TX}	Effective transmit power of BS m
p^{UL}	Uplink transmission power
p^{tot}	Total power consumed by the network
p_m	Power consumed by a given BS m
r_k	Capacity of UE k tranmission
x_k	Signal sent by UE k
$x_{m,k}$	Signal sent by BS m and received by UE k
y_k	Downlink signal received by UE k
$\lvert \cdot \rvert$	Cardinality of a set or absolute values of matrices/vectors

SUMMARY

1 INTRODUCTION

Over the last 40 years, mobile communication networks have evolved five generations. The discussions about the requirements of the fifth generation (5G) began around 2012, and the first set of 5G standards were delivered in December 2017 and June 2018 [1]. However, the 5G term is often used in a wider context, not just referring to the radio access technology but also to the next range of services enabled by 5G new features. Based on the academic and industry discussions and agreements, the International Telecommunication Union (ITU) has pointed out three main use cases [2]:

- **Enhanced mobile broadband (eMBB)** is the direct evolution of fourth generation (4G) mobile-broadband services, enabling very large data rates to improve the user experience.
- **Massive machine-type communication (mMTC)** represents services where a massive amount of devices are connected to the network, for example, remote sensors. In this use case, low-cost devices with a long-life battery, low energy consumption, and small amounts of data to be transmitted/received are expected. Therefore, the requirement of high data rates is less important in this case than energy efficiency.
- **Ultra-reliable and low latency communication (URLLC)** includes services that require fast and critical actions, making low latency and high reliability the main key peformance indicators (KPIs) of this use case.

It is worth highlighting that these three use cases are a mix of economic and social demands for 5G, as well as a simplification of requirements. A quantitative comparison of the main 4G and 5G KPIs is shown in Table 1.1.

Table 1.1 – Main KPIs of 4G and 5G.

KPI	4G	5G
Peak data rate (GHz)	1	20
User experienced data rate (Mbit/s)	10	100
Connection density (devices/km^2)	10^5	10^6
Mobility support (km/h)	350	500
Area traffic capacity (Mbit/s/m^2)	0.1	10
Latency (ms)	10	1
Reliability (%)	99	99.99
Positioning accuracy (m)	1	0.01
Spectral efficiency (bps/Hz)	3	10
Network energy efficiency (J/bit)	1	0.01

Source: [3]

In order to achieve 5G requirements and move towards the beyond fifth generation (B5G), the research community identified three plausible ways: network densification, increase of the spectrum bandwidth, and massive multiple-input multiple-output (MIMO) antennas [4].

These three solutions are complementary in many aspects. Densification increases the network capacity by deploying a large amount of base stations (BSs) with short coverage, and thus, increases the reuse of radio resources. Also, it is a practical solution for crowded areas, where each BS may serve a reduced set of user equipment (UE). Another direct benefit of network densification is the short distance between transmitter and receiver nodes, which reduces the path loss effect on transmitted signals. On the other hand, the inter-cell interference increases. Despite this, the network densification associated with advanced signal processing techniques can improve the spectral efficiency, but not by orders of magnitude [5]. Therefore, increasing the multiplexing gains and extending the useful bandwidth are important to fulfill the upcoming traffic and data rate demands.

Increasing the bandwidth implies on exploring a higher frequency spectrum. The millimiter wave (mmWave) band has been adopted as solution by researchers and industry due to the existence of a large amount of unused continuous spectrum (30-300 GHz) [4, 6, 7]. The half-wavelength dipole antennas are small at such frequencies, which enables the use of a massive number of antennas. Nonetheless, the propagation channels are different in such frequencies when compared with the spectrum below 6 GHz, due to the short wavelengths. mmWave signals have issues to overcome blockages, including the human body [4]. Furthermore, the signal in such frequencies experiences more attenuation than centimeter wave (cmWave) ones.

Massive MIMO is a technology where each BS is equipped with tens to hundreds of antennas [8]. It has the potential to increase the spectral efficiency exploiting the spatial dimension for beamforming and diversity gains, thus combating deep fading effects. Besides, due to the huge number of antennas, the beamforming can create narrower beams compared with conventional MIMO, concentrating radiated energy in a narrower area. This improves energy efficiency and reduces path loss effects.

We can note that those prominent solutions are complementary in some aspects. Networks operating in mmWave spectrum have a short-range communication that leads naturally to the network densification. mmWave makes it possible to reduce the antenna's size, enabling massive MIMO. Also, the antenna gain and large number of spatial resources are important to overcome mmWave propagation issues. At the same time, the high path loss in mmWave might reduce the interference that is a problem in dense networks. The amalgam of dense networks, mmWave spectrum and massive MIMO is illustrated in Fig. 1.1.

Despite the benefits of those solutions, each one of them has some challenges. With network densification, fast fluctuations on downlink and uplink traffic become an issue for the legacy time division duplex (TDD) methods. Regarding mmWave, the elevated cost and power consumption of some circuit components can be a limitation for massive MIMO in such frequencies. In the next section, we provide details about key technologies to handle those

Figure 1.1 – Prominent solutions for 5G and B5G.

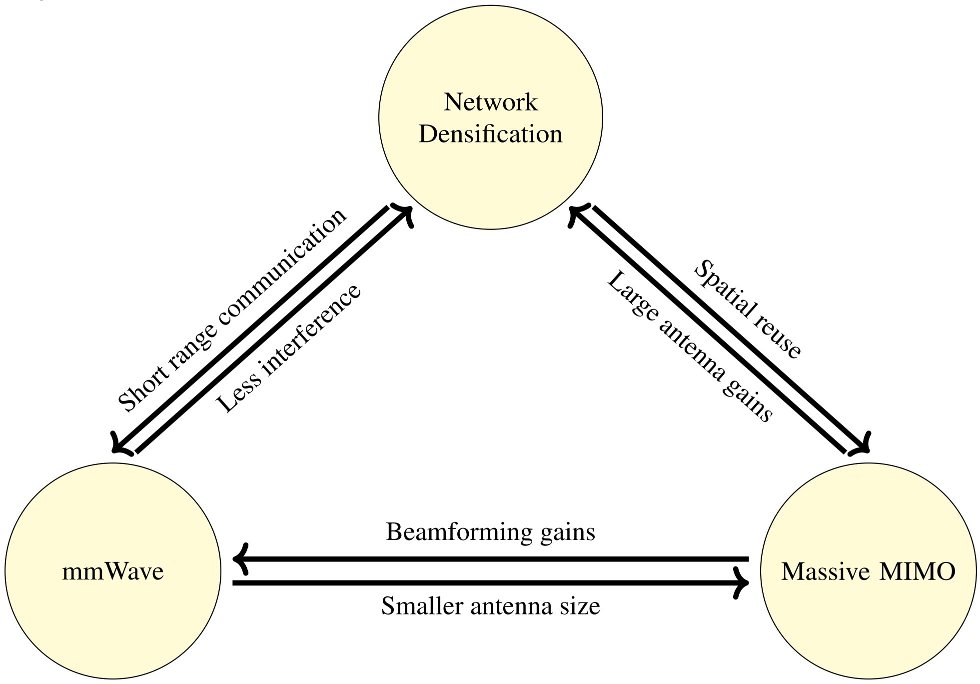

Source: Modified from [4].

challenges and which are considered in this thesis.

1.1 Key technologies

1.1.1 Dynamic TDD

Traditionally, mobile networks operate in half-duplex mode using frequency division duplex (FDD) or TDD. In FDD, different spectrum bands are allocated for uplink and downlink transmission at the same time, while in TDD the same spectrum is used for both transmission directions in different time slots. Therefore, TDD can exploit the whole available bandwidth in each direction and accommodate downlink/uplink traffic asymmetry by adjusting the transmission duration of each direction in accordance with traffic demands.

In the long term evolution (LTE) Releases 8 to 12, BSs are able to adapt uplink/downlink transmission duration by selecting one of 7 configurations from Table 1.2. The "D" and "U" labels indicate the downlink and uplink subframes, respectively, while "S" is a special subframe used when switching from downlink to uplink. In static TDD, all BSs update the uplink/downlink frame structure following the same configuration [9]. This means that all BSs will operate at the same transmission direction simultaneously.

With network densification, the downlink/uplink traffic demands have fast variation due to the small number of UEs associated with each BS. Despite this, the traffic demands become significantly different among BSs in the same networks [9]. Hence, static TDD in a dense network will make some BSs operate in an inadequate downlink/uplink configuration, which will increase the network latency.

Dynamic time division duplex (DTDD) is a solution for asymmetric traffic demands

Table 1.2 – Uplink-Downlink subframes in the LTE-TDD frame structure [10].

Pattern	0	1	2	3	4	5	6	7	8	9	D subframes	U subframes	S subframes
0	D	S	U	U	U	D	S	U	U	U	2	6	2
1	D	S	U	U	D	D	S	U	U	D	4	4	2
2	D	S	U	D	D	D	S	U	D	D	6	2	2
3	D	S	U	U	U	D	D	D	D	D	6	3	1
4	D	S	U	U	D	D	D	D	D	D	7	2	1
5	D	S	U	D	D	D	D	D	D	D	8	1	1
6	D	S	U	U	U	D	S	U	U	D	3	5	2

Source: Created by the author.

in dense networks, where each BS can adapt the downlink/uplink configuration based on its own traffic conditions. In dynamic TDD scenarios, there are two types of inter-cell interference, which will be called in this work as co-channel and cross-channel interference. The co-channel interference happens when the interfering cells are operating in the same direction, whereas the cross-channel interference happens when interfering cells are operating in opposite directions. Therefore, the co-channel interference represents BS-to-UE or UE-to-BS interference and the cross-channel interference could be UE-to-UE or BS-to-BS interference. A typical DTDD scenario is shown in Figure 1.2, where two cells are in the downlink direction and the other cell is in the uplink direction, each cell serving one UE.

Figure 1.2 – Typical DTDD scenario.

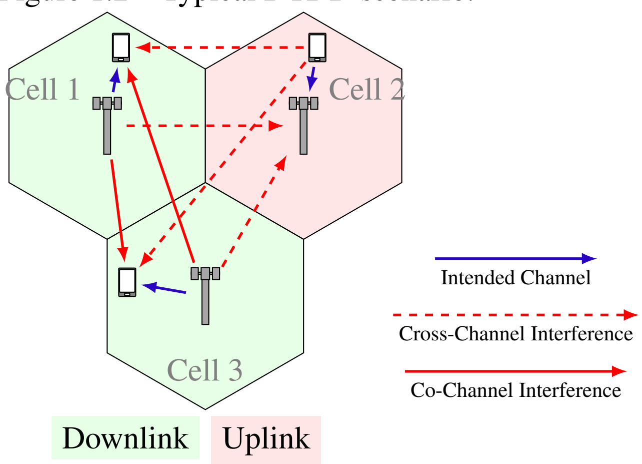

Source: Created by the author.

The direct step to move from static TDD to DTDD is considering that each BS can select one of the predefined subframe configurations shown in Table 1.2 based on local traffic conditions [11, 12, 13, 14, 15, 16]. The most sophisticated implementation of DTDD is when the uplink/downlink direction adaptation is done subframe by subframe, regardless of other BSs' decisions [17, 18, 19, 20, 21].

1.1.2 Hybrid beamforming

MIMO is a transmission scheme where there are multiple antennas transmitting and receiving signals. It brings gains in terms of spectral efficiency (SE) due to its capability of transmitting multiple data streams using the same time and frequency resource. After years of contributions on MIMO from industry and academia, the massive MIMO concept was introduced, where each BS can have tens to hundreds of antennas [8]. This technology allows increasing data streams massively while employing computationally cheap signal processing. The large number of antennas allows for a fine spatial resolution for beamforming design, which is capable to suppress small-scale fading and creates a “channel hardening” effect [22]. Massive MIMO also reduces the required transmission power due to the large beamforming gain. Despite its many benefits, massive MIMO has two major challenges:

- Large number of required radio frequency (RF) chains. In regular MIMO, there is one RF chain per antenna element. This architecture can be prohibitive for massive MIMO due to the large cost and energy consumption of considering those components in a massive scale.
- The channel estimation also becomes an issue due to the large dimension of channel matrices in massive MIMO.

An RF chain is a cascade of electronic components which may include amplifiers, filters, mixers, detectors, etc. Due to the high cost and energy consumption of RF chains, especially in mmWave frequencies, hybrid beamforming (HBF) has been considered as a candidate to handle those issues [23]. In HBF, the number of RF chains is smaller than the number of transmitting antennas and the complete beamforming is separated into digital and analog beamforming. The digital beamforming is performed on RF chains, and it is the beamforming considered in regular MIMO. Note that the amplifiers are located at RF chains, thus, the digital precoder can variate the amplitude and phase of transmitted signals. Afterwards, the output from digital beamforming is processed by an analog phase-shift circuit before being sent by the antennas. In this step, the beamforming only varies the phase of the signal to be transmitted at each antenna.

Figure 1.3 illustrates the main beamforming architectures considered in this thesis. In Figure 1.3a, the fully digital architecture considered in regular MIMO is illustrated. Each antenna has one dedicated RF chain. In Figures 1.3b and 1.3c, the fully and partially connected architectures are illustrated, respectively.

In fully-connected HBF, each RF chain is connected to all antennas, providing more beamforming gains at the cost of more complex hardware. On the other hand, in partially-connected HBF, each RF chain is connected to one independent sub-array. This second architecture is more practical and exploit the diversity/multiplexing gains that can be improved by analog beamforming.

1.1.3 C-RAN

Despite the asymmetric and heterogeneous traffic demands caused by the network densification, the inter-cell interference, capital expenditure (CAPEX), and operation expenditure (OPEX) are also challenges in those scenarios. To reduce the cost of the network and suppress the

Figure 1.3 – Block diagram of main beamforming architectures.

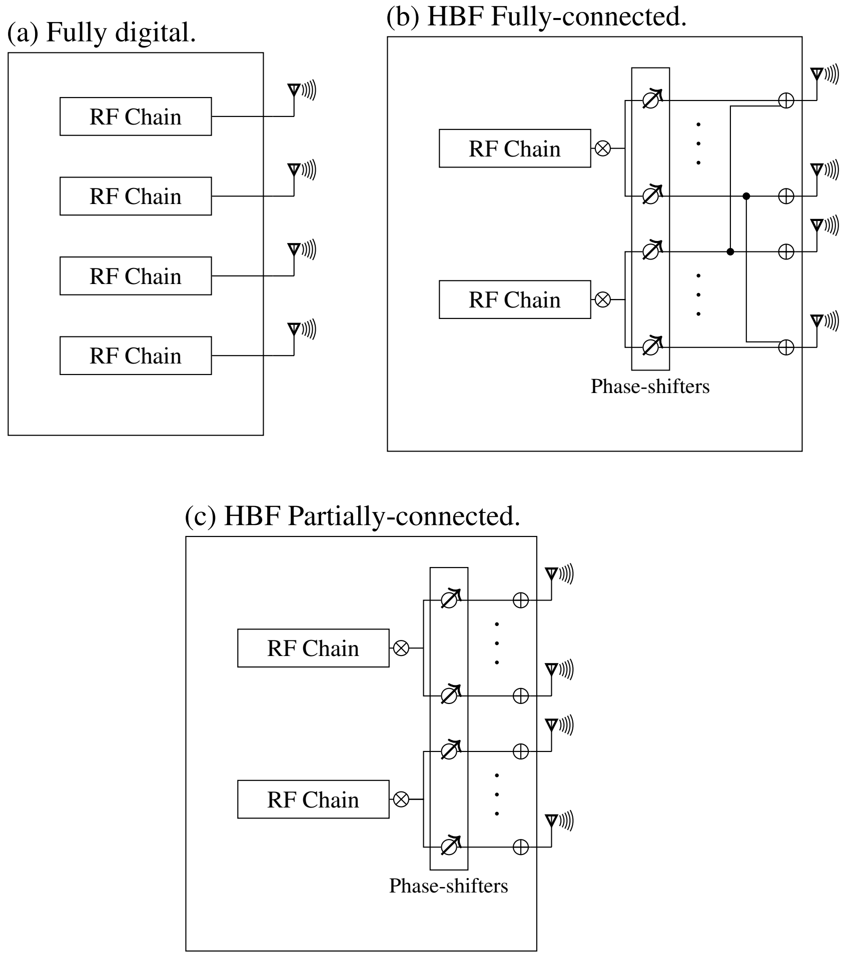

Source: Created by the author.

inter-cell interference efficiently, the cloud radio access network (C-RAN) has gained significant attention due to its network optimization capability and cost-effectiveness [24].

C-RAN was originally introduced by China Mobile [25], which proposed to move the baseband unit (BBU) from BSs to a cloud infrastructure. This architecture can handle a large amount of BSs using the concept of virtualization, allowing better cooperation among BSs in order to improve the user experience. With respect to BBU functions, C-RAN can be separated into two types: Fully centralized and partially centralized [26].

- Fully centralized: Functions related to Layer 1 (such as sampling, modulation, resource block mapping, and antenna mapping), Layer 2 functions (transport media access control), and Layer 3 (radio resource control) are performed by the BBUs in the cloud infrastructure. A fully-centralized C-RAN solution enhances the network resource sharing and multi-cell signal processing.

- Partially centralized: Functions of higher layers are performed by BBUs located in the cloud infrastructure. Specifically, Layer 1 functions are delegated to remote radio heads (RRHs), whereas Layer 2 and Layer 3 related functions are performed within BBUs.

The original C-RAN architecture has three main components:

- RRH: Composed of RF components that include power amplifiers, analog-to-digital converters, duplexers, antenna array, etc. It assumes part of the functionality of a conventional BS without baseband processing functions. In general, the RRHs are placed in a distributed way and require a reduced power supply, when compared to regular BSs [27].
- Baseband unit (BBU) pool: In a regular mobile network, each BS has one BBU, which is usually placed on the ground at the BS site. In C-RAN, those BBUs are placed in a cloud infrastructure named BBU pool, central office or point of concentration [24]. A given BBU can be connected to one or multiple RRHs dynamically, enabling a full BS cooperation.
- Fronthaul: This is a fast link between cloud infrastructure and RRHs. In general, it consists of an optical link, but wireless links can also be used.

Figure 1.4 illustrates a C-RAN network.

Figure 1.4 – C-RAN network.

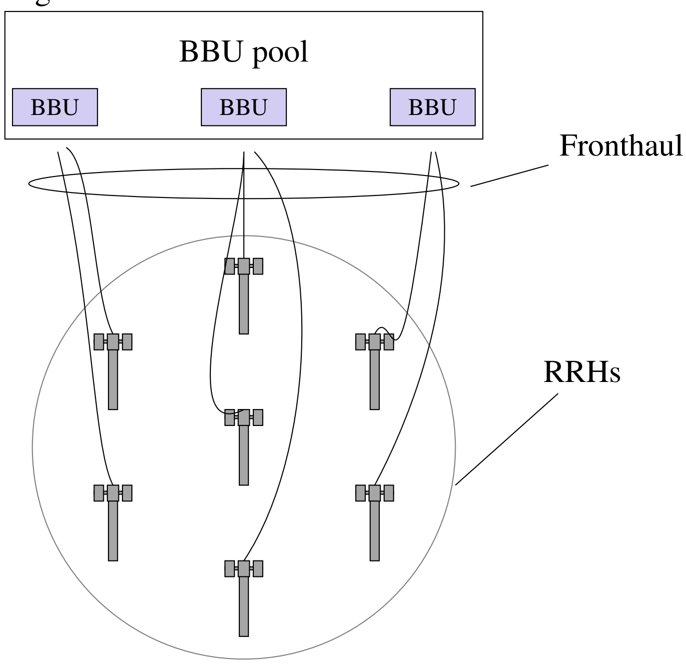

Source: Created by the author.

1.2 Resource allocation and spatial compatibility

In a radio system the resource allocation (RA) algorithms manage the time/frequency and power resources. Considering a proper frequency and time synchronization, those resources can be made orthogonal, that is, signals transmitted in a different set of resources (frequency and/or time) do not interfere with each other. This assumption simplifies the RA solutions, specially in single input single output (SISO) single cell scenarios, where the system is limited by the noise power. However, in single cell multi-user (MU)-MIMO systems, multiple signals could be transmitted and received using the same time/frequency resources, if they are separated in space through space division multiple access (SDMA). Therefore, there can be intra-cell interference in these scenarios.

In RA for MU-MIMO the time/frequency resources can be extended in a new dimension and can be thought as elements of a 3D structure represented by frequency, time and space resources [28]. In orthogonal frequency division multiple access (OFDMA) systems, this 3D resource structure is represented by subcarriers or physical resource blocks (PRBs) (time/frequency resources), subframes (time resources) and spatial layer (space resources). Due to the large number of resources to be managed in MU-MIMO scenarios, the RA solutions are more complex [29].

The set of UEs in the same cell that are transmitting or receiving signals in the same frequency-time resource, which have signals separated in the space domain, is denoted as SDMA group [30, 31, 32, 33]. The quality of signals in an SDMA group in a single cell scenario is affected by:

- Spatial compatibility: A set of channels that can be efficiently separated in the space domain are said spatially compatible. As example, spatially uncorrelated channels can have signals efficiently separated in the space domain.
- Precoding and decoding methods: Different precoding and decoding methods can suppress totally or partially the interference, which influences the spectral efficiency.
- Power allocation: The power of signals transmitted in an SDMA group has an effect on the signal-to-interference-plus-noise ratio (SINR) perceived by each UE in the group. Allocating more power to a signal can enhance the SINR at a receiver, but if the precoding and decoding methods do not efficiently suppress the interference, then the perceived SINR at other receivers in the same SDMA group can be decreased.

These three criteria are related. If UEs in the same SDMA group have spatially compatible channels, then the precoding and decoding methods can efficiently isolate the signals and the signal power allocation has more flexibility. Otherwise, more robust precoding, decoding and power allocation methods would be required.

SDMA grouping is the method to select spatially compatible channels on each frequency-time resource. Some RA schemes in the literature based on MU-MIMO scenarios consider the SDMA grouping problem, where the decision of which UEs are spatially compatible is naturally an integer and combinatorial problem [30, 31, 33]. Integer optimization problems have a discrete domain and, consequently, are not convex. These problems cannot be solved using convex optimization methods and the optimal point solution requires an exhaustive search. In general, integer problems are combinatorial problems, where the search spaces grow exponentially, hence a lower complexity suboptimal solution to SDMA grouping is preferred for a realistic system. There are in the literature several proposals to solve SDMA grouping problems. These solutions are usually based on two main components:

1. **Spatial compatibility metric**: Function of channel state information (CSI) that maps the channel properties of MU-MIMO into a scalar value that quantifies how such channels are separable in the space domain.

2. **Grouping algorithm**: Builds an SDMA group based on a grouping metric. The main goal of a grouping algorithm is to find an efficient solution avoiding the exhaustive search.

The authors in [31] and [33] present three SDMA grouping metrics which measure how efficiently UEs can be separated in space. These metrics were proposed for a single cell MU-MIMO scenario with FDD, where they were tested in a downlink transmission. Since they were formulated for single cell downlink scenarios, they are not suitable to multi-cell DTDD scenarios.

The decision of which UEs are spatially compatible is naturally an integer and combinatorial problem and the optimal solution requires an exhaustive search. The set of UEs that are transmitting or receiving signals in the same frequency-time resource, which have signals separated in the space domain, is denoted as SDMA group [30, 31, 32, 33, 34].

1.3 Objectives and thesis structure

Considering the overview about DTDD, HBF, C-RAN, resource allocation and spatial compatibility presented in previous sections of this chapter, the main objective of this thesis is to study spatial compatibility for resource allocation in 5G/B5G.

Two different radio resources are the focus of this thesis: frequency and spatial resources. In both cases, we consider a C-RAN network composed of small-cells. Figure 1.5 presents a thesis diagram separating each chapter in accordance with the type of resource studied.

Initially, in Chapter 2, we evaluate frequency resource allocation in DTDD C-RAN networks. More specifically, Chapter 2 presents proposals of a spatial metric for multi-cell DTDD scenarios and an SDMA grouping optimization problem. The optimal solution to the formulated problem can only be found through an exhaustive search algorithm. To handle this computational complexity issue, we reformulate the problem into a mixed integer quadratically constrained program (MIQCP) that can be optimally solved through the branch and bound (BB) algorithm. Besides this, two low-complexity greedy sub-optimal solutions are also presented. The proposed metric and solutions are evaluated through system-level simulations, where the relation between SINR and system capacity is compared with the spatial metric minimization.

Figure 1.5 – Thesis structure.

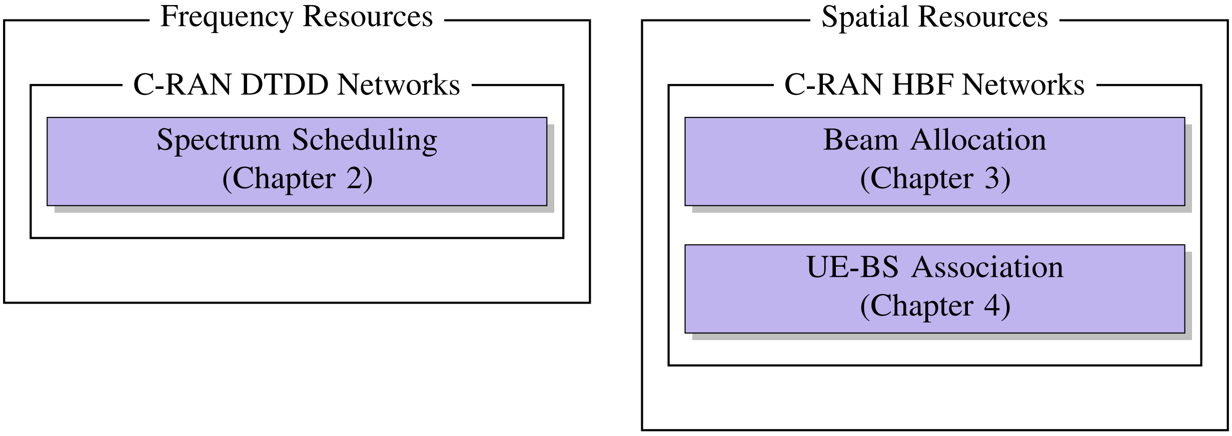

Source: Created by the author.

Then, in Chapters 3 and 4 we study spatial resource allocation problems. In Chapter 3, we present a spatial metric for analog beamforming assignment based on codebook for sum data rate maximization. The presented optimization problem is non-convex and the optimal solution can only be found through an exhaustive search. Due to a large number of possible solutions in realistic scenarios, exhaustive search is an impractical strategy. For this, we propose a greedy solution based on a spatial compatibility metric for analog beamforming assignment. The proposal aims to create equivalent channels, which will be used to design the digital beamforming with favorable spatial compatibility characteristics.

In Chapter 4, we propose a complete framework for UE-BS association as well as analog and digital beamforming design. The UE-BS association is achieved considering the similarity among channel statistics and it is used to identify and reduce high co-channel interference situations. In this context, we formulate a power minimization problem that is solved using semi-definite relaxation (SDR). In our simulations, we also consider the circuit energy consumption of the proposed and baseline solutions.

1.4 Related works

In this section we present a literature review of topics evaluated in this thesis. The related works are separated into resource allocation for DTDD networks and multi-cell HBF.

1.4.1 Resource allocation for DTDD network

Many works have proposed methods to allocate radio resources and mitigate the interference effects in DTDD networks with different goals and scenarios. In [19, 35, 36, 37, 38, 39, 40, 41, 42, 43], frequency resource allocation methods have been proposed.

Specifically in [35, 36, 37], a comparison is presented between centralized and distributed approaches for frequency scheduling in order to reduce the packet delay. In [35], beamforming and receiver design are abstracted and the simulated analyses consider a predetermined SINR based on interference levels from previous transmissions. A reduction in packet delays was perceived for DTDD, however, only marginal gains of a centralized approach were achieved when compared with a distributed one. In [36, 37], scheduling approaches were proposed for a DTDD with device-to-device (D2D) communication, where communication between UEs is enabled during the uplink time slot. In these cases, the results show gains in terms of throughput and delay for the centralized method.

Scheduling solutions for DTDD considering SISO transmission were proposed in the works [38, 39, 40]. In [38] a framework based on service requirements was proposed, where a two-step solution is considered. In the first step, the transmission direction and slicing of resources is made in order to reach the requirements of the service. Afterwards, in the second step, a resource allocation is made in order to ensure traffic demands. A strategy based on the probability that interfering BSs be transmitting in one of the directions is presented in [39]. The proposed solution considered a fully distributed scheduling approach. Finally, the work in [40] evaluates an energy efficiency (EE) scheduling problem. The problem is a mixed-integer non-linear programming that is separated into sub-problems to achieve a sub-optimal solution. The authors have found throughput gains in DTDD when compared with static TDD. However, no advantage in terms of EE has been noticed when comparing static TDD and DTDD.

Scheduling solutions for DTDD scenarios considering MIMO transmission schemes were studied in [19, 41, 42, 43]. A clustering of BSs based on geographic distance was proposed in [41]. The idea is that BSs in the same cluster operate at the same transmission direction, thus avoiding cross-link interference (CLI). The interference within a cluster is fully mitigated by zero-forcing beamforming and the frequency scheduling is made in order to satisfy the traffic demand of each UE. In [42], a Lyapunov optimization is applied to determine user scheduling, BS transmission directions and spatial design. The solution is distributed and based on interference achieved from previous transmission times. The minimum mean square error (MMSE) is considered as downlink and uplink precoder/decoder found through a sucessive convex approximation (SCA) approach. Despite considering frequency scheduling and MIMO, both works [41] and [42], do not consider the spatial compatibility and the scheduling approach does not take into account the impact of spatial filtering.

On the other hand, in [19] a user scheduling approach that considers a Gram-Schmidt process in UE-to-UE channels is proposed. The idea is to perform the Gram-Schmidt process in the UE-to-UE channels and determine the quality of the channel subspace totally free of interference. This is a spatial compatibility metric that the proposed scheduling approach considers in order to avoid solutions with high UE-to-UE interference. Note that the number of UE-to-UE channels grows exponentially, which makes the network signaling and computational complexity an issue for realistic scenarios.

In [43], we propose a spatial compatibility metric that is a convex combination of BS-to-BS, BS-to-UE channels and attenuation of the intended channel. This work is an extension for DTDD networks of the spatial compatibility metric proposed in [31] for MU-multiple-input single-output (MISO) single-cell scenarios. The idea is to have a metric that considers the channel orthogonality and channel quality at the same time. This proposal is part of this thesis, and it is presented in details in Chapter 2.

In Table 1.3, we compare the related works and the DTDD chapter of this thesis in terms of considered resources. Since transmission direction has to be properly scheduled, we assume it as a resource in our framework.

We can note that most of the cited works consider spectrum and/or space without any spatial compatibility metric. This means the effects of scheduling over spatial filtering are not considered, which can limit the gains of the approaches. The unique exception is [19], which evaluates a spatial metric between UE-to-UE channels in order to avoid scheduling frequency resources that create harmful interference.

In Chapter 2, we propose new spatial metrics for BS-to-UE and BS-to-BS channels and evaluate it in a more complex scheduling scenario.

Table 1.3 – Related works in DTDD.

References	Resources			Spatial compatibility
	Space	Trans. direction	Spectrum	
[36, 37]	✓		✓	none
[35, 39, 40]			✓	none
[38]		✓	✓	none
[42]	✓	✓	✓	none
[44]	✓	✓		none
[19]	✓	✓	✓	UE-to-UE
Chapter 2 ([43])	✓		✓	BS-to-BS and BS-to-UE

Source: Created by the author.

1.4.2 *Multi-cell hybrid beamforming*

In [45, 46, 47], methods for user-beam scheduling are evaluated for C-RAN networks, considering full BS cooperation. In [45], a scheduling method considering received power statistics for each beam is considered. Solutions based on codebooks for analog beamforming were evaluated in [46] and [47], where instantaneous channel state information (ICSI) is required by the proposed algorithms for the analog and digital precoders. Specifically in [47], we proposed a spatial compatibility metric to associate beams. In the proposal, the spatial compatibility metric is considered in order to create an equivalent channel for the digital precoders with subspaces as uncorrelated as possible. This proposal is a contribution of this thesis, and it is discussed in more details in Chapter 3. In order to mitigate the bottleneck in the fronthaul, the authors of [48] and [49] evaluate methods to optimize the analog and digital beamforming and fronthaul constraints. Both works consider full cooperation among BSs and the cell-free concept is not adopted.

The cell-free paradigm with regular MIMO is evaluated in [50, 51, 52, 53]. In [50], an optimization problem for digital precoders/decoders is solved considering the scenario with soft-handover, where UEs are considered in a handover region when the mean signal power received from a candidate BS is higher than a threshold. The authors in [51] and [52] demonstrate a significant gain in terms of spectral efficiency by considering dynamic grouping of cooperative BSs, instead of fixed cooperative configurations using conventional MIMO. In [53], the authors proposed an approximation of the ergodic capacity in the high signal-to-noise ratio (SNR) region with randomly distributed BSs and one antenna per BS. In that study, the set of cooperative BSs can jointly design beamforming.

The authors in [54] and [55] evaluate the cell-free concept from a C-RAN perspective. Despite the presented benefits, the authors point out some challenges to use those technologies, such as the amount of required CSI and the cost of RF chains in a massive MIMO array. Specifically in [55], the use of massive MIMO, small-cells and joint transmission (JT) coordinated multi-point (CoMP) is proposed to improve the spectral efficiency of the network. For that purpose, *cover-shifts* are considered, which are coverage regions where the inter-cell interference is high and JT CoMP is required. In massive-MIMO, the inter-cell interference is reduced due to the high directive beams, however, inter-cell interference can still be present when multiple BSs illuminate nearby regions. The use of cell-free massive-MIMO was also studied in [56], where a framework for joint initial access, pilot assignment, and BS cooperation cluster formation is proposed. In that approach, each UE appoints a master BS that has the largest mean channel power. Afterwards, neighboring BSs decide whether they will also serve the UE based on channel power. This method reduces the CSI fronthaul signaling and computational complexity since just a subset of BSs will serve each UE in the network.

The use of HBF for the cell-free paradigm is evaluated in [57, 58, 59]. The work in [57] proposes a channel estimation method and HBF design considering zero-forcing (ZF) as digital precoder. In [58], the work is extended to include a power allocation method. In both works, the ICSI of the complete channel matrix is required for the HBF design. In [59], the second-order channel statistics are considered for the analog beamforming. Such second-order statistics vary much slower than the ICSI, so that the analog beamforming can be considered for a longer period of time than when it was based on ICSI. Once the analog beamforming is defined, the resulting equivalent channel matrices have dimensions equal to the number of RF chains and should be considered for the digital precoder. Since there are less RF chains than antennas in the system, this represents a large reduction of the required ICSI for the cloud infrastructure to design the digital precoder. In [59], a power allocation solution for max-min SINR is proposed considering ZF as beamforming.

In Chapter 4, we propose a framework to determine the UE-BS association based on second order channel statistics. The similarity of UE-BS channel statistics is evaluated as spatial compatibility metric and it is considered for UE-BS association. Besides this, we propose a solution to maximize the system capacity and another solution to minimize the total power in the system with minimum SINR constraints as quality of service (QoS) requirements. There are, in the literature, many studies on the cell-free paradigm, HBF and CoMP with different objectives, but most of them do not consider a scenario with all technologies operating together.

In Table 1.4, we compare the related works and the hybrid beamforming chapters of this thesis in terms of beamforming method and scenario.

Table 1.4 – Related works in HBF multi-cell.

References	MIMO	Beamforming	Cell-free	Spatial Compatibility
[45, 46, 48, 49]	Massive MIMO	HBF		
[50, 51, 52, 53, 54]	Regular	Digital	✓	
[55, 56]	Massive MIMO	Digital	✓	
[57, 58, 59]	Massive MIMO	HBF	✓	
Chapter 3 [47]	Massive MIMO	HBF		✓
Chapter 4	Massive MIMO	HBF	✓	✓

Source: Created by the author.

1.5 Scientific contributions

During this Ph.D., the following papers have been published or submitted:

- COSTA, L. R.; SILVA, Y. C. B.; LIMA, F. R. M.; KLEIN, A. **Beam Allocation based on Spatial Compatibility for Hybrid Beamforming C-RAN Networks**. In: PROCEEDINGS of the IEEE Workshop on Smart Antennas. [S.l.: s.n.], 2019. P. 1–6

- COSTA, L. R.; LIMA, F. R. M.; SILVA, Y. C.; CAVALCANTI, F. R. P. Radio resource allocation in multi-cell and multi-service mobile network based on QoS requirements. **Computer Communications**, v. 135, p. 40–52, 2019. ISSN 0140-3664. DOI: `https://doi.org/10.1016/j.comcom.2018.12.007`

- COSTA, L. R.; MOREIRA, D. C.; SILVA, Y. C. B.; FREITAS, W. C.; LIMA, F. R. M. **User Grouping Based on Spatial Compatibility for Dynamic-TDD Cooperative Networks**. In: PROCEEDINGS of the IEEE Global Telecommunications Conference (GLOBECOM). [S.l.: s.n.], 2018. P. 1–6

- MOREIRA, D. C.; COSTA, L. R.; SILVA, Y. C. B.; GUERREIRO, I. M. Interference Mitigation for Dynamic TDD Networks Employing Sounding Signals. **Journal of Communication and Information Systems**, v. 35, n. 1, p. 320–332, 2020

It is worth mentioning that this thesis was developed under the context of the following Ericsson/UFC technical cooperation project:

- Nov/2016-Oct/2018: *TIDE5G - Dynamic Time Division Duplex for 5G Systems*, in which four technical reports have been delivered. Furthermore, a sandwich Ph.D. internship took place during this period:

- Nov/2018-Oct/2019: sandwich Ph.D. at Technische Universität Darmstadt, Germany.

2 SPATIAL COMPATIBILITY METRICS FOR DTDD NETWORKS

In the present chapter, we deal with an SDMA grouping problem for DTDD networks. More specifically, the SDMA grouping is the problem of selecting the best set of UEs to transmit at the same time/frequency resource. The signals of downlink and uplink UEs in the network are isolated in the space resource by downlink beamforming and uplink reception filter. In this context, we propose a new spatial compatibility metric and an optimization problem. This problem can be reformulated as an MIQCP and can be solved through a BB algorithm. However, the worst case complexity of the BB algorithm is exponential, which might be prohibitive for realistic systems. For this reason, we propose two greedy algorithms to search for a feasible solution of the SDMA grouping problem with polynomial complexity.

2.1 Contributions and chapter organization

This chapter has the following main contributions.

- We propose a new spatial compatibility metric for a multi-cell DTDD network. The proposed metric is a convex combination of intended channel attenuation and correlation among intended channels and interfering channels. In order to include BS-to-BS cross-channels, we propose to consider equivalent channels between BSs that represent the subspace with strongest channel power where the uplink BSs can receive the intended signals.
- We formulate an SDMA grouping optimization problem that can be optimally solved through an exhaustive search method. Besides this, we provide a reformulation of the original problem into an MIQCP that can be solved through a BB algorithm, which has average-case time complexity smaller than that of an exhaustive search. However, its worst-case time complexity is exponential, which might be prohibitive for applying BB solutions in realistic scenarios.
- To handle the time complexity issue, we propose best-fit and sequential removal greedy algorithm solutions based on the proposed spatial compatibility metric. The main difference between solutions is the direction where the SDMA grouping solution is built. In the best-fit solution, at each iteration of the algorithm, one new UE is selected considering the spatial compatibility metric. On the other hand, for the sequential removal algorithm, an initial SDMA group containing all UEs is considered. At each iteration, one new UE is excluded from the group by considering the SDMA grouping metric until a feasible solution is found.

This chapter is organized as follows. Section 2.2 describes the system model, including the downlink and uplink received signals and SINR considered in this work. Section 2.3

presents the proposed spatial compatibility metric used in the SDMA grouping. In Section 2.4, the optimization problem, its reformulation as MIQCP and the greedy solutions are presented and discussed. Afterwards, Section 2.5 describes a ZF method for DTDD networks that will be considered in this chapter. Section 2.6 presents numerical results of the proposed grouping solutions. Finally, Section 2.7 enumerates the main chapter conclusions and perspectives.

The following notation is adopted: upper/lower boldface letters are used for matrices/vectors. The notations $(\cdot)^{\mathrm{T}}$ and $(\cdot)^{\mathrm{H}}$ are the transpose and complex conjugate transpose. The notation $|\cdot|$ is used to represent the element-wise absolute value for matrices/vectors and cardinality for sets and $\|\cdot\|$ is the norm operator. The symbol $\leftarrow$ represents uplink direction and is used to distinguish between uplink and downlink precoders, decoders and channels.

2.2 System model

In this work, we consider a DTDD C-RAN network composed of a set $\mathcal{M}$ of BSs, each one equipped with N antennas. Let $\mathcal{K}$ be the set of single-antenna UEs in the system and $\mathcal{K}_m$ be the set of UEs served by BS m. The BSs can operate in either uplink or downlink independently. Let $\mathcal{U}$ denote the set of BSs in the uplink and $\mathcal{D}$ the set of BSs in the downlink. The vector $\mathbf{h}_{m,k} \in \mathbb{C}^{1\times N}$ represents the downlink channel between BS m and UE k. Considering that channel reciprocity holds in TDD systems, the uplink channel between BS m and UE k can be defined as

$$\mathbf{h}^{\mathrm{H}}_{m,k} = \overleftarrow{\mathbf{h}}_{m,k}. \tag{2.1}$$

The signal received by a BS m in uplink direction is given by:

$$\overleftarrow{\mathbf{y}}_m = \underbrace{\sum_{k\in\mathcal{K}_m} \overleftarrow{\mathbf{h}}_{m,k}\sqrt{p^{\mathrm{UL}}}x_k}_{\text{Intended signals}} + \underbrace{\sum_{p\in\mathcal{U}\setminus\{m\}}\sum_{b\in\mathcal{K}_p} \overleftarrow{\mathbf{h}}_{m,b}\sqrt{p^{\mathrm{UL}}}x_b}_{\text{UE-to-BS interfering signal}} + \underbrace{\sum_{p\in\mathcal{D}}\sum_{b\in\mathcal{K}_p} \mathbf{H}_{m,p}\mathbf{w}_{p,b}x_{p,b}}_{\text{BS-to-BS interfering signal}} + \mathbf{n}_m, \tag{2.2}$$

where x_k is the signal sent by UE k, $x_{p,b}$ is the signal sent by BS p to UE b, $\mathbf{n}_m$ is the noise vector perceived by BS m and $\mathbf{w}_{p,b} \in \mathbb{C}^{N\times 1}$ is the downlink precoder from BS p to UE b. The uplink transmission power is represented by p^{UL}. The matrix $\mathbf{H}_{m,p} \in \mathbb{C}^{N\times N}$ is the BS-to-BS channel between BSs m and p. The downlink transmission power of BS p is given by $\|\mathbf{w}_{p,b}\|^2$.

In order to isolate a signal from a specific UE $k \in \mathcal{K}_m$, the BS m must apply a receive beamforming to the received signal defined in (2.2). Therefore, the estimated received signal is given by

$$\hat{x}_k = \overleftarrow{\mathbf{w}}_{m,k}\overleftarrow{\mathbf{y}}_m, \tag{2.3}$$

where $\overleftarrow{\mathbf{w}}_{m,k} \in \mathbb{C}^{1\times N}$ is the receive beamforming vector with unit-norm. Note that the transmission power is applied into the downlink beamforming, therefore, $\mathbf{w}_{m,k}$ do not have unit-norm.

Similarly, the downlink signal received by a UE $k \in \mathcal{K}_m$ is given by

$$y_k = \underbrace{\mathbf{h}_{m,k}\mathbf{w}_{m,k}x_{m,k}}_{\text{Intended signal}} + \underbrace{\sum_{b\in\mathcal{K}_m\backslash\{k\}} \mathbf{h}_{m,k}\mathbf{w}_{m,b}x_{m,b}}_{\text{Intra-cell interfering signals}} + \underbrace{\sum_{p\in\mathcal{D}\backslash\{m\}}\sum_{b\in\mathcal{K}_p} \mathbf{h}_{p,k}\mathbf{w}_{p,b}x_{p,b}}_{\text{BS-to-UE interfering signals}} + \underbrace{\sum_{p\in\mathcal{U}}\sum_{b\in\mathcal{K}_p} h_{k,b}\sqrt{p^{\mathrm{UL}}}x_b}_{\text{UE-to-UE interfering signals}} + n_k, \tag{2.4}$$

where $h_{k,b} \in \mathbb{C}^{1\times 1}$ is the channel between UE k and UE b and n_k is the noise. Note that we consider a MU-MISO scenario where UEs have only one antenna. Therefore, the estimated intended signal is exactly the received signal, i.e., $y_k = \hat{x}_{m,k}$. Since the UEs are equipped with a single antenna, they cannot design a reception filter. In this way, the unique possible method to mitigate interference using space resources is through the downlink beamforming design.

Following the presented assumptions, the uplink SINR is given by

$$\overleftarrow{\gamma}_{m,k} = \frac{\left|\overleftarrow{\mathbf{w}}_{m,k}\overleftarrow{\mathbf{h}}_{m,k}\sqrt{p^{\mathrm{UL}}}\right|^2}{\overleftarrow{i}_{m,k} + \sigma_m^2}, \tag{2.5}$$

where σ_m^2 is the noise power and $\overleftarrow{i}_{m,k}$ is the interference power perceived by BS m regarding the signal sent by UE k that is calculated as:

$$\overleftarrow{i}_{m,k} = \underbrace{\sum_{b\in\mathcal{K}_m\backslash\{k\}} |\overleftarrow{\mathbf{w}}_{m,k}\overleftarrow{\mathbf{h}}_{m,k}\sqrt{p^{\mathrm{UL}}}|^2}_{\text{intra-cell interference power}} + \underbrace{\sum_{p\in\mathcal{U}\backslash\{m\}}\sum_{b\in\mathcal{K}_p} |\overleftarrow{\mathbf{w}}_{m,k}\overleftarrow{\mathbf{h}}_{m,b}\sqrt{p^{\mathrm{UL}}}|^2}_{\text{UE-to-BS interference power}} + \underbrace{\sum_{p\in\mathcal{D}}\sum_{b\in\mathcal{K}_p} |\overleftarrow{\mathbf{w}}_{m,k}\mathbf{H}_{m,p}\mathbf{w}_{p,b}|^2}_{\text{BS-to-BS interference power}}. \tag{2.6}$$

Finally, the downlink SINR in this scenario is calculated as:

$$\gamma_k = \frac{|\mathbf{h}_{m,k}\mathbf{w}_{m,k}|^2}{i_k + \sigma_k^2}, \tag{2.7}$$

where i_k is the total interference perceived by UE k in downlink transmission, defined as

$$i_k = \underbrace{\sum_{b\in\mathcal{K}_m\backslash\{k\}} |\mathbf{h}_{m,k}\mathbf{w}_{m,b}|^2}_{\text{Intra-cell interference power}} + \underbrace{\sum_{p\in\mathcal{D}\backslash\{m\}}\sum_{b\in\mathcal{K}_p} |\mathbf{h}_{p,k}\mathbf{w}_{p,b}|^2}_{\text{BS-to-UE interference power}} + \underbrace{|h_{b,k}\sqrt{p^{\mathrm{UL}}}|^2}_{\text{UE-to-UE interference power}}. \tag{2.8}$$

2.3 Spatial compatibility metric

In this proposal, we aim to schedule UEs served by different BSs within the DTDD network to the same time/frequency resource. Signals have been separated through downlink beamforming or uplink decoder. Note that the SINRs in (2.5) and (2.7) depend on channel conditions and spatial filters. Therefore, the method to optimally determine the best SDMA group is to design a spatial filter for each possible SDMA group and estimate the SINR of each scheduled UE. The number of possible groups grows exponentially, which is impractical for realistic scenarios. To handle this issue, we propose a spatial compatibility metric for DTDD networks as an alternative to evaluate SDMA group candidates, without designing all spatial filters.

In general, BS-to-BS channels have a higher rank than BS-to-UE channels, due to the larger number of antennas. In this case, when two BSs are operating in different directions, the precoder used by the downlink transmission will cause interference in a subspace of the BS-to-BS channel matrix. Moreover, the uplink decoder must isolate the interference received by the downlink BS in a subspace of the BS-to-BS channel matrix. Hence, we propose to consider an equivalent BS-to-BS channel, which represents a subspace where the BS should cause/perceive interference. This assumption ensures that the grouping proposed in this work takes into account the effective interference received/caused from/by one BS to another one, without designing all spatial filters.

For this specific case, we consider the interfering channel subspace from a BS m (transmitting in the dowlink) to a BS p (receiving data in the uplink from a UE $k \in \mathcal{K}_p$). The subspace can be measured by the equivalent channel $\bar{\mathbf{h}}_{m,k}$, created by considering the matched filter based on channel vector $\overleftarrow{\mathbf{h}}_{p,k}$. Due to the channel reciprocity property, the spatial compatibility of downlink channels is also valid in the uplink direction. In summary, the channels considered for the spatial metric are defined as:

$$\bar{\mathbf{h}}_{m,k} = \begin{cases} \left(\dfrac{\overleftarrow{\mathbf{h}}_{p,k}}{\left\|\overleftarrow{\mathbf{h}}_{p,k}\right\|}\right)^{\mathrm{H}} \mathbf{H}_{m,k}, & \text{for } k \in \mathcal{K}_p \text{ and } m, p \text{ in different directions,} \\ \mathbf{h}_{m,k}, & \text{for } k \in \mathcal{K}_p \text{ and } m, p \text{ in the same direction.} \end{cases} \tag{2.9}$$

The spatial compatibility metric maps the CSI of a given BS m into a real value. In a multi-cell scenario, we have different spatial compatibility metrics for each BS CSI in accordance with evaluated UEs. Since the intended signal must be separated from interfering signals, the spatial compatibility must be calculated only between intended UE and interfering UE channels. Despite the spatial filters, the channel gain also has an impact on the SINRs described in (2.5) and (2.7). In order to consider channel gain and correlation in the spatial metric, we propose to combine both in the same metric. The combination of those two elements was proposed in [31] for a regular MIMO single-cell scenario. The proposed metric was a convex combination of channel attenuation and channel correlation.

Differently from [31], our scenario is multi-cell, and the channel attenuation of interfering UEs can be beneficial for the SINR. Therefore, we propose a different metric considering each BS as a reference. The concatenation of all channels perceived by a BS m is given as:

$$\mathbf{H}_m = \begin{bmatrix} \bar{\mathbf{h}}_{m,1}^{\mathrm{H}} & \bar{\mathbf{h}}_{m,2}^{\mathrm{H}} & \cdots & \bar{\mathbf{h}}_{m,K}^{\mathrm{H}} \end{bmatrix}^{\mathrm{H}}, \tag{2.10}$$

where each row has dimension $1 \times N_m$ and corresponds to a vector channel from BS m and a receiver element, which can be a UE antenna or a row of cross-interfering equivalent channel generated by (2.9).

Let the attenuation vector of each channel element of matrix $\mathbf{H}_m$ be given by:

$$\mathbf{a}_m = \left[\|\mathbf{h}_{m,1}\|^{-1} \quad \|\mathbf{h}_{m,2}\|^{-1} \quad \cdots \quad \left\|\mathbf{h}_{m,K}\right\|^{-1} \right]^T. \tag{2.11}$$

Then, using (2.10) and (2.11), it is possible to write a real and non-negative correlation matrix $\mathbf{R}_m \in \mathbb{R}_+^{K\times K}$ containing all pairs of vector channel correlation calculated as

$$\mathbf{R}_m = \left| \left(\sqrt{\mathrm{diag}(\mathbf{a}_m)}\mathbf{H}_m\mathbf{H}_m^H\sqrt{\mathrm{diag}(\mathbf{a}_m)} \right) \right|, \tag{2.12}$$

where the diag$(\cdot)$ operator creates a matrix with the main diagonal composed by the input vector. The correlation between interfering channels can improve the interference mitigation by helping to isolate the interference in the same subspace. Note that in matrix (2.12), some elements represent the correlation of two interfering or two intended channels. Therefore, we have to exclude some elements of the matrix $\mathbf{R}_m$ for the SDMA grouping problem.

Next, let the association between a UE k and a BS m be represented by the binary vector $\mathbf{o}_m$, where the element $o_{m,k}$ assumes 1 if k belongs to BS m. Similarly, the vector $\mathbf{d}_m$ is a binary vector indicating if an interfering UE is operating in the same link direction of BS m, which does not include UEs served by BS m. The opposite link direction is represented by the vector $\overline{\mathbf{d}}_m$, where the element assumes 1 if UE k is operating in the opposite link direction, otherwise it assumes 0.

Let $\mathbf{O}_m = (\mathbf{o}_m)$, $\mathbf{D}_m = \mathrm{diag}(\mathbf{d}_m)$ and $\overline{\mathbf{D}}_m = \mathrm{diag}(\overline{\mathbf{d}}_m)$. The elements of matrix $\mathbf{R}_m$, which represents the correlation between the desired BS-to-UE channels and the BS-to-UE interfering channels, can be isolated by

$$\mathbf{Q}_m = \mathbf{O}_m\mathbf{R}_m\mathbf{D}_m + \mathbf{D}_m\mathbf{R}_m\mathbf{O}_m + \mathbf{O}_m\mathbf{R}_m\mathbf{O}_m. \tag{2.13}$$

Similarly, the correlation elements between the intended BS-to-UE channels and interfering equivalent channels between BSs are given by:

$$\overline{\mathbf{Q}}_m = \mathbf{O}_m\mathbf{R}_m\overline{\mathbf{D}}_m + \overline{\mathbf{D}}_m\mathbf{R}_m\mathbf{O}_m. \tag{2.14}$$

The operations in (2.13) and (2.14) zero out all components representing the correlation of two interfering channel elements. The matrices $\mathbf{Q}_m$ and $\overline{\mathbf{Q}}_m$ have dimension $K \times K$. Let $\mathbf{x} \in \mathbb{B}^{K\times 1}$ be a binary variable that indicates if a UE has been chosen to the SDMA group. Also, let $\bar{\mathbf{a}}_m = \mathbf{o}_m \odot \mathbf{a}_m$ be the attenuation vector containing only intended UEs attenuation of BS m where $\odot$ is the Hadamard product. The convex combination grouping metric for BS m is given by

$$f_{CC}^m(\mathbf{x}) = (1-\beta)\,\mathbf{x}^T\left((1-\alpha)\frac{\overline{\mathbf{Q}}_m}{\left\|\overline{\mathbf{Q}}_m\right\|_F} + \alpha\frac{\mathbf{Q}_m}{\|\mathbf{Q}_m\|_F} \right)\mathbf{x} + \beta\mathbf{x}^T\frac{\bar{\mathbf{a}}_m}{\|\bar{\mathbf{a}}_m\|}. \tag{2.15}$$

The α component can assume values in the range from 0 to 1. It represents a trade-off between the correlation of intended channels with UE interfering channels or BS interfering equivalent channels. Similarly, the β value represents the trade-off between correlation channels and channel gains. The best α and β values depend on propagation channel properties. As an example, for a noise-limited system, the best β is 1, for which UEs with the best channel condition will be selected and the interfering channel are not a problem.

Note that the spatial metric of (2.15) is exclusively dependent on the CSI measured by BS m. This is an alternative to predict how beneficial for UE k will it be when jointly scheduled with UE b, without designing the beamforming and/or uplink decoder. The CSI of intended and interfering signals can be measured by different methods. One possible way is through sounding signals, such as the sounding reference signal (SRS) presented in [60]. The CSI acquisition procedure is not the focus of this thesis and we assume that it is available for each BS of the system.

2.4 SDMA grouping problem and greedy solutions

To select the best set of UEs to be scheduled based on the proposed spatial compatibility metric, we consider an SDMA grouping optimization problem, which aims at minimizing the largest metric $f_{CC}^{m}(\mathbf{x}) \quad \forall m$. The SDMA grouping problem is formulated as

$$\mathbf{x}^* = \arg\min \left\{ \max_{m \in \mathcal{M}} f_{CC}^{m}(\mathbf{x}) \right\} \tag{2.16a}$$

$$\text{s.t} \quad \mathbf{1}^{\mathrm{T}}\mathbf{x} = G, \tag{2.16b}$$

$$\mathbf{o}_m^T \mathbf{x} \geq 1 \quad \forall m \in \mathcal{M}, \tag{2.16c}$$

$$\mathbf{x} \in \mathbb{B}^{K \times 1}. \tag{2.16d}$$

The objective of problem (2.16) is to select a set of UEs that reduces the maximum metric value $f_{CC}^{m}(\mathbf{x})$ among $m \in \mathcal{M}$. The amount of UEs in the SDMA group is controlled by constraint (2.16b), i.e, this guarantees a group size equal to G and should be used to fulfill the degrees of freedom requirements. Constraint (2.16c) ensures that at least one UE will be selected in each BS, thus avoiding to mute frequency resources in BSs. Finally, constraint (2.16d) restricts the values of $\mathbf{x}$ to the binary domain.

2.4.1 MIQCP formulation

The solution of problem (2.16) is assuredly found by exhaustive search. Nevertheless, the BB algorithm [61] can find the optimal point without testing all UE combinations. This approach consists of an enumeration of all candidate solutions subdivided as a rooted tree, where each solution has branches representing a subset of solutions. The full solutions set is represented by the root of the tree. The algorithm goes through the branches of this tree searching for new feasible solutions, while comparing them against the upper and lower bound solution found so far. When the algorithm finds a UE combination that cannot produce a feasible solution or a solution better than the best one found so far, the algorithm discards this UE combination, and all solution branches deriving from it. Thus, the search space is reduced, preventing the algorithm from checking for infeasible/suboptimal combinations. The BB solution is the most common tool used for combinatorial problems and it is used by solvers such as CPLEX [62].

In this work, we employ CPLEX to evaluate an optimal metric solution in the numerical results. For this purpose we have to rewrite the problem in (2.16) as an MIQCP as follows

$$\min_{t,\mathbf{x}} \quad t \tag{2.17a}$$

$$\text{s.t} \quad \mathbf{1}^{\mathrm{T}}\mathbf{x} = G, \tag{2.17b}$$

$$\mathbf{o}_m^T\mathbf{x} \geq 1 \quad \forall m \in \mathcal{M}, \tag{2.17c}$$

$$(1-\beta)\,\mathbf{x}^T\left((1-\alpha)\frac{\overline{\mathbf{Q}}_m}{\left\|\overline{\mathbf{Q}}_m\right\|_F} + \alpha\frac{\mathbf{Q}_m}{\|\mathbf{Q}_m\|_F}\right)\mathbf{x} + \beta\mathbf{x}^T\frac{\bar{\mathbf{a}}_m}{\|\bar{\mathbf{a}}_m\|} \leq t \quad \forall m \in \mathcal{M}, \tag{2.17d}$$

$$\mathbf{x} \in \mathbb{B}^{K\times 1}, \tag{2.17e}$$

$$t \in \mathbb{R}, \tag{2.17f}$$

where t is a new continuous variable. The problem in (2.17) seeks to minimize the t value, which is limited by the maximum convex combination metric of all BSs in the constraint (2.17c). Hence, the optimal solution of problem (2.17) is the group of UEs (variable $\mathbf{x}$), which reduces the minimum t value.

The BB could be used to find the solution of problem (2.17) testing the UE combinations of the solution tree and obtaining the optimal t by

$$t = \max_{m\in\mathcal{M}}\left\{(1-\beta)\,\mathbf{x}^T\left((1-\alpha)\frac{\overline{\mathbf{Q}}_m}{\left\|\overline{\mathbf{Q}}_m\right\|_F} + \alpha\frac{\mathbf{Q}_m}{\|\mathbf{Q}_m\|_F}\right)\mathbf{x} + \beta\mathbf{x}^T\frac{\bar{\mathbf{a}}_m}{\|\bar{\mathbf{a}}_m\|}\right\}. \tag{2.18}$$

2.4.2 Heuristic solutions - greedy algorithms

Even though the BB algorithm can find the solution of (2.17) faster than the exhaustive search, BB still has a worst case exponential complexity, which is not suitable for realistic scenarios. Therefore, a low-complexity heuristic to find suboptimal solutions is a good strategy for combinatorial problems, and hence for the SDMA grouping problem of this work.

In the following, we describe two greedy algorithms that can be used to search for a feasible point for the SDMA grouping problem in (2.16). Both algorithms have polynomial complexity. In Algorithm 2.1, the best-fit algorithm for the SDMA grouping solution is briefly described, whereas in Algorithm 2.2 the sequential removal heuristic is described.

Both algorithms are quite similar. The difference is the direction in which the solution is built. In line 1 of both algorithms, the search space is defined as a set including all UEs. In

Algorithm 2.1 Best Fit Algorithm for problem (2.16)

1: Define the search space as $\mathcal{S} = \mathcal{K}$.
2: Define the solution vector $\mathbf{x} = \mathbf{0}_{K\times 1}$.
3: **while** $\mathbf{1}^T\mathbf{x} < G$ **do**
4: Define $\mathbf{x}_k$ $\forall k \in \mathcal{S}$ as the grouping solution including the UEs already selected in $\mathbf{x}$ and the UE k.
5: Select the solution $\mathbf{x}_k^* = \arg\min \left\{ \max\limits_{\forall m \in \mathcal{M}} f_{CC}^m(\mathbf{x}_k) \right\}$
6: If $\mathbf{x}_k^*$ fulfills the constraints (2.16b) and (2.16c) do $\mathbf{x} = \mathbf{x}_k^*$
7: $\mathcal{S} \setminus \{k\}$.
8: **end while**

Algorithm 2.2 Sequential Removal Algorithm for problem (2.16)

1: Define the search space as $\mathcal{S} = \mathcal{K}$.
2: Define the solution vector $\mathbf{x} = \mathbf{1}_{K\times 1}$.
3: **while** $\mathbf{1}^T\mathbf{x} > G$ **do**
4: Define $\mathbf{x}_k$ $\forall k \in \mathcal{S}$ as the grouping solution removing the UE k from solution $\mathbf{x}$.
5: Select the solution that $\mathbf{x}_k^* = \arg\min \left\{ \max\limits_{\forall m \in \mathcal{M}} f_{CC}^m(\mathbf{x}_k) \right\}$
6: If $\mathbf{x}_k^*$ fulfills the constraints (2.16b) and (2.16c) do $\mathbf{x} = \mathbf{x}_k^*$
7: $\mathcal{S} \setminus \{k\}$.
8: **end while**

line 2, the initial solution is defined. In the best fit algorithm, the initial solution is a vector of zeros, indicating that no UEs are in the current solution. On the other hand, the sequential removal algorithm is a vector of ones, indicating that all UEs in the system are in the initial solution.

In each iteration from line 3 to line 8 of both algorithms, new solution candidates are evaluated. Each candidate considers a UE from the search space set $\mathcal{S}$ as a reference. In the best fit algorithm, the solution candidates correspond to the current solution including the reference UE while in the sequential removal, the candidates are the current solution without the reference UE. If the selected solution candidate meets the constraints (2.16b) and (2.16c), the current solution is updated with the selected candidate. In each iteration, the reference UE of the selected solution is removed from the search space set. The problem is solved when the current solution contains G UEs. The performance of both algorithms is analyzed in the numeric results section.

2.5 Zero-forcing for DTDD

Note that the interfering BS-to-BS channel matrix has dimension $N \times N$ that can be full rank in the worst case. In this way, the cross-interference mitigation must align the interfering signal in a subspace of the BS-to-BS channel matrix. To perform ZF spatial filter for a DTDD network, we propose a ZF method where downlink precoders are initially designed considering a channel subspace where the uplink BSs will possibly receive their signal. Afterwards, the uplink filters are designed by uplink BSs, considering the downlink precoders already calculated. For this, we consider an equivalent channel between BSs within the best subspace where the uplink BS can receive signals from its UEs. The selection of those subspaces is made in the equivalent channel considered for the SDMA grouping problem and given by (2.9).

Let $\mathbf{\Sigma}_{m,k} \in \mathbb{C}^{G-1\times N}$ be the interfering channel matrix perceived by a BS m in downlink regarding UE k intended channel and let it be defined as

$$\mathbf{\Sigma}_{m,k} = \begin{bmatrix} \bar{\mathbf{h}}_{m,[b]_1} \\ \bar{\mathbf{h}}_{m[b]_2} \\ \vdots \\ \bar{\mathbf{h}}_{m,[b]_{|\overline{\mathcal{K}}|-1}} \end{bmatrix}_{\mathbf{b}=(\mathcal{K}\setminus\{k\})^+}, \tag{2.19}$$

where the operator $(\cdot)^+$ represents the sorting elements of a set in ascending order. In this case, $\mathbf{b}$ is a vector of scheduled UEs without the UE k, and b_i is the i^{th} element of vector $\mathbf{b}$. Therefore, the downlink interfering channel $\mathbf{\Sigma}_{m,k}$ is the row concatenation of all equivalent channels $\bar{\mathbf{h}}_{m,b}$ excluding the channel of intended UE k. Considering $\mathbf{V}^{(0)}$ as the matrix whose columns span the nullspace of matrix $\mathbf{\Sigma}_{m,k}$ calculated using singular value decomposition (SVD) operation, the ZF downlink precoder is calculated as:

$$\mathbf{w}_{m,k} = \sqrt{p^{\text{DL}}_{m,k}} \frac{\mathbf{V}^{(0)}_{m,k}\left(\mathbf{V}^{(0)}_{m,k}\right)^{\text{H}}\mathbf{h}^{\text{H}}_{m,k}}{\left\|\mathbf{V}^{(0)}_{m,k}\left(\mathbf{V}^{(0)}_{m,k}\right)^{\text{H}}\mathbf{h}^{\text{H}}_{m,k}\right\|}, \tag{2.20}$$

where $p^{\text{DL}}_{m,k}$ is the allocated downlink transmission power.

The ZF downlink precoder will suppress the interference of all downlink UEs, excluding the UE-to-UE interference, which cannot be mitigated by spatial filtering, since UEs are single-antenna. Even though the beamforming mitigates the BS-to-BS interference in a given subspace, the uplink BSs have to design a proper uplink reception decoder to correctly isolate the interference coming from downlink and uplink transmissions. For this, let us consider the uplink equivalent channel for a given BS m and UE k defined as

$$\overleftarrow{\mathbf{h}}_{m,k} = \begin{cases} \mathbf{H}_{m,p}\mathbf{w}_{m,k}, & \text{for } k \in \mathcal{K}_p \text{ and } p \in \mathcal{D}, \\ \overleftarrow{\mathbf{h}}_{m,k}, & \text{for } k \in \mathcal{K}_p \text{ and } p \in \mathcal{U} \end{cases}, \tag{2.21}$$

where the vectors $\mathbf{w}_{m,k}$ were calculated using (2.20).

Similarly as downlink beamforming, the uplink interfering channel can be calculated as

$$\overleftarrow{\mathbf{\Sigma}}_{m,k} = \begin{bmatrix} \overleftarrow{\mathbf{h}}_{m,[b]_1} & \overleftarrow{\mathbf{h}}_{m[b]_2} & \cdots & \overleftarrow{\mathbf{h}}_{m,[b]_{|\overline{\mathcal{K}}|-1}} \end{bmatrix}_{\mathbf{b}=(\mathcal{K}\setminus\{k\})^+}. \tag{2.22}$$

Considering the matrix $\overleftarrow{\mathbf{U}}_{m,k}$ whose rows are vectors that span the nullspace of matrix $\overleftarrow{\mathbf{\Sigma}}_{m,k}$, obtained from an SVD operation, the uplink receive decoder is defined as

$$\overleftarrow{\mathbf{w}}_{m,k} = \frac{\overleftarrow{\mathbf{h}}^{\mathrm{H}}_{m,k} \overleftarrow{\mathbf{U}}^{(0)}_{m,k} \left(\overleftarrow{\mathbf{U}}^{(0)}_{m,k}\right)^{\mathrm{H}}}{\left\| \overleftarrow{\mathbf{h}}^{\mathrm{H}}_{m,k} \overleftarrow{\mathbf{U}}^{(0)}_{m,k} \left(\overleftarrow{\mathbf{U}}^{(0)}_{m,k}\right)^{\mathrm{H}} \right\|}. \tag{2.23}$$

The use of spatial filters (2.20) and (2.23) requires the degrees of freedom constraint to be fulfilled by the scheduling algorithm (or SDMA grouping solution), i.e., the number of active UE antennas in the cooperative cell cluster must satisfy $G \leq \mathrm{rank}(\mathbf{\Sigma}_{m,k}), \forall m \in \mathcal{M}$ and $\forall k \in \mathcal{K}$.

2.6 Numerical results

In order to evaluate the beamforming and grouping methods discussed in this chapter, we perform computational simulations. The simulation scenario considered in this work is composed by 4 cells with 50 meters radius in a hexagonal grid. Each cell can operate in the downlink or uplink according to the traffic demands. The scenario follows the third generation partnership project (3GPP) recommendations [63] and corresponds to the outdoor pico environment deployed in a 5 MHz bandwidth system. The main simulation parameters used in all simulations are specified in Table 2.1 and the pathloss conditions are described in Table 2.2.

Table 2.1 – General simulation parameters of DTDD simulations.

Number of BSs	4 (Hexagonal grid)
Number of BS antennas	4
Number of UE antennas	1
BS antenna array	uniform linear array (ULA) (half wavelength element separation)
BS transmit power	24 dBm
UE transmit power	23 dBm
Cell radius	50 m
Fast fading model	one-ring local scattering model
Angular spread (Δ)	65°
Number of scatterers	11
Power allocation	equal power allocation (EPA)
Noise density	−174 dBm/Hz
Monte carlo samples	1,000

Source: Created by the author.

2.6.1 *Interference mitigation results*

In order to analyze the interference conditions in the environment, we performed simulations considering the following precoder and decoder configurations:

Table 2.2 – Propagation Characteristics [63].

BS to BS
if $l < 2/3$ km: $PL(l) = 98.4 + 20\log_{10}(l)$, l in km
if $l \geq 2/3$ km: $PL(l) = 101.9 + 40\log_{10}(l)$, l in km
BS to UE
$PL(l) = 103.8 + 20.9\log_{10}(l)$, l in km
UE to UE
If $l < 50$ m: $PL(l) = 98.45 + 20\log_{10}(l)$, l in km
If $l \geq 50$ m: $PL(l) = 55.78 + 40\log_{10}(l)$, l in m.

Source: Created by the author.

- **ZF**: this approach achieves the total interference mitigation. We consider BSs operating in downlink using the ZF beamforming from (2.20) and uplink BSs using the ZF reception filter described in (2.23).

- **Maximum ratio transmission (MRT)/maximum ratio combining (MRC)**: this configuration completely ignores the interference and BSs select the subspace that maximize the signal strength. In this approach, we consider downlink BSs using MRT as beamforming precoder and uplink BSs using MRC as reception filter.

Each configuration represents extreme cases, in the sense that in the ZF approach the interference is fully suppressed, whereas for MRT/MRC the interference is fully ignored.

Figure 2.1 shows the cumulative distribution function (CDF) of the mean SINR when all BSs are operating in the same direction. These scenarios have no cross-channel interference and represent a small-cell network operating in legacy TDD.

Figure 2.1 – Mean SINR for ZF and MRT/MRC configurations when all BSs are operating in uplink or downlink.

(a) Downlink SINR for all BSs in the downlink. (b) Uplink SINR for all BSs in the uplink.

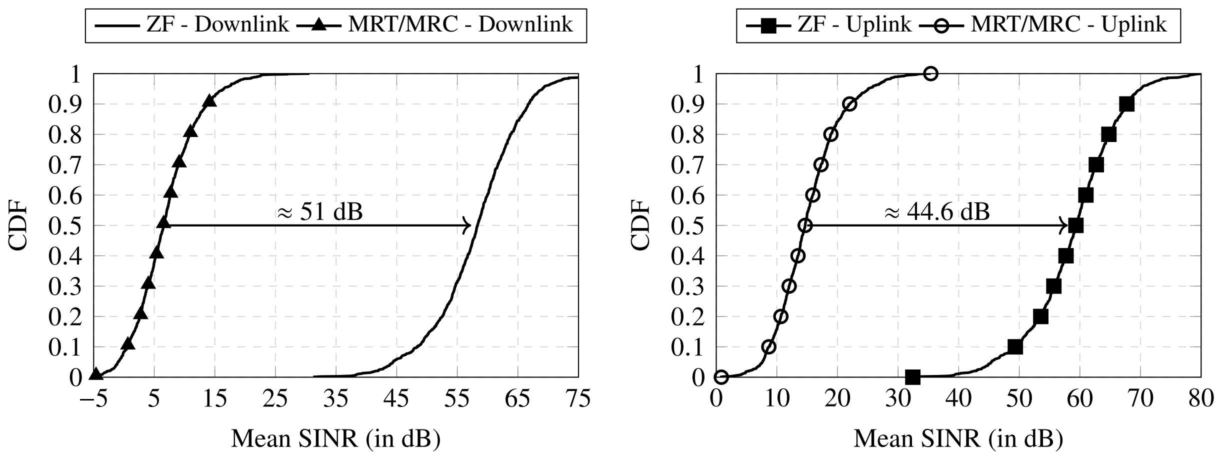

Source: Created by the author.

By analyzing Figure 2.1 we can note that, for the cases in which either all BSs are in the uplink or the downlink, the ZF approach achieves better SINR. This result shows that the

Figure 2.2 – Mean SINR for ZF and MRT/MRC configurations when only one of 4 BSs is operating in a different direction.

(a) Uplink and downlink SINR for 3 BSs in the uplink and 1 BS in the downlink.

(b) Uplink and downlink SINR for 3 BSs in the downlink and 1 BS in the uplink.

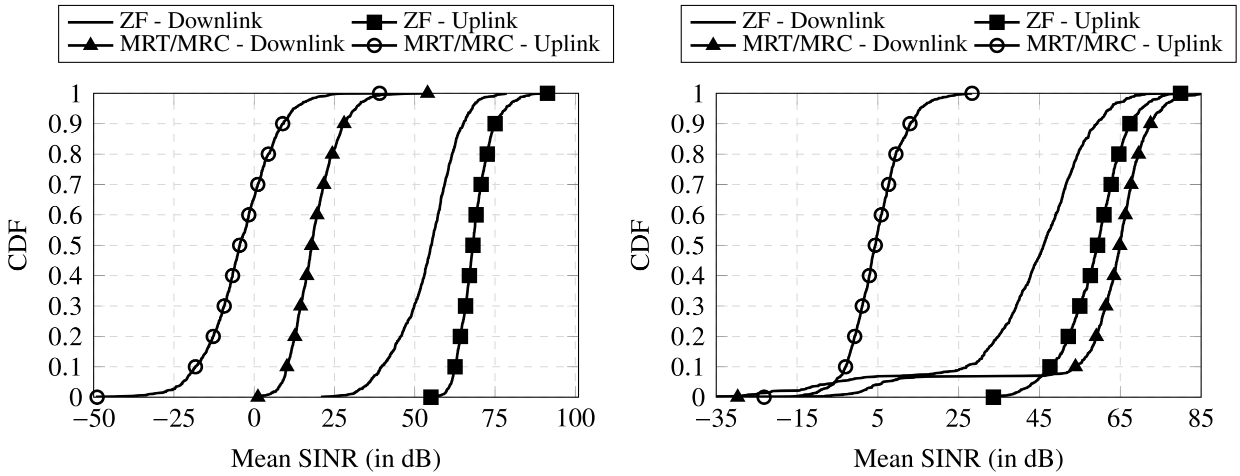

Source: Created by the author.

simulated scenario is subject to high co-channel interference and some interference mitigation approach should be employed to improve the system performance.

The CDF of the mean SINR of UEs in uplink and downlink when one BS is operating in the downlink and the others are operating in the uplink is shown in Figure 2.2a. In this scenario, comparing the ZF SINRs in uplink against downlink, we can note that the uplink SINR achieved better performance than the downlink. For the considered ZF beamforming, the downlink BSs design the beamforming considering the subspace chosen by the uplink BSs to receive the signal. Therefore, uplink BSs are free to select the strongest subspace, while the downlink BSs design the beamforming to avoid interference in these subspaces. For this reason, the uplink SINRs are higher than the downlink SINRs when the ZF approach is adopted.

The opposite behavior between uplink and downlink SINRs can be noted for the MRT/MRC approach, in the sense that downlink UEs achieve better SINR than uplink UEs. The reason is that in the model described in Table 2.2 the path-loss between BSs is smaller than BS-to-UE. The MRT/MRC approach does not perform any interference mitigation and the cross-interference from the downlink BS has a high impact on the uplink SINR.

In Figure 2.2b, the SINR CDFs are shown for the case where one BS is operating in the uplink and the others are operating in the downlink. When analyzing the ZF results for downlink and uplink SINRs, we can note the same behavior as in Figure 2.2a, in which the uplink SINRs are higher than downlink SINRs.

However, in this scenario, the downlink SINR of the MRT/MRC approach achieves the best performance among all SINR CDFs. This behavior is a consequence of the model described in Table 2.2, where the cross-interference channel between UEs has a larger path-loss coefficient than other links for distances larger than 50 m. In other words, the downlink UEs will receive less interference than the uplink UEs due to the lower path-loss of BS-to-UE and UE-

Figure 2.3 – Mean SINR in uplink and downlink when there are 2 BSs operating in uplink and 2 BSs operating in downlink.

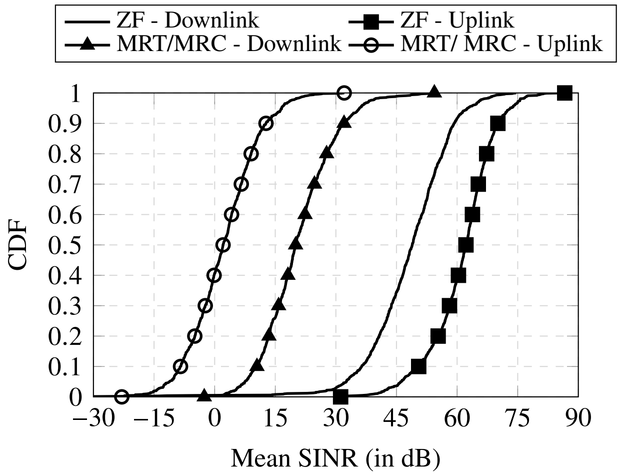

Source: Created by the author.

to-UE interfering channels when compared with BS-to-BS channel. Note that the interference between UEs is not mitigated in any of the approaches, but that is not a problem, since the interference from other UEs is small, given that the mean distances between UEs are larger than 50 m.

Finally, the CDFs for the case with 2 BSs operating in the uplink and 2 BSs operating in the downlink are shown in Figure 2.3. By comparing the behavior of uplink and downlink SINR curves for the ZF and MRT/MRC approaches we can note that they are similar to the scenario in which only one BS is in the downlink. The main difference is that lower SINR values are obtained in this scenario.

2.6.2 SDMA grouping results

Simulations considering 7 active UEs in each cell were performed to assess the performance of the SDMA grouping solutions described in this chapter. Besides the proposed grouping solution, we consider as a benchmark a random selection of UEs, which represents a scheduling solution without any SDMA grouping criterion. The UE positions are generated randomly in each cell. The capacity of each UE in a group is calculated using Shannon's capacity expression defined as

$$r_k = B\log_2(1+\gamma_k), \tag{2.24}$$

where B is the bandwidth in Hz of resource block (RB) and γ_k is the SINR of UE k.

In the grouping simulations, the target group size is 4, which represents a group formed by one UE per cell. The main simulation parameters are specified in Table 2.3.

In Figure 2.4 we compare the mean of the lowest link capacity when all BSs are transmitting in the same link direction. This scenario does not have any cross-channel interference

Table 2.3 – Parameters of SDMA grouping simulations.

Precoder	ZF (2.20)
Decoder	ZF (2.23)
Number of UEs per BS	7
Group Size	4 UEs
Grouping Algorithms	BB, Best Fit, Sequential Removal, and Random

Source: Created by the author.

Figure 2.4 – Mean of the lowest capacity of BB, Best Fit, Sequential Removal and Random grouping for different β values from (2.15).

(a) All BSs in the downlink. (b) All BSs in the uplink.

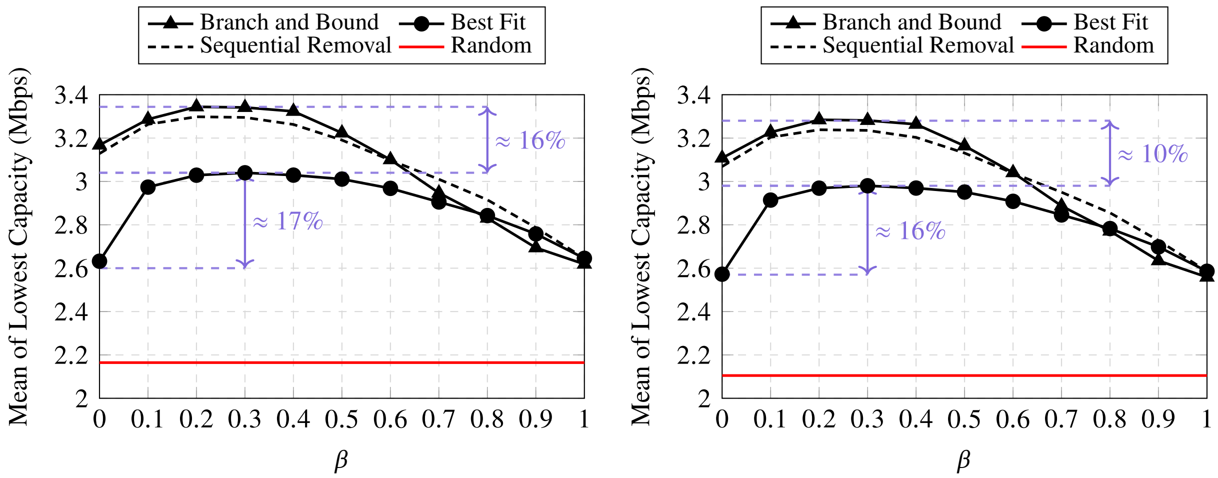

Source: Created by the author.

and represents a legacy TDD network. For this reason, the impact of α is not analyzed in this scenario, since α represents the trade-off between the correlation of intended channels and the cross-channel interference, from interfering UE channels and BS interfering equivalent channels. Therefore, we consider $\alpha = 1$ for all grouping methods, which represents the total correlation component of (2.15) in interfering UE channels.

When comparing the performance of all grouping methods in uplink and downlink illustrated in Figure 2.4, it can be seen that the performance in both link directions is quite similar. This result is expected and this behavior was perceived in the numerical results of the ZF method analyzed in Section 2.6.1. The reason is the channel reciprocity between downlink and uplink channels and the fact that all BSs are operating in the same direction, avoiding cross-interference. In both scenarios, the capacity achieved by grouping algorithms varies with the β values from (2.15), indicating the importance of adjusting the trade-off between correlation and channel gain.

The best β value in the downlink scenario is roughly 0.2, for all simulated grouping methods, and the BB algorithm achieves the best performance. For this β value, BB achieves 3.34 Mbps, while Sequential Removal, Best Fit and Random achieve 3.30 Mbps, 3 Mbps and 2.16 Mbps, respectively. When all BSs are in the uplink, the best β is roughly 0.3, where BB, Sequential Removal, Best Fit and Random achieve 3.28 Mbps, 3.23 Mbps, 2.98 Mbps and 2.10 Mbps, respectively.

Although BB achieves the best performance for the indicated β value, it has expo-

Figure 2.5 – Contour map of the lowest capacity of BB solution when 2 BSs are operating in the downlink and 2 BSs in the uplink. The black circle marks the optimal point.

(a) Mean lowest downlink capacity. (b) Mean lowest uplink capacity.

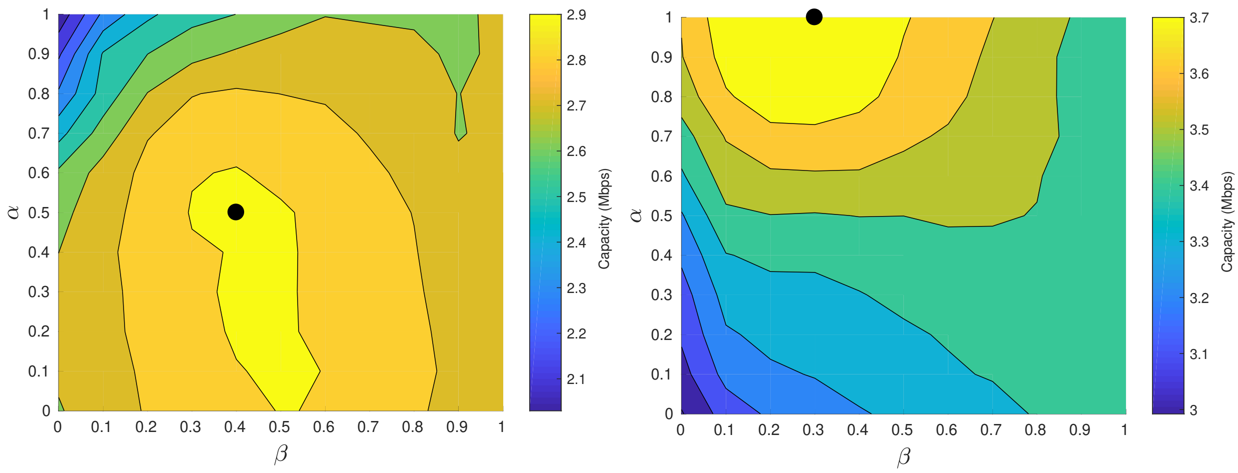

Source: Created by the author.

nential complexity, while the complexity of Sequential Removal and Best Fit is polynomial. Among the greedy solutions, the Sequential Removal reaches the best performance. The reason is that the Best Fit algorithm builds the SDMA group selecting one UE in each iteration. Thus, in the first iteration, the algorithm selects the UE with the best channel condition, which might not be the best choice. From this point on, to select new UEs the algorithm has to consider the channel gain and channel correlation with UEs already selected. On the other hand, the Sequential Removal algorithm builds the SDMA group by removing UEs. Hence, this approach considers the correlation component and channel gain from the first iteration, avoiding unfair solutions.

For scenarios with BSs operating in different link directions, the α component becomes relevant, due to the cross-channel interference. Therefore, it is important to show how grouping solutions behave for different α and β values. This analysis should identify the best range of α and β values for different interference conditions in the simulated scenario.

In this way, Figure 2.5 illustrates the contour curves of the lowest capacity in downlink and uplink UEs for the BB grouping solution, assuming that there are two BSs operating in the uplink and two BSs operating in the downlink. The black circle in the figures marks the best α and β values in terms of capacity.

When comparing the downlink capacity map in Figure 2.5a and uplink capacity map in Figure 2.5b, it can be seen that the best capacity regions are different for each situation. Good values of lowest downlink capacity are reached in the region within $0.3 \leq \beta \leq 0.6$ and $0 \leq \alpha \leq 0.6$, while for uplink capacity the region is $0.1 \leq \beta \leq 0.5$ and $0.7 \leq \alpha \leq 1$.

For both link directions, the correlation is important and has an impact on capacity. The main difference corresponds to the influence of the α value in the best capacity regions on each link direction. This difference can be explained by the ZF method of (2.20) and (2.23). According to these equations, BSs in the uplink are free to select the best subspace to receive

Figure 2.6 – Contour map of the lowest capacity of best fit solution when 2 BSs are operating in the downlink and 2 BSs in the uplink. The black circle marks the optimal point.

(a) Mean lowest downlink capacity.

(b) Mean lowest uplink capacity.

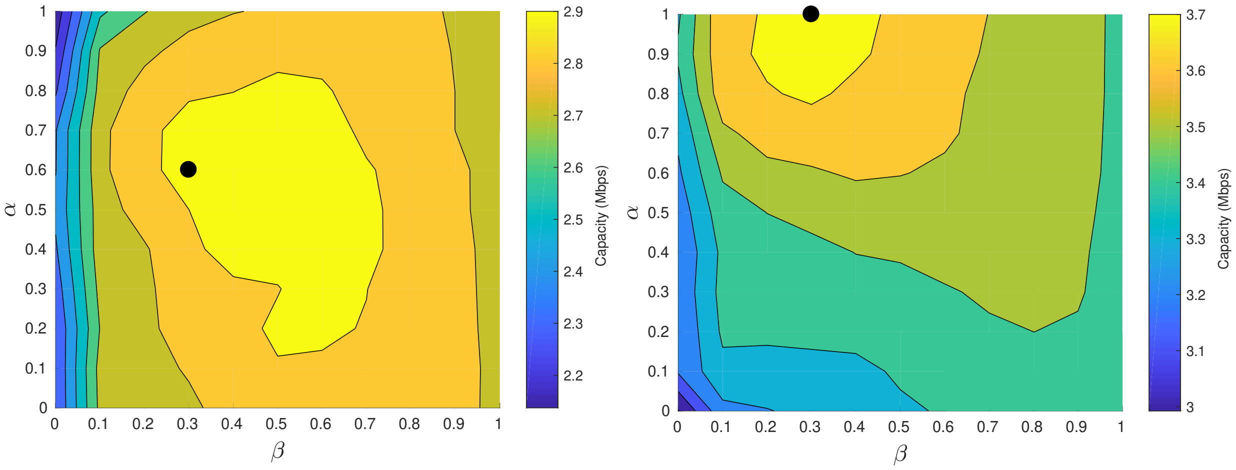

Source: Created by the author.

signals from their own UEs, while BSs in downlink have to cancel out the interference on these subspaces. Thus, if a downlink channel and a BS-to-BS interfering channel are highly correlated, the downlink ZF beamforming will have a negative impact on the signal received by the downlink UE, since it will try to cancel the caused interference while neglecting the direct channel. In this situation, the downlink UE is affected when the downlink BS protects the uplink UE. For this reason, the cross-interference channel does not have any impact on the uplink transmission when ZF is used.

This fact can be verified in the regions with the worst capacity of each link direction map. Either for uplink or downlink, the worst capacity region includes the $\beta = 0$ value, which represents a solution fully based on correlated channels. However, the worst capacity for the downlink is for $\alpha = 1$, which represents a solution fully based on BS-to-UE channels. The worst capacity for uplink BSs is for $\alpha = 0$, which is a solution based on correlations between the intended channel and BS-to-BS interfering equivalent channels.

Figure 2.6 illustrates the contour map of the lowest capacity of downlink and uplink transmissions for the Best Fit grouping solution, assuming that there are two BSs in uplink and two BSs in downlink.

Comparing the uplink capacity map of BB against the Best Fit, it can be seen that the best and worst capacity regions are quite similar, as well as the optimal capacity point. The downlink capacity for the Best Fit map includes the region $0.3 \leq \beta \leq 0.7$ and $0.2 \leq \alpha \leq 0.8$, which has a large intersection with the best capacity region of the BB solution. When analyzing the range of values of the color capacity bar of the Best Fit and BB solutions, it can be seen that they resemble each other, indicating the similarity of performance for both solutions. The best uplink capacity region for the Best Fit solution includes $0.2 \leq \beta \leq 0.4$ and $0.8 \leq \alpha \leq 1$, which is completely contained within the best capacity region of the BB solution.

Finally, Figure 2.7 shows the capacity contour maps for the Sequential Removal

Figure 2.7 – Contour map of the lowest capacity of sequential removal solution when 2 BSs are operating in the downlink and 2 BSs in the uplink. The black circle marks the optimal point.

(a) Mean lowest downlink capacity. (b) Mean lowest uplink capacity.

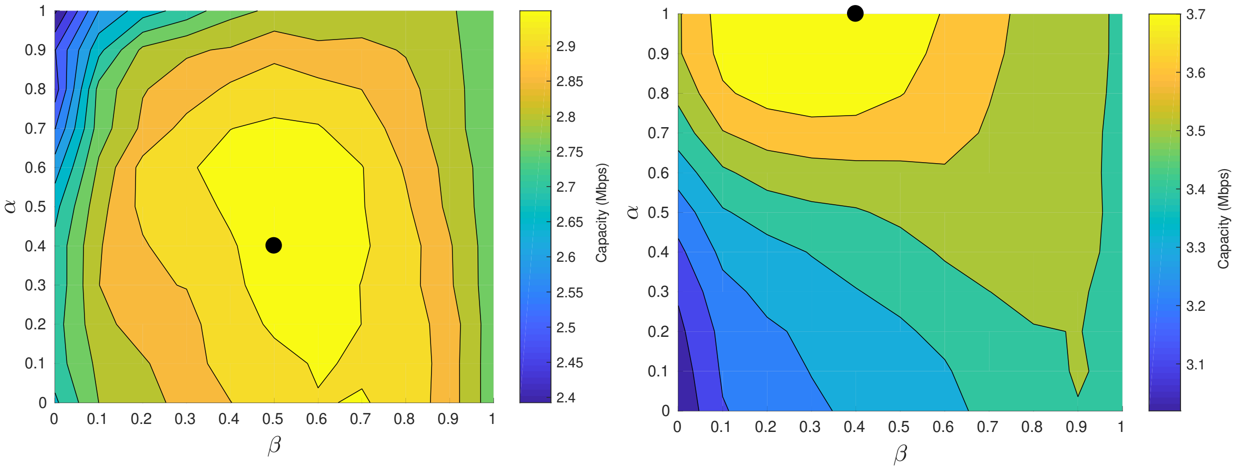

Source: Created by the author.

grouping solution with two BSs operating in downlink and two BSs operating in uplink.

An analysis of the contour maps, comparing them against the BB and Best Fit solutions, leads to similar conclusions. The best region for downlink capacity includes $0.4 \leq \beta \leq 0.7$ and $0.1 \leq \alpha \leq 0.7$, while for uplink it includes $0.1 \leq \beta \leq 0.6$ and $0.8 \leq \alpha \leq 1$.

Despite small changes in the best capacity regions, the good and bad regions of all methods present a large intersection and any SDMA grouping algorithm can find a good solution considering the α and β contained in this region.

2.7 Conclusions and future works

In this chapter, we have presented new insights on how to perform frequency resource allocation in MU-MIMO DTDD networks. In networks of small cells, the traffic demands can have quick fluctuations. Furthermore, if there are multiple services with different requirements, there can be an asymmetric traffic demand between downlink and uplink in the different cells. DTDD is a promising technology that can handle these problems and reduce network latency. However, cross-channel interference becomes an issue that must be taken into account.

To mitigate the interference in a small DTDD network, the intended channel and the interfering channels should have a low spatial correlation, which we address as being spatially compatible. With more spatially compatible channels the efficiency of the spatial precoders and decoders is increased and, hence, the cross-channel interference can be better mitigated. We have investigated grouping the UEs into SDMA groups, where an SDMA group corresponds to a set of channels transmitting signals in a frequency-time resource.

More precisely, we have proposed a new SDMA grouping problem to evaluate the quality of a group based on the spatial compatibility and the quality of the channels for a

DTDD network. The proposed problem takes into account the cross-interference and co-channel interference. The goal of the optimization problem is to minimize an SDMA metric composed of a convex combination between channel correlations and channel gains. This utility function has two trade-off parameters. One of them represents a trade-off between channel correlation and channel gain. The other one is the trade-off of cross-interfering channel correlation and co-interfering channel. Due to the combinatorial nature of the SDMA grouping problem, the solution can only be found with exponential complexity, which might be impractical for realistic scenarios. For this reason, we formulated the best fit and sequential removal algorithms, which are greedy heuristics with polynomial complexity. We also analyzed the performance of SDMA grouping solutions to find the best trade-off parameters when a ZF approach is adopted as an interference mitigation method. We concluded that these parameters have a different impact on the UE capacity and the best parameter values have been identified for each algorithm.

The content of this chapter can be extended in some directions. In the following, some of the possible future works are pointed out.

- Optimize the α and β parameters based on channel propagation, BS transmission direction and network requirements. As verified in this chapter, the best α and β values depend on the network state and on the considered spatial precoder and decoder. An efficient method to determine those values dynamically is an open question.

- Apply the proposed metric to scheduling algorithms taking into account QoS requirements, such as packet delay and target throughput. The performance of the scheduling algorithm, such as exponential proportional fair [64], could be improved by the SDMA grouping.

- Extend the proposal for a new distributed SDMA grouping strategy for a DTDD network. In the scenario considered in this chapter, the scheduling decision is made by the central unit. However, scheduling resources requires a fast response of the system. A distributed method where each BS can take its own decisions based on a small amount of signaling between BSs can improve the applicability of the metric in a realistic network, especially for low latency and reliable services.

3 SPATIAL COMPATIBILITY FOR BEAM ALLOCATION IN HYBRID BEAMFORMING

The use of codebook-based HBF requires a selection of pre-defined codewords representing the set of phase-shifts of each transmit antenna. The optimal design of HBF must jointly consider the analog-beamforming selection and digital precoder. However, the combinatorial nature of codeword selection makes the joint optimization a challenge due to the computational complexity. In general, the codeword choice is made independently of the digital precoder design.

In this chapter, we propose a beam allocation method based on the spatial compatibility of the equivalent channel created by phase-shifts of analog-beamforming. This criterion is intended to aid the digital precoder in isolating different signals sent in the network.

3.1 Contributions and chapter organization

This chapter has the following main contributions:

- We propose a spatial compatibility metric for a multi-cell HBF network for the case where all BSs cooperate in a JT-CoMP.
- We propose a greedy beam allocation method based on the proposed spatial compatibility metric. The beam allocation process is made considering a combination of channel gain and correlation of equivalent channels among served UEs created by phase-shifts of antennas.
- We present numerical results for our proposal and baseline solutions. We verify that exploiting spatial compatibility can improve the system capacity when a regularized zero-forcing (RZF) is considered as digital precoder.

This chapter is organized as follows. Section 3.2 describes the system model, including the network assumptions, digital and analog beamforming structure, and SINR. Section 3.3 describes the general optimization problem for codebook-based HBF, the low-complexity greedy solutions and the spatial compatibility metric. Furthermore, Section 3.4 presents and analyzes the numerical results of the beam allocation methods studied in this chapter. Finally, Section 3.5 presents the main chapter conclusions.

3.2 System model

In this work, we consider the downlink of an HBF C-RAN scenario composed of a set $\mathcal{M}$ of M BSs, each one equipped with N antennas and R RF chains. Each BS has a fully connected HBF architecture, which means that all antennas from one BS are connected to all R

RF chains. The BSs are serving a set $\mathcal{K}$ of K single-antenna UEs in a JT-CoMP, as illustrated in Figure 3.1.

Figure 3.1 – C-RAN system implementing JT-CoMP.

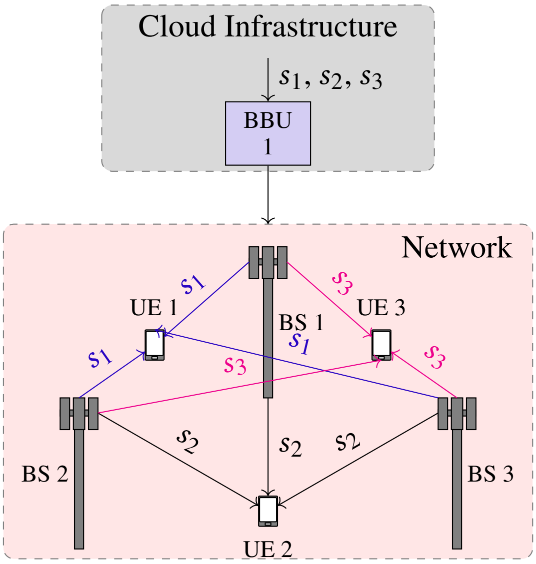

Source: Created by the author.

The analog beams designed by each BS m are composed of phase-shifts applied at each transmit antenna, which is represented by the vector $\mathbf{f}_{m,r} \in \mathbb{C}^{N\times 1}$, r is the index of the RF chain associated with the analog beam. Each element of $\mathbf{f}_{m,r}$ is given by $\frac{1}{\sqrt{N}}e^{j\theta_n}$, where θ_n is a quantized angle in antenna n. The complete analog beamforming matrix considering all beams of BS m is defined as

$$\mathbf{F}_m = \begin{bmatrix} \mathbf{f}_{m,1} & \cdots & \mathbf{f}_{m,R} \end{bmatrix} \in \mathbb{C}^{N\times R}, \tag{3.1}$$

where each column of matrix $\mathbf{F}_m$ represents an analog beam. Therefore, each BS is capable of designing R analog beams using N antennas, where $R < N$. For simplicity, let us consider $MR \geq K$, which means that it is possible to point at least one analog beam to each UE considering the overall system.

Let the vector $\mathbf{h}_{m,k} \in \mathbb{C}^{1\times N}$ represent the downlink channel between BS m and UE k. The concatenation of channel vectors between a UE k and all BSs is represented as

$$\mathbf{h}_k = \left[\mathbf{h}_{m,k}, \cdots, \mathbf{h}_{M,k}\right] \in \mathbb{C}^{1\times MN}. \tag{3.2}$$

Let $\mathbf{w}_{m,k} \in \mathbb{C}^{R\times 1}$ be the digital beamforming designed by the cloud processing unit to UE k in BS m. In this chapter, we consider the case that all BSs in the system will cooperate to design the digital precoder of each UE in the system. From this assumption, the overall digital precoder to UE k considering the RF chains from all BSs can be expressed as

$$\mathbf{w}_k = \begin{bmatrix} \mathbf{w}_{1,k}^{\mathrm{T}} & \cdots & \mathbf{w}_{M,k}^{\mathrm{T}} \end{bmatrix}^{\mathrm{T}}, \tag{3.3}$$

with $\mathbf{w}_k \in \mathbb{C}^{MR\times 1}$.

The block diagonal matrix containing the analog beamforming matrices from all cooperative BSs is defined as

$$\mathbf{F}^{\mathrm{b}} = \mathrm{blkdiag}\left(\mathbf{F}_1, \cdots, \mathbf{F}_M\right) \in \mathbb{C}^{MN \times MR}, \tag{3.4}$$

where the blkdiag$(\cdot)$ operator returns a block diagonal matrix with the input matrices as the main-diagonal blocks.

Therefore, the SINR of a UE k can be calculated by

$$\gamma_k = \frac{|\mathbf{h}_k \mathbf{F}^{\mathrm{b}} \mathbf{w}_k|^2}{\sum\limits_{\substack{b \in \mathcal{K} \\ b \neq k}} |\mathbf{h}_k \mathbf{F}^{\mathrm{b}} \mathbf{w}_b|^2 + \sigma^2}, \tag{3.5}$$

where σ^2 is the received additive white Gaussian noise (AWGN) power and the transmit symbols are assumed to have unit variance.

3.3 Beam allocation problem

In this work, we consider that each analog beam at each BS is taken from a predefined codebook $\mathcal{Q}$ composed of Q codewords. Each codeword corresponds to a phase-shift vector applied to the transmitting antennas. In order to optimize some utility function $f(\cdot)$, the cloud processing unit has to determine the analog beams of each BS, as well as design a digital beam for each UE. For simplicity, let us define the set of analog beamformers as $\mathcal{F} \triangleq \{\mathbf{F}_m\}_{m \in \mathcal{M}}$ and digital precoders as $\mathcal{W} \triangleq \{\mathbf{w}_k\}_{k \in \mathcal{K}}$, where $\triangleq$ represents equality by definition. Considering the power transmission budget of each BS as $p^{\max}$, a general HBF optimization problem for a C-RAN HBF network based on codebook is expressed as

$$\max_{\mathcal{F},\, \mathcal{W}} \quad f(\mathcal{K}, \mathcal{F}, \mathcal{W}) \tag{3.6a}$$

$$\text{s.t.} \quad \sum_{k \in \mathcal{K}_m} \mathbf{w}_{m,k}^{\mathrm{H}} \mathbf{F}_m^{\mathrm{H}} \mathbf{F}_m \mathbf{w}_{m,k} \leq p^{\max}, \quad \forall m \in \mathcal{M}, \tag{3.6b}$$

$$\mathbf{f}_{m,r} \in \mathcal{Q}, \quad \forall m \in \mathcal{M} \text{ and } r \in [0, R], \tag{3.6c}$$

where the constraint (3.6b) guarantees power budget of each BS, and (3.6c) guarantees that each analog beam belongs to the codebook.

The utility function in (3.6) can represent any objective such as system sum rate, energy efficiency, power minimization, etc. Although problem (3.6) is non-convex due to the nature of the optimization variables, the overall complexity also depends on the objective function. For each possible codebook selection, we have a possible solution for the digital precoder. In this way, the solution with best objective for any version of problem (3.6) is achieved by testing all combinations of beam allocation and by designing a proper digital precoder. In the end, the solution with the largest utility is selected.

In general, the analog beamforming selection is solved independently from the digital precoder. In this context, the focus of this work is on the analog beam allocation step. In this step, we evaluate low-complexity solutions considering different criteria to estimate the final network performance. The first solution is based on capacity estimates without considering the digital precoder. The second one is a solution that takes into account the spatial compatibility among interfering effective channels created by the analog beam selection.

3.3.1 Low-complexity sub-optimal solutions

Let the codebook set $\mathcal{Q}$ also be represented by the matrix $\mathbf{C} \in \mathbb{C}^{N\times Q}$, where each column is an analog beam of $\mathcal{Q}$. For simplicity, let us consider the same codebook for all BSs and let the matrix $\overline{\mathbf{F}}$ be a block diagonal matrix containing the codebooks from all BSs, defined as

$$\overline{\mathbf{F}} = \mathbf{I}_M \otimes \mathbf{C} \in \mathbb{C}^{MN\times MQ}, \tag{3.7}$$

where $\mathbf{I}_M$ is an identity matrix of dimension M and $\otimes$ is the Kronecker product.

Further, let $\mathbf{Y}_{m,k} \in \mathbb{B}^{Q\times R}$ be the binary matrix representing beam allocations of BS m to UE k. The columns of $\mathbf{Y}_{m,k}$ correspond to the different RF chains, while its rows represent codeword indices from the codebook, i.e., a given column from matrix $\mathbf{C}$. Let be the operator $[\cdot]_{c,r}$ represents the element in row c and column r of a matrix. When the codeword c is associated with the RF chain r from a BS m in order to point a beam towards UE k, the matrix element $\left[\mathbf{Y}_{m,k}\right]_{c,r}$ is set to 1, otherwise it is zero.

The block diagonal matrix containing all beams allocated to UE k is given by

$$\mathbf{Y}_k = \text{blkdiag}\left(\mathbf{Y}_{1,k}, \cdots, \mathbf{Y}_{M,k}\right) \in \mathbb{B}^{MQ\times MR}, \tag{3.8}$$

and the total beams allocated in the system considering all BSs is given by matrix

$$\mathbf{Y} = \sum_{k=1}^{K} \mathbf{Y}_k, \in \mathbb{B}^{MQ\times MR}. \tag{3.9}$$

In this chapter, we evaluate two low-complexity sub-optimal solutions for the analog beam allocation step. In order to describe the algorithms, let us define some auxiliary sets and variables. Let C_m be the set of codewords available to be allocated at BS m. Further, let $\overline{\mathcal{M}}$ and $\overline{\mathcal{K}}$ be the sets of BSs and UEs available to the beam allocation, respectively. Finally, let the vector $\mathbf{c}_c \in \mathbb{C}^{N\times 1}$ define the c-th column of the codebook matrix $\mathbf{C}$. The algorithms follow the structured pseudo-code presented in Algorithm 3.1. The main difference between them is the criterion to select the tuple codeword-BS-UE to be assigned, which will be further discussed.

In Algorithm 3.1, one analog beam is associated with one UE in each iteration. The first assignment is made in line 3 of the algorithm considering only the channel quality between all combinations of UE, BS and beam. Since this step is faced with a large number of possibilities, this selection could be made by using a lookup table process, assuming that the cloud has access to the gains of all beams in the network, which can be estimated and reported by each BS, with the largest one being selected. Afterwards, the iteration from line 7 to line 12 performs a sequential assignment of beams, considering the metrics that will be later discussed.

Algorithm 3.1 Greedy beam allocation algorithm

1: Define $\overline{\mathcal{M}}$ and $\overline{\mathcal{K}}$ as the set of all BSs and UEs in the system, respectively.
2: Define $\mathcal{Q}_m$ as the set of all codewords for all BSs.
3: Select the tuple codeword-BS-UE (c^*, m^*, k^*) which has the largest expected received power $|\mathbf{h}_{m^*,k^*}\mathbf{c}_{c^*}|^2$
4: Set $\left[\mathbf{Y}_{m^*,k^*}\right]_{c^*,q^*} = 1$, where q^* is the index of an RF chain at BS m without assigned codeword.
5: Update $\overline{\mathcal{K}} = \overline{\mathcal{K}} \setminus \{k^*\}$ and $C_m = C_m \setminus \{\mathbf{c}_{c^*}\}$.
6: In the specific case that $B = 1$, do $\mathcal{M} = \mathcal{M} \setminus \{m^*\}$.
7: **while** $\overline{\mathcal{K}} \neq \emptyset$ **do**
8:     Select the tuple codeword-BS-UE (c^*, m^*, k^*) which maximizes metric (3.10) or minimizes (3.12).
9:     Set $\left[\mathbf{Y}_{m^*,k^*}\right]_{c^*,b^*} = 1$
10:     $\overline{\mathcal{K}} = \overline{\mathcal{K}} \setminus \{k^*\}$ and $C_m = C_m \setminus \{\mathbf{c}^*_{c^*}\}$.
11:     If all RF chains in BS m^* have been allocated, do $\overline{\mathcal{M}} = \overline{\mathcal{M}} \setminus \{m^*\}$.
12: **end while**
13: **if** $\overline{\mathcal{M}} \neq \emptyset$ and $\overline{\mathcal{K}} = \emptyset$ **then**
14:     Update $\overline{\mathcal{K}} = \mathcal{K}$.
15: **end if**
16: **while** $\overline{\mathcal{M}} \neq \emptyset$ **do**
17:     Select the tuple codeword-BS-UE (c^*, m^*, k^*) which maximizes metric (3.10) or minimizes (3.12).
18:     Set $\left[\mathbf{Y}_{m^*,k^*}\right]_{c^*,b^*} = 1$
19:     $\overline{\mathcal{K}} = \overline{\mathcal{K}} \setminus \{k^*\}$ and $C_m = C_m \setminus \{\mathbf{c}^*_{c^*}\}$.
20:     If all RF chains in BS m^* have been allocated, do $\overline{\mathcal{M}} = \overline{\mathcal{M}} \setminus \{m^*\}$.
21: **end while**

At each iteration of this loop, one UE, BS and beam from sets $\overline{\mathcal{K}}$, $\overline{\mathcal{M}}$, and $C_m, \forall m \in \overline{\mathcal{M}}$, are assigned. The selected UE k^* is removed from the set $\overline{\mathcal{K}}$ of possible assignments. In this way, one UE will be associated with at least one beam. Also in this loop, the number of RF chains without codeword at the selected BS m^* is verified in line 11. If the BS has all RF chains assigned to an analog beam, it cannot be considered in the next iterations, so it is removed from the set $\overline{\mathcal{M}}$.

Note that after assigning one beam for each UE in the loop from line 7 to line 12, it is possible that some BSs have RF chains without any codeword. In this case, all UEs are re-included in set $\overline{\mathcal{K}}$ and a new loop to associate the remaining beams is performed from line 16 to line 21 until all RF chains are assigned with one codeword.

The first algorithm is the greedy estimated capacity (GEC), which is an adaptation of the algorithm proposed in [46]. This algorithm considers the expected signal power after the beam allocation to predict system capacity. The GEC expression is defined as

$$f_{\text{CAP}}(c^*, m^*, k^*) = \sum_{k \in \overline{\mathcal{K}}} \log_2 \left(1 + \frac{||\mathbf{h}_k \mathbf{F}^b \mathbf{Y}_k||^2}{\sum\limits_{\substack{b \in \overline{\mathcal{K}} \\ b \neq k}} ||\mathbf{h}_k \mathbf{F}^b \mathbf{Y}_b||^2 + \sigma^2} \right), \tag{3.10}$$

where the relationship between intended signal power and the interfering signal power is made considering the equivalent channel without digital precoder. Considering this SINR estimation, a simplification of the expected capacity is the metric considered to guide the analog beam allocation.

The second criterion is the greedy correlation (GC), which is our proposal and considers the correlation between equivalent channels after the beam allocation and the channel attenuation on the tuple codeword-BS-UE (c^*, m^*, k^*). Hence, we can calculate the complete downlink equivalent channel to one given UE considering the beam allocation of all BSs by

$$\mathbf{h}_k^{\text{eq}} = \mathbf{h}_k \mathbf{F}^b \mathbf{Y}. \tag{3.11}$$

The GC criterion is defined by

$$f_{\text{COR}}(c^*, m^*, k^*) = \|\mathbf{h}_{k^*,m^*}\mathbf{c}_{c^*}\|^{-2} \sum_{\substack{b\in\mathcal{K} \\ b\neq k}} \frac{|\mathbf{h}_k^{\text{eq}}\left(\mathbf{h}_b^{\text{eq}}\right)^{\text{H}}|}{\|\mathbf{h}_k^{\text{eq}}\|\|\mathbf{h}_b^{\text{eq}}\|}, \tag{3.12}$$

where the term $\|\mathbf{h}_{k^*,m^*}\mathbf{c}_{c^*}\|^{-2}$ is the channel attenuation and the term $\frac{|\mathbf{h}_k^{\text{eq}}(\mathbf{h}_b^{\text{eq}})^{\text{H}}|}{\|\mathbf{h}_k^{\text{eq}}\|\|\mathbf{h}_b^{\text{eq}}\|}$ is the channel correlation.

Note that, to efficiently isolate the signals in the space domain by digital beamforming, an analog beam assignment that reduces the correlation among the downlink equivalent channels is desired. Analog beams that have good signal reception by UEs are also desired. Therefore, the GC method will allocate analog beams with low correlation and good channel quality. It is worth to mention that the correlation and channel attenuation could be acquired by evaluating the statistics of the channel, therefore, the metric could be calculated without considering the instantaneous CSI. To evaluate the performance of the greedy analog beam allocation, we consider a classical RZF digital precoder that acts on the equivalent channel created by analog beamforming. In this approach, we calculate the digital precoders for each UE k considering the equivalent channels after the analog beamforming solution. The RZF for the HBF scenario is given by

$$\mathbf{w}_k = \zeta \left((\mathbf{H}^{\text{eq}})^{\text{H}} \mathbf{H}^{\text{eq}} + \rho M R \mathbf{I}_{MR} \right)^{-1} \left(\mathbf{h}_k^{\text{eq}}\right)^{\text{H}}, \tag{3.13}$$

where $\mathbf{H}^{\text{eq}}$ is the concatenation of channels relative to UEs served by BSs in $\mathcal{M}_k$, defined as $\mathbf{H}^{\text{eq}} = \begin{bmatrix} \mathbf{H}_1^{\text{eq}} & \cdots & \mathbf{h}_K^{\text{eq}} \end{bmatrix}$, ζ is a normalization parameter to fulfill the power constraint at each BS and ρ is the regularization parameter which controls the interference. In this work, we consider $\rho = (K\sigma^2)/(p^{\max}M)$, which maximizes the SINR in a single-cell scenario [65, 66].

For the power allocation step, we have to consider the per-BS power constraints. This means that if we normalize each BS digital precoder, the total combined digital precoder will no longer cancel the interference [67, 68]. Therefore, we apply a sub-optimal power allocation according to

$$\zeta = \left\{ \min_{m=1,\cdots,M} \sqrt{\frac{p^{\max}}{\sum_{k\in\mathcal{K}_m} \mathbf{w}_{m,k}^{\text{H}} \mathbf{F}_m^{\text{H}} \mathbf{F}_m \mathbf{w}_{m,k}}} \right\}. \tag{3.14}$$

This power allocation solution guarantees that all BSs will fulfill the power transmit budget without modifying the ZF effect. However, this solution will typically lead to a situation where only one BS transmits with total power, which is not optimal in terms of system capacity.

3.4 Numerical results

To evaluate the analog beamforming solutions presented in Section 3.3.1, simulations have been performed. The simulated system corresponds to an outdoor micro-cell environment deployed in a system with 100 MHz bandwidth and line-of-sight (LOS) at all links. We have simulated a scenario considering a square environment with 4 BSs at each vertex and with the antenna array pointing towards the center of the square, as illustrated in Figure 3.2. We have considered 24 dBm of transmission power budget, which is equally divided among 124 frequency resources. The proposed algorithm has been applied at each frequency resource, considering the amount of power reserved for it. The main parameters used in the simulations are specified in Table 3.1.

In our simulations, we consider two reference cases: full digital and random. The full digital approach is the method where we consider that each BS has the number of RF chains equal to the number of antennas. In this case, only the digital precoder with all antennas is considered. As for the random approach, it considers a random allocation of codewords and users, while satisfying the constraints in problem (3.6). The position of each UE is generated randomly considering a uniform area distribution.

Figure 3.3 shows the sum data rate at one frequency resource of the system for the

Figure 3.2 – Simulated environment with 4 UEs in the system.

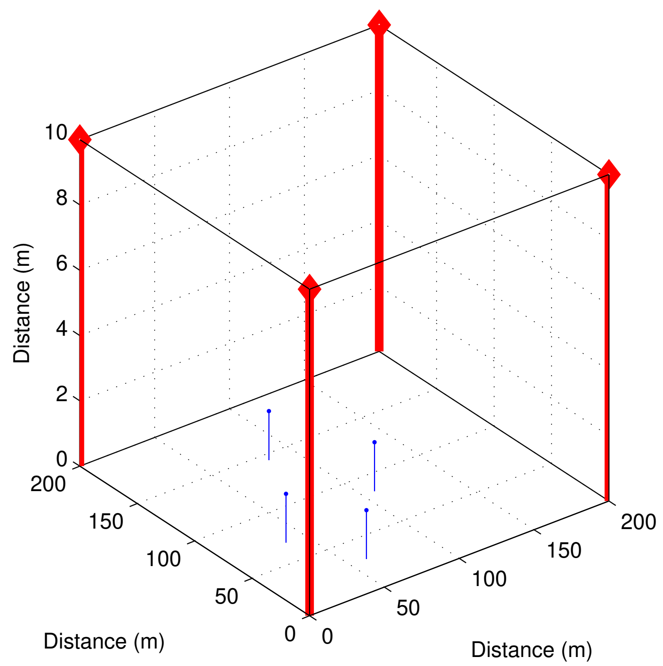

Source: Created by the author.

Table 3.1 – Parameters of beam allocation simulations.

Num. of BSs	4
Num. of BS antennas	64
Num. of UE antennas	1
Carrier frequency	60 GHz
BS height	10 m
UE height	1.50 m
BS antenna downtilt	12 degrees
Distance between neighbor BSs	200 m
BS antenna array	uniform plannar array (UPA) 8x8
UE antenna array	Omni-directional
Maximum transmit power	24 dBm
Num. frequency resources	124
Noise density	-174 dBm/Hz
Monte Carlo samples	500
Digital precoder	RZF
Codebook	discrete Fourier transform (DFT)
Channel model	QuaDRiGA [69]
Scenario	3GPP 3D Urban Micro-Cell LOS

Source: Created by the author.

Figure 3.3 – Sum data rate in a frequency resource versus number of UEs considering 2 RF chains per BS.

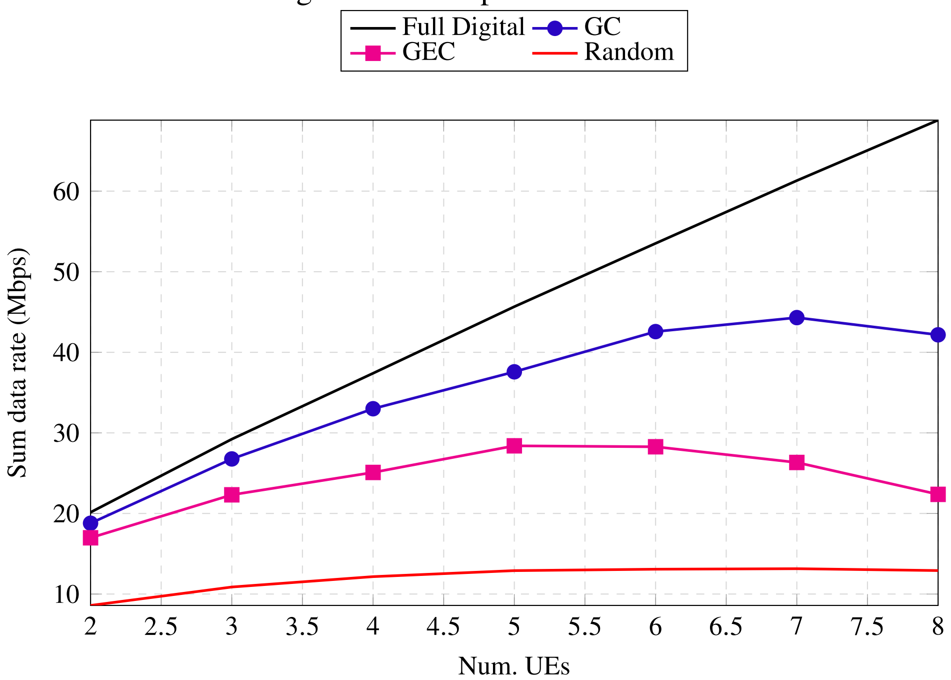

Source: Created by the author.

simulated algorithms, considering 2 RF chains per BS and that the number of UEs increases from 2 to 8. It can be seen that the fully digital and random approaches present the best and worst performance, respectively, as expected. The sum data rate increases with the number of UEs up to a certain point, after which it starts to decrease for all HBF algorithms. The reason is that the maximum number of possible analog beams in the system is limited to 8 (two RF chains per BS). The consequence is that the algorithm does not have enough degrees of freedom to find a good solution when the number of users tends to 8, in the sense that each UE will be allocated to each

Figure 3.4 – Mean data rate in a frequency resource versus number of UEs considering 2 RF chains per BS.

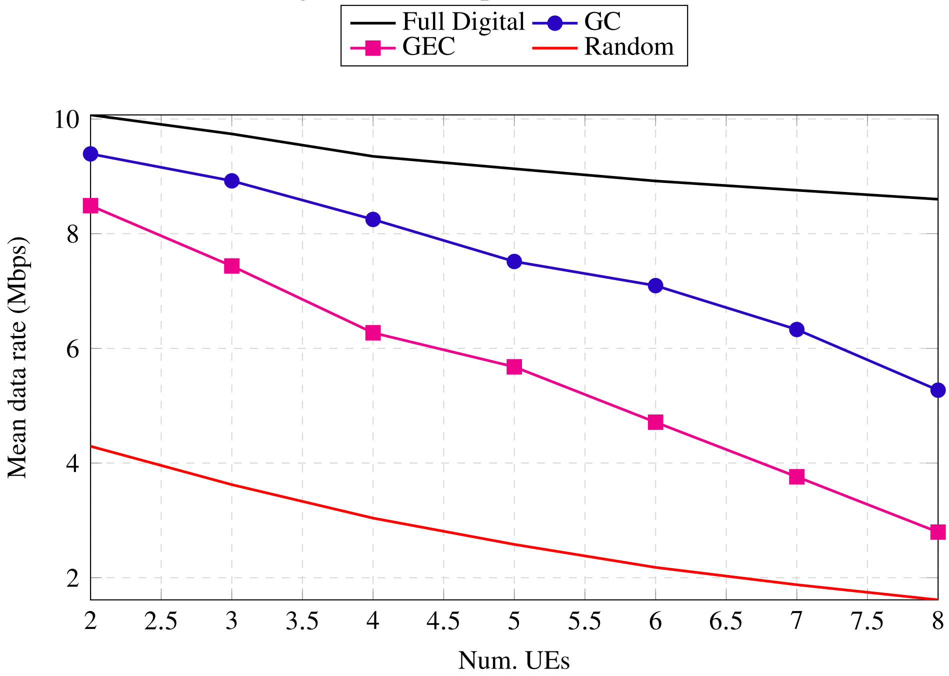

Source: Created by the author.

possible RF chain. Beside this, the power resource is divided among all UEs, which naturally reduces the received signal power. The GC solution presents better performance than the GEC. This behavior demonstrates that spatial compatibility has an impact on the system capacity and should not be neglected. In the case with 5 UEs, the GC approach reaches 37.50 Mbit/s against 28.42 Mbit/s for GEC, which represents a gain of 30%. The full digital approach reaches 45.60 Mbit/s in the case with 5 UEs, representing a loss of 21% of GC.

Figure 3.4 shows the mean user data rate considering 2 RF chains per BS when the number of UEs increases. In this result, it can be noted that the mean data rate is reduced when the number of UEs increases for all simulated algorithms. This result supports the reduction of sum data rate in Figure 3.3 when the number of UEs increases. All methods have a reduction in data rate per UE when the number of UEs increases, but this reduction is larger for the HBF methods. The reason for that is the decreased orthogonality of the channels when the number of UEs in the system increases and the reduction of transmit power per UE. The mean capacity achieves better performance for the GC solution when compared with all other hybrid beamforming algorithms. Considering the extreme case with 8 UEs, the GC approach reaches 5.27 Mbit/s, against 8.60 Mbit/s of full digital and 2.80 Mbit/s of GEC.

In Figure 3.5, the performance in terms of data rate is shown considering 6 UEs and increasing the number of RF chains per BS. It can be seen that GC still outperforms the other HBF solutions for all numbers of RF chains. We can also observe a similiar behavior as that of the sum data rate of Figure 3.5a and mean data rate of Figure 3.5b. In general, the data rate of the HBF techniques increases with the number of extra RF chains, until saturation. Although an increase in the number of analog beams at each BS also improves the degrees of freedom for the

Figure 3.5 – Sum and mean data rate in a frequency resource versus number of RF chains considering 6 UEs in the system.

(a) Sum data rate. (b) Mean data rate.

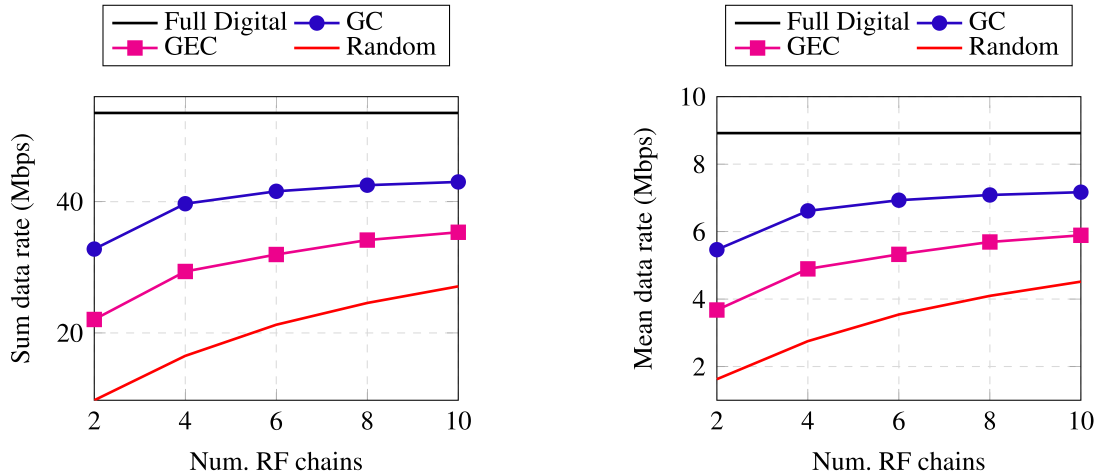

Source: Created by the author.

digital precoder, the number of beam candidates with a reasonable channel quality is limited and this saturation is expected.

In all simulations, GC outperformed GEC, demonstrating that the correlation metric has a significant effect on the simulated scenarios. Note that GC considers the orthogonality of the spaces and the channel quality to perform the analog beam allocation, which improves the ability of the digital beamforming to isolate the interfering signals.

3.5 Conclusions and future works

In this chapter, we have formulated an analog beam allocation problem in Hybrid Beamforming C-RAN networks. The presented problem considers codebook-based analog beamforming applied at the RF chains of each BS and the digital beamforming performed at the C-RAN BBU.

In general, joint analog beamforming and digital precoder optimization problems are non-convex and cannot be directly solved. Therefore, we have presented a solution decoupling the analog beam allocation, digital beamforming design, and power allocation. The focus of this work is on the analog beam allocation step, for which we evaluate a new metric that considers both channel correlation and attenuation. The metric measures the spatial orthogonality created by the analog beamforming, which can improve the interfering signal isolation performed by the digital precoder. To analyze its performance, a greedy algorithm from the literature has been adapted to the considered scenario, taking into account different beam allocation criteria.

Our results have demonstrated that the correlation criterion has a considerable influence on the simulated scenario, leading to gains when compared with the baseline approach.

The content of this chapter can be extended in some directions. In the following, some of the possible future works are pointed out:

- The greedy solution proposed is centralized and requires a large amount of information at the central entity that will solve the problem. Note that the CSI required for the digital precoder is the equivalent channel created by analog beamforming and has dimension equal to the number of RF chains. Distributed solutions for a proper beam assignment can reduce the amount of CSI reported by BSs even for JT-CoMP.
- The presented solution considers codebooks to design the analog beamforming. However, continuous analog beamforming design is expected to lead to equivalent channels that are more separable in the space. Note that analog beamforming has the constraint of constant amplitude, which makes any optimization problem hard to solve. A non-codebook-based analog beamforming design based on spatial compatibility is an interesting topic that can be investigated.

4 SPATIAL COMPATIBILITY FOR USER-BS ASSOCIATION IN HYBRID BEAMFORMING MULTI-CELL NETWORKS

In this chapter, we propose a framework to determine the UE-BS association based on second order channel statistics. In the proposed approach, the similarity of channel statistics indicates when a set of UEs are spatially compatible. This information is considered to identify high inter-cell interference situations when UEs are served by different BSs. Besides that, we propose a solution to maximize the system capacity and another one to minimize the total power in the system with minimum SINR constraints as QoS requirements.

4.1 Contributions and chapter organization

This chapter has the following main contributions:

- We propose a new framework solution where UE clustering, UE-BS association and HBF design are sequentially solved. In order to avoid inter-cell interference, the proposed framework considers that a given UE can be served by one or multiple BSs.
- The UE-BS association is made considering a UE clustering approach based on second-order channel statistics from the point of view of each BS. To the best of our knowledge, this is the first work that performs UE clustering based on channel statistics to mitigate inter-cell interference in a C-RAN network operating in mmWave frequencies.
- In the proposed framework, in order to save energy, we consider that the number of active RF chains in each BS is equal to the number of associated UEs. We provide an energy efficiency analysis of our framework considering a realistic power consumption model that takes into account the transmission power and the circuit energy of RF chains and discrete phase-shift circuits.
- For the digital beamforming part in HBF, we formulate optimization problems for maximizing system capacity and minimizing the transmission and circuit power with minimum SINR constraints. The former is solved suboptimally by adapting a successive convex approximation approach proposed in [70]. The latter corresponds to a non-convex mixed-integer problem, which is impractical to be solved using classical optimization. To handle this, we use SDR to obtain a semi-definite program (SDP). Considering that the solution of the relaxed problem is not necessarily a rank-1 matrix, we propose for such cases a new power reallocation step to be used in a Gaussian randomization method.

- We prove that the solution found to digital precoders using SDR is guaranteed to be optimal for two cooperative BSs. Furthermore, the simulation results indicate that this also applies for the considered scenario with four BSs, for which only optimal rank-1 solutions have been found.

This chapter is organized as follows. Section 4.2 describes the system model, including the network assumptions, SINR and power consumption model considered in this work. Section 4.3 presents the optimization problems for UE-BS association and HBF design. Section 4.4 describes the proposed low complexity framework solution with reduced ICSI requirements. Afterwards, Section 4.5 presents and analyzes the numerical results of the proposal. Finally, Section 4.6 enumerates the main chapter conclusions.

4.2 System model

In this work, we consider the downlink of an HBF C-RAN network. The network is composed of a set $\mathcal{M}$ of BSs, each one equipped with N antennas using HBF architecture. Let $\mathcal{K}_m$ be the set of single-antenna UEs in the system and $\mathcal{K}_m$ be the set of UEs associated with BS m. It is possible that $\mathcal{K}_m \cap \mathcal{K}_b \neq \emptyset$ for any BS $b \neq m$. Let the operator $|\cdot|$ be the cardinality of a set and let us denote $\mathcal{M}_k$ as the set of BSs serving the UE k and $|\mathcal{M}_k| = M_k$. In cases that $M_k > 1$, the UE k will receive the messages from multiple BSs in a JT-CoMP. The association of one UE with multiple BSs might improve the quality of the received signal by exploiting diversity or by suppressing the interference if the UE is placed in a high interference region.

Figure 4.1 illustrates an example of the system considered in this chapter. In the example, there are three BSs and UEs, where each UE k receives a respective message s_k. The UE 1 receives its message from BSs 1 and 2, UE 3 from BS 1 and UE 2 from all three BSs. For each combination of BSs transmitting cooperatively, we have a dedicated BBU allocated in the cloud infrastructure.

In the evaluated network, the BSs are connected to BBUs located at the cloud infrastructure. All baseband processing is performed by BBUs, including the digital precoder. However, the RF chains are placed at the BSs and they are connected to BBUs at the cloud infrastructure through a fronthaul link. Note that if multiple BSs jointly precode the same message, a baseband processing that considers the RF chains of those BSs is required. Therefore, in our scenario it is possible for one BBU to be associated with multiple BSs. To reduce the circuit power consumption of RF chains, we consider that a BS m operates with $|\mathcal{K}_m|$ RF chains, which is the minimum to guarantee that each BS can design one analog beamforming vector for each associated UE.

In the special case where all UEs receive their signal from a single BS, we have the classical multi-cell MIMO scenario. We can say that the system has multiple virtual cells represented by BBUs, which may share the same BS infrastructure.

Let the vector $\mathbf{h}_{m,k} \in \mathbb{C}^{1\times N}$ represent the downlink channel between BS m and UE k

Figure 4.1 – C-RAN system implementing cell-free concept.

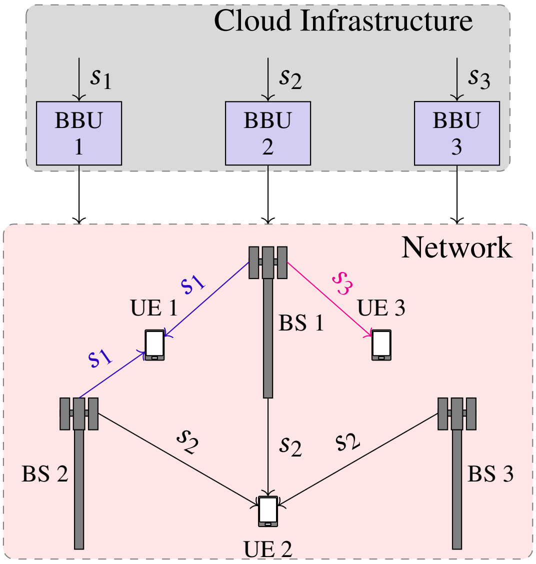

Source: Created by the author.

and let the matrix $\mathbf{F}_m \in \mathbb{C}^{N \times |\mathcal{K}_m|}$ be the analog beamforming matrix of BS m. The dimension of matrix $\mathbf{F}_m$ changes in accordance with the number of associated UEs, where we consider one active RF-chain for each UE associated with BS m. This indicates that each BS has the minimum degrees of freedom to design an analog beam for each associated UE. The small number of active RF-chains leads to a reduced complexity of the digital precoder design. The total equivalent channel to send a signal to a UE k is the concatenation of channels multiplied by the analog beamforming from BSs in $\mathcal{M}_k$.

The channel related to the transmission of a signal intended to UE b and perceived by UE k is defined as

$$\mathbf{h}_{k,b}^{\text{eq}} = \left[\mathbf{h}_{[\mathbf{m}]_1,k} \mathbf{F}_{[\mathbf{m}]_1} \cdots \mathbf{h}_{[\mathbf{m}]_{M_b},k} \mathbf{F}_{[\mathbf{m}]_{M_b}} \right]_{\mathbf{m}=(\mathcal{M}_b)^+}, \tag{4.1}$$

with $\mathbf{h}_{k,b}^{\text{eq}} \in \mathbb{C}^{1 \times \sum_{m \in \mathcal{M}_b} |\mathcal{K}_m|}$, where $\mathbf{m}$ is a vector created by the operator $(\mathcal{M}_b)^+$, which represents the sorting of elements from the set $\mathcal{M}_b$ in ascending order, and $[\cdot]_i$ is the i^{th} element of vector $\mathbf{m}$. If $b = k$, the equivalent channel $\mathbf{h}_{k,b}^{\text{eq}}$ is the intended channel.

Since the dimension of (4.1) created by the analog beamforming varies with the number of UE-BS associations, the dimensions of the digital precoder should vary in accordance.

Let the vector $\mathbf{w}_{m,k} \in \mathbb{C}^{|\mathcal{K}_m| \times 1}$ be the digital precoder used by BS $m \in \mathcal{M}_k$ to transmit a signal to UE k. If a UE k receives signals jointly precoded from multiple BSs, the effective digital precoder to be considered is the concatenation of the beamformers of all BSs in $\mathcal{M}_k$. Therefore, in this work we consider the concatenation of digital precoders of a UE k given by

$$\mathbf{w}_k = \left[\mathbf{w}_{[\mathbf{m}]_1,k}^{\text{T}} \cdots \mathbf{w}_{[\mathbf{m}]_{M_k},k}^{\text{T}} \right]_{\mathbf{m}=(\mathcal{M}_k)^+}^{\text{T}}, \tag{4.2}$$

with $\mathbf{w}_k \in \mathbb{C}^{\left(\sum_{m \in \mathcal{M}_k} |\mathcal{K}_m|\right) \times 1}$.

The signal received by UE k is defined as

$$y_k = \mathbf{h}^{\text{eq}}_{k,k}\mathbf{w}_k s_k + \sum_{\substack{b\in\mathcal{K}\\ b\neq k}} \mathbf{h}^{\text{eq}}_{k,b}\mathbf{w}_b s_b + n_k, \tag{4.3}$$

where s_k is the message to be sent to UE k and $n_k \sim \mathcal{CN}(0,\sigma^2)$ denotes the additive noise with zero mean and variance σ^2. The SINR of UE k, assuming that the symbols have unit variance, is defined as

$$\gamma_k = \frac{\left|\mathbf{h}^{\text{eq}}_{k,k}\mathbf{w}_k\right|^2}{\sum\limits_{\substack{b\in\mathcal{K}\\ b\neq k}} \left|\mathbf{h}^{\text{eq}}_{k,b}\mathbf{w}_b\right|^2 + \sigma^2}. \tag{4.4}$$

4.2.1 Power consumption model

In this work, we consider an adaptation of the power consumption model presented in [71] for the fully connected phase-shifter architecture, where the power consumption for a given BS m is

$$p_m = p_m^{\text{TX}} + p^{\text{RF}}|\mathcal{K}_m| + p^{\text{PS}}|\mathcal{K}_m|N + p^{\text{BB}}, \tag{4.5}$$

where p_m^{TX} is the transmit power of BS m, p^{RF} is the power consumed by an RF chain circuit, p^{PS} is the power consumed by the phase-shifter circuit of BS m and p^{BB} is the baseband processing power. Note that the power consumption of RF chains and phase-shift circuits depends on the number of active RF chains. Therefore, the assumption of just one RF chain per UE keeps the system operating with the minimum number of RF chains required to serve all UEs.

The model in (4.5) represents the power consumption of one BS where the baseband processing is performed locally. In our scenario, however, the baseband processing is performed at the cloud and we can have more baseband units than BSs in the system. As a consequence, the baseband processing power does not consume energy of BSs. Since in this work we focus on the BS energy consumption, the baseband power component will be dropped from the model. The total power consumption in the system is then given by

$$p^{\text{tot}} = \sum_{m\in\mathcal{M}} \left(p_m^{\text{TX}} + p^{\text{RF}}|\mathcal{K}_m| + p^{\text{PS}}|\mathcal{K}_m|N\right). \tag{4.6}$$

4.3 UE-BS association and hybrid beamforming design

In this chapter, we consider two optimization problems: weighted sum-capacity maximization and power minimization with SINR constraints.

For simplicity, let us define the set of analog beamformers as $\mathcal{F} \triangleq \{\mathbf{F}_m\}_{m\in\mathcal{M}}$ and digital precoders as $\mathcal{W} \triangleq \{\mathbf{w}_k\}_{k\in\mathcal{K}}$, where $\triangleq$ represents equality by definition. The weight a_k is the priority of UE k defined by the system scheduler. Considering the power transmission budget of each BS as $p^{\max}$, the weighted sum-capacity problem is expressed as

$$\max_{\substack{\mathcal{K}_m,\,\mathcal{F},\,\mathcal{W}\\ \forall m}} \quad \sum_{k=1}^{|\mathcal{K}|} a_k \log_2\left(1+\frac{\left|\mathbf{h}_{k,k}^{\mathrm{eq}}\mathbf{w}_k\right|^2}{\sum_{\substack{b\in\mathcal{K}\\ b\neq k}}\left|\mathbf{h}_{k,b}^{\mathrm{eq}}\mathbf{w}_b\right|^2+\sigma^2}\right), \tag{4.7a}$$

$$\text{s.t.} \quad \bigcup_{m=1}^{M}\mathcal{K}_m=\mathcal{K}, \tag{4.7b}$$

$$\sum_{k\in\mathcal{K}_m}\mathbf{w}_{m,k}^{\mathrm{H}}\mathbf{F}_m^{\mathrm{H}}\mathbf{F}_m\mathbf{w}_{m,k}\leq p^{\max}, \quad \forall m\in\mathcal{M}, \tag{4.7c}$$

$$|\mathbf{F}_m|=\frac{1}{\sqrt{N}}\mathbf{1}_{N\times|\mathcal{K}_m|}, \quad \forall m\in\mathcal{M}, \tag{4.7d}$$

where $\mathbf{1}$ is a matrix of ones with appropriate dimensions.

The objective function of problem (4.7) is the sum weighted capacity of the system. The variables are UE-BS association, represented by the sets $\mathcal{K}_m$, BS analog precoders and digital precoders. The constraints (4.7b) and (4.7c) guarantee that all UEs will be associated with at least one BS and that no individual BS will exceed the transmission power budget $p^{\max}$, respectively. Constraint (4.7d) guarantees that the analog beamformer elements are composed only by phase-shifters.

Also in this work, we consider a power minimization problem with minimum SINR constraints formulated as

$$\min_{\substack{\mathcal{K}_m,\,\mathcal{F},\,\mathcal{W}\\ \forall m}} \sum_{m=1}^{M}\left(p^{\mathrm{RF}}|\mathcal{K}_m|+p^{\mathrm{PS}}N|\mathcal{K}_m|+\sum_{k\in\mathcal{K}_m}\|\mathbf{F}_m\mathbf{w}_{m,k}\|^2\right), \tag{4.8a}$$

$$\text{s.t.} \quad \bigcup_{m=1}^{M}\mathcal{K}_m=\mathcal{K}, \tag{4.8b}$$

$$\frac{\left|\mathbf{h}_{k,k}^{\mathrm{eq}}\mathbf{w}_k\right|^2}{\sum_{\substack{b\in\mathcal{K}\\ b\neq k}}\left|\mathbf{h}_{k,b}^{\mathrm{eq}}\mathbf{w}_b\right|^2+\sigma^2}\geq r_k, \quad \forall k\in\mathcal{K}, \tag{4.8c}$$

$$\sum_{k\in\mathcal{K}_m}\mathbf{w}_{m,k}^{\mathrm{H}}\mathbf{F}_m^{\mathrm{H}}\mathbf{F}_m\mathbf{w}_{m,k}\leq p^{\max}, \quad \forall m\in\mathcal{M}, \tag{4.8d}$$

$$|\mathbf{F}_m|=\frac{1}{\sqrt{N}}\mathbf{1}_{N\times|\mathcal{K}_m|}, \quad \forall m\in\mathcal{M}, \tag{4.8e}$$

where the objective function is the minimization of the sum transmission power of BSs and circuit power. Note that the circuit power consumption grows with the number of UEs associated with BSs. The set of constraints is the same from problem (4.7) with the addition of constraint (4.8c), which guarantees a minimum SINR r_k for each UE.

Problems (4.7) and (4.8) are difficult to be solved due to the non-convexity of constraints (4.7d), (4.8c) and the objective function (4.7a). Furthermore, the sets $\mathcal{K}_m$ represent combinatorial variables, which make it impossible to use classical non-convex optimization solutions. In terms of practical applicability both problems require ICSI, which is a difficult requirement for massive-MIMO, and even more significant if the cloud needs to receive this ICSI.

4.4 Low-complexity solution

Given the huge ICSI requirements of channel matrices and non-convexity of problems (4.7) and (4.8), we propose a low-complexity framework with reduced ICSI requirements. In the framework, we split our solution into different parts, which are based on the second-order statistics and ICSI, as illustrated in Figure 4.2.

Steps based on second-order statistic find a solution for UE-BS association variables $\mathcal{K}_m$ and analog beamforming matrices $\mathbf{F}_m$, while digital precoders $\mathbf{w}_k$ are based on ICSI. Note that the analog beamforming $\mathbf{F}_m$ has larger dimension than digital precoder and can be updated in a long time interval. Therefore, the ICSI considered for the digital precoder part is the channel perceived through the analog beamforming, i.e., the equivalent channel defined in (4.1), which has dimension equal to the number of active RF chains.

Figure 4.2 – Steps of the proposed framework solution.

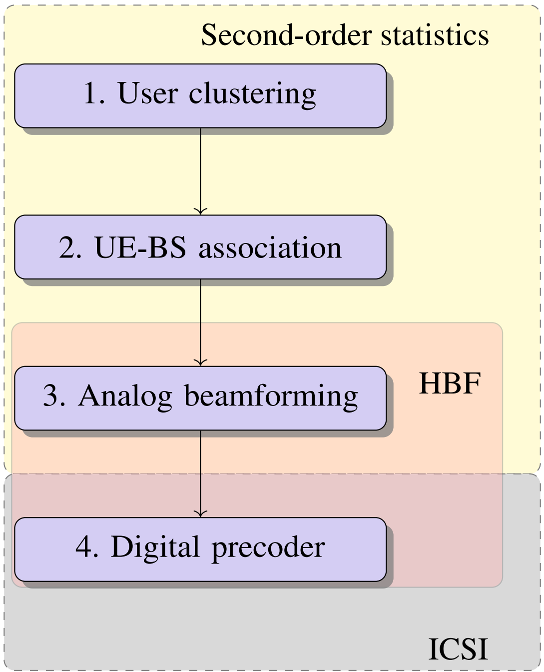

Source: Created by the author.

The first step is the UE clustering, that aims to group UEs that have correlated channels from the point of view of each BS. This can be determined by evaluating the similarity of second-order statistics. This indicates that if the BSs which have performed the clustering transmit a signal to one of the UEs in a cluster, the signal will fall in a well-correlated channel subspace of other UEs inside the same cluster. The idea is to associate entire clusters of UEs with BSs. In this way, the assignment of UEs to BSs (step 2 of the framework) will prevent UEs with similar subspaces from being served by different BSs, thus isolating the inter-cell interference.

In the UE-BS step, we consider a greedy algorithm that takes into account the Frobenious norm of correlation matrices of UEs in the cluster. The idea is to quantify the mean channel power of UEs in a given cluster in order to associate it with the BS that will provide the best overall received signal.

After UE clustering and UE-BS association, each BS will design an analog beamforming based on the covariance of intended channels (step 3 of the framework). Due to the UE-BS association based on clustering, the interfering channel space from different BSs will be as orthogonal as possible. This step will facilitate the task of the digital precoder to isolate the interference, since all interfering signals from other BSs will fall into an orthogonal channel space. Therefore, in our solution we design the analog beamforming with the purpose of improving the channel quality of the intended UEs. This step will reduce the effective channel dimension for the digital precoder step.

Finally, the digital precoder is designed considering the ICSI of the equivalent channel in (4.1) after the analog beamforming. The digital precoder is performed by the BBUs at the cloud infrastructure and the equivalent channel will reduce significantly the instantaneous CSI reported from BSs. At this point, the framework tries to find the best solution for the objective functions of problems (4.7) or (4.8).

4.4.1 User clustering

The first part of our framework solution is the UE clustering, which will be later used in the UE-BS association step. The clustering aims to group UEs with similar channel statistics, which indicates that their signals are received in a similar space. Therefore, we will separate the UEs into groups which will cause significant interference in each other. In this work, we consider that the channel statistics are collected by the BSs independently.

The covariance matrix for a BS m and a UE k can be approximated from the channel samples as

$$\tilde{\mathbf{R}}_{k,m} = \frac{1}{T}\sum_{t=1}^{T}\left(\mathbf{h}_{m,k}^{(t)}\right)^{\mathrm{H}}\mathbf{h}_{m,k}^{(t)}, \tag{4.9}$$

where $\mathbf{h}_{m,k}^{(t)}$ is the channel between BS m and UE k at the t-th channel sample and T is the total number of samples. The covariance matrix approximated by (4.9) will be equal to the real covariance matrix when $T \to \infty$.

In this work, we consider the K-means algorithm, which is a well-known solution of partitioning observations into clusters with the nearest mean [72]. As input for K-means, we consider the eigenvector $\mathbf{v}_{k,m}$ relative to the strongest eigenvalue from the covariance matrix in (4.9), which represents the subspace with the best signal reception.

The algorithm determines the cluster of UEs based on the similarity of their eigenvectors, calculated by means of the Euclidean distance, as considered in [73]. The number of desired clusters is an input of the algorithm. The methods to determine the optimal number of clusters, however, are not the focus of this work.

The idea is not to associate UEs with BSs independently, but associate entire clusters of UEs with BSs. In this way, the assignment of UEs to BSs can be made avoiding UEs with similar subspace be served by different BSs. This solution will reduce situations with large interference among signals from different BSs. Furthermore, the cluster based association will make it possible that all correlated channel subspaces be used as useful subspace instead of interfering subspace. After the clustering solution step, we have UE clustering solutions for each BS.

In other words, our solution aims to avoid high interference in an HBF multi-cell network. Despite this, our solution also creates a good orthogonality between the intended and interfering channels using clustering solution for UE-BS association.

In general, the clustering solutions of different BSs are similar due to the geographical position of UEs, which has influence on the angle of arrival (AoA) and other channel parameters. However, it is possible to have different cluster solutions in different BSs due to the antenna array position and different UE-BS distances.

4.4.2 UE-BS association

After the clustering solution step, we have UE clustering solutions for each BS. The idea of our UE-BS assignment solution is to always assign UEs from the same cluster to one BS, thus avoiding that the transmission from another BS falls into a highly correlated subspace. In other words, we aim to orthogonalize as much as possible the intended and interfering channels by using the clustering solution for UE-BS association.

Let $C_{m,c}$ represent a cluster solution c found by BS m, where c is the cluster index. If the clustering solutions of all BSs are equal, it is possible for each BS to transmit in an uncorrelated channel subspace reducing inter-cell interference. As example, let us consider the following clustering solutions found by two BSs: $C_{1,1} = \{1, 2\}$, $C_{1,2} = \{3, 4\}$, $C_{2,1} = \{1, 2\}$ and $C_{2,2} = \{3, 4\}$. Note that if BS 1 transmits to UEs 1 and 2, while BS 2 transmits to UEs 3 and 4, the inter-cell interfering channels are uncorrelated.

On the other hand, if the clustering solutions of some BSs are different, it could be impossible to guarantee that two or more BSs transmit in an almost uncorrelated channel subspace. As example, let us consider the following clustering solutions found by two BSs: $C_{1,1} = \{1, 2, 3\}$, $C_{1,2} = \{4\}$, $C_{2,1} = \{1\}$ and $C_{2,2} = \{2, 3, 4\}$. Note that it is impossible to find a UE-BS association solution using both BSs to serve all UEs without transmiting in an almost correlated subspace of another BS. If all UEs are uniquely associated with the same BS, the network will waste half of the transmit power resources. On the other hand, if all UEs are associated with all BSs, the amount of active RF chains will increase, thus increasing the circuit energy consumption. The association which reduces the cluster intersection while still satisfying (4.7b) is to assign UEs 1, 2 and 3 to BS 1 and UEs 3 and 4 to BS 2. Considering this solution, UE 3 will have a strong subspace correlation with channels of some UEs in both BSs. However, by associating UE 3 with both BSs, the interference could be controlled by the digital precoder.

In addition to clusters found by each BS, we consider a metric to evaluate the mean channel quality of UEs within the cluster to decide on the UE-BS association. For this, let the quality of a given cluster from BS m be given by $g_{m,c} = \|\overline{\mathbf{R}}_{m,c}\|_F^2$, where $\overline{\mathbf{R}}_{m,c} = \frac{1}{|C_{m,c}|}\sum_{k\in C_{m,c}} \tilde{\mathbf{R}}_{m,k}$. High values of $g_{m,c}$ indicate that the UEs in cluster c of BS m have high channel power in average. The goal of our proposal is to associate, in a greedy way, clusters of UEs with the BSs considering the values of $g_{m,c}$. Algorithm 4.1 summarizes the UE-BS assignment approach.

Algorithm 4.1 UE-BS association algorithm

1: Define the set of assigned UEs as $\mathcal{K}^* = \emptyset$
2: Define the sets $\mathcal{K}_m = \emptyset, \quad \forall m$, and $\mathcal{M}_k = \emptyset, \quad \forall k$
3: Define C_m as the set of clusters from BS m
4: **while** $\mathcal{M}_k = \emptyset$ for any k **do**
5: Select the BS-cluster pair such that $(m^*, c^*) = \underset{m\in\mathcal{M},\ c\in C_m}{\arg\max}\ g_{m,c}$, where $c^* \in C_{m^*}$
6: **if** $|C_{m^*,c^*} \cap \mathcal{K}^*| < |C_{m^*,c^*}|$ **then**
7: $\mathcal{K}^* = \mathcal{K}^* \cup C_{m^*,c^*}$ and $\mathcal{K}_{m^*} = \mathcal{K}_{m^*} \cup C_{m^*,c^*}$
8: $\mathcal{M}_k = \mathcal{M}_k \cup \{m^*\}\ \forall k \in C_{m^*,c^*}$
9: **end if**
10: $C_{m^*} = C_{m^*} \setminus \{c^*\}$
11: **end while**

In line 1, the set $\mathcal{K}^*$ of UEs to be associated with BSs is defined as empty. In line 2 the associated UEs set $\mathcal{K}_m\ \forall m$ and associated BSs set $\mathcal{M}_k\ \forall k$ are defined as empty sets. Lines 4 to 11 correspond to a loop, where in each iteration the pair BS m^* and cluster c^* with the largest $g_{m,c}$ is selected. If there is at least one non-served UE in C_{m^*,c^*}, all UEs in the selected set are associated with BS m^*. In this way, UEs in C_{m^*,c^*} already associated with another BS will be served by more than one BS.

4.4.3 Analog beamforming

After defining the UE-BS association, we have to handle the analog beamforming and digital precoder design. Similarly to the UE clustering, we consider the second order statistics to design the analog beamforming in order to reduce the ICSI requirements for the digital precoder step. In this work, we consider two methods to perform the analog beamforming design, which are described as follows:

4.4.3.1 Codebook based

Let Q be the codebook and $\mathbf{f}_q \in \mathbb{C}^{N\times 1}$ a codeword that can be placed in one of the analog beamforming matrix columns. The idea of this approach is to associate codewords from Q that guarantee a good channel quality for the intended UEs. Algorithm 4.2 summarizes the codeword allocation performed by each BS.

Algorithm 4.2 Codeword allocation for a BS m

1: Define the set of UEs to receive a codeword $\mathcal{K}^* = \mathcal{K}_m$
2: Define the analog beamforming matrix $\mathbf{F}_m$ as an empty matrix
3: **while** $\mathcal{K}^* \neq \emptyset$ **do**
4: Select a UE and codeword such that $(k^*, \mathbf{f}_{q^*}) = \underset{k\in\mathcal{K}^*,\ \mathbf{f}_q\in\mathcal{Q}}{\arg\max}\ ||\tilde{\mathbf{R}}_{m,k}\mathbf{f}_q||^2$
5: Concatenate the selected codeword with the analog beamforming matrix $\mathbf{F}_m = \left[\mathbf{F}_m,\ \mathbf{f}_{q^*}\right]$
6: Update the sets $\mathcal{K}^* = \mathcal{K}^* \setminus \{k^*\}$ and $\mathcal{Q} = \mathcal{Q} \setminus \left\{\mathbf{f}_{q^*}\right\}$
7: **end while**

In each loop of the algorithm, the pair (UE k^*, codeword $\mathbf{f}_{q^*}$) with the largest $||\tilde{\mathbf{R}}_{m,k}\mathbf{f}_q||^2$ is selected and the codeword is concatenated with the current analog beamforming matrix $\mathbf{F}_m$. At the end of each iteration, the selected k^* is removed from the possible choices in order to prevent k^* from being selected in the next iterations. Also, the codeword $\mathbf{f}_{q^*}$ is removed from the possibilities in order to ensure that all columns of $\mathbf{F}_m$ will be different, thus providing the minimum degrees of freedom for the digital precoder step.

4.4.3.2 Eigenvector approximation

In this method, we define the analog beamforming $\mathbf{F}_m \in \mathbb{C}^{N\times|\mathcal{K}_m|}$ based on the dominant eigenvector $\mathbf{v}_{m,k}$ of the covariance matrix $\tilde{\mathbf{R}}_{m,k}$ in (4.9) for each UE $k \in \mathcal{K}_m$. The goal is to design the analog beamforming as close as possible to the best subspace of each UE without the codebook limitation. However, due to constraint (4.7d) we have to find a feasible phase-shift vector with minimum distance to the eigenvector. The optimal solution can be found by considering the phase-shift of the eigenvector [74]. Therefore, the analog beamforming matrix for the eigenvector approximation can be defined as

$$\mathbf{F}_m = \frac{1}{\sqrt{N}}\left[e^{j\angle\mathbf{v}_{[\mathbf{k}]_1,m}},\ \ldots,\ e^{j\angle\mathbf{v}_{[\mathbf{k}]_{|\mathcal{K}_m|},m}}\right]_{\mathbf{k}=(\mathcal{K}_m)^+}. \tag{4.10}$$

4.4.4 Digital precoder

Finally, we present two methods to calculate the digital precoders: weighted sum-capacity and power minimization with SINR constraints. The former aims to maximize the total system capacity without any QoS constraint. Since the objective function is not convex, we consider a SCA method to find a feasible solution. The second method, on the other hand, aims to reduce the transmission power while guaranteeing a required SINR for each UE. To solve this problem we consider an approach based on semi-definite relaxation (SDR).

4.4.4.1 Weighted sum-capacity

After the UE-BS association and analog beamforming steps, the weighted sum-capacity problem considering the fixed UE-BS association $\mathcal{K}_m$ and analog beamforming $\mathbf{f}_m$ can be reformulated as

$$\max_{\mathcal{W}} \quad \sum_{k\in\mathcal{K}} a_k \log_2\left(1+\frac{\left|\mathbf{h}_{k,k}^{\mathrm{eq}}\mathbf{w}_k\right|^2}{\sum_{\substack{b\in\mathcal{K}\\ b\neq k}}\left|\mathbf{h}_{k,b}^{\mathrm{eq}}\mathbf{w}_b\right|^2+\sigma^2}\right), \tag{4.11a}$$

$$\text{s.t.} \sum_{k\in\mathcal{K}_m} \mathbf{w}_{m,k}^{\mathrm{H}}\mathbf{F}_m^{\mathrm{H}}\mathbf{F}_m\mathbf{w}_{m,k} \leq p^{\max}, \quad \forall m\in\mathcal{M}, \tag{4.11b}$$

The objective function in (4.11a) is still non-convex. To deal with this problem, we perform a successive convex approximation based on the lower bound of the capacity function, as considered in [70], which is defined as:

$$\log_2\left(1+\frac{\left|\mathbf{h}_{k,k}^{\mathrm{eq}}\mathbf{w}_k\right|^2}{\sum_{\substack{b\in\mathcal{K}\\ b\neq k}}\left|\mathbf{h}_{k,b}^{\mathrm{eq}}\mathbf{w}_b\right|^2+\sigma^2}\right) \geq \frac{1}{\ln 2}\left(\ln j_k - j_k e_k\left(\mathcal{W},u_k\right)+1\right), \tag{4.12}$$

where $j_k \geq 0$ and u_k are arbitrary values and $e_k\left(\mathcal{W},u_k\right)$ is the mean squared error function defined as

$$e_k(\mathcal{W},u_k) = |1-u_k^*\mathbf{h}_{k,k}^{\mathrm{eq}}\mathbf{w}_k|^2 + |u_k|^2\left(\sum_{\substack{b\in\mathcal{K}\\ b\neq k}}|\mathbf{h}_{k,b}^{\mathrm{eq}}\mathbf{w}_b|^2+\sigma^2\right). \tag{4.13}$$

The equality in (4.12) is reached, according to [70], when u_k and j_k are

$$u_k = \left(|\mathbf{h}_{k,k}^{\mathrm{eq}}\mathbf{w}_k|^2 + \sum_{\substack{b\in\mathcal{K}\\ b\neq k}}|\mathbf{h}_{k,b}^{\mathrm{eq}}\mathbf{w}_b|^2+\sigma^2\right)\mathbf{h}_k^{\mathrm{eq}}\mathbf{w}_k, \tag{4.14}$$

$$j_k = (e_k(\mathcal{W},u_k))^{-1}. \tag{4.15}$$

Considering the defined lower capacity bound in (4.12), the corresponding optimization problem can be formulated as:

$$\max_{\mathcal{W},\,\mathcal{U},\,\mathcal{J}} \quad \sum_{k\in\mathcal{K}} a_k\left(\ln j_k - j_k e_k\left(\mathcal{W},u_k\right)+1\right), \tag{4.16}$$

$$\text{s.t.} \quad \text{(4.11b)},$$

where $\mathcal{U} \triangleq \{u_k\}_{k\in\mathcal{K}}$ and $\mathcal{J} \triangleq \{j_k\}_{k\in\mathcal{K}}$. The objective function in (4.16) is still not convex for $\mathcal{W}$, $\mathcal{U}$ and $\mathcal{J}$, however, it is convex in $\mathcal{W}$ if we consider $\mathcal{U}$ and $\mathcal{J}$ fixed. Therefore, we consider an iterative algorithm where $\mathcal{W}$, $\mathcal{U}$ and $\mathcal{J}$ are updated sequentially, creating a successive iterative approximation. The complete procedure is described in Algorithm 4.3.

The SCA in Algorithm 4.3 is an adaptation of the solution proposed in [70] for a beamforming and fronthaul quantization problem, and its convergence is proved in [75].

4.4.4.2 Power minimization with minimum SINR constraints

In problem (4.8), the objective function is the minimization of the transmission power and circuit power. Notice that the circuit power components in (4.8a) are determined by

Algorithm 4.3 Centralized solution for weighted sum-capacity using SCA

1: Initialize the digital precoders $\mathcal{W}$ with one feasible solution which meets constraints (4.11b).
2: Update $\mathcal{J}$ considering the initial $\mathcal{W}$.
3: **repeat**
4: Update $\mathcal{U}$ using (4.14) considering current $\mathcal{W}$ and $\mathcal{J}$
5: Update $\mathcal{J}$ using (4.15) considering current $\mathcal{W}$ and $\mathcal{U}$
6: Update $\mathcal{W}$ by solving (4.16) considering $\mathcal{U}$ and $\mathcal{J}$ fixed
7: **until** convergence criterion is met

UE-BS association. Hence, after fixing variables $\mathcal{K}_m$ and $\mathbf{F}_m$, the power minimization problem for calculating the digital precoder can be formulated as

$$\min_{\mathcal{W}} \sum_{m\in\mathcal{M}} \sum_{k\in\mathcal{K}_m} ||\mathbf{F}_m \mathbf{w}_{m,k}||^2, \tag{4.17a}$$

$$\text{s.t.} \quad \frac{\left|\mathbf{h}^{\text{eq}}_{k,k}\mathbf{w}_k\right|^2}{\sum_{\substack{b\in\mathcal{K}\\ b\neq k}} \left|\mathbf{h}^{\text{eq}}_{k,b}\mathbf{w}_b\right|^2 + \sigma^2} \geq r_k, \quad \forall k \in \mathcal{K}, \tag{4.17b}$$

$$\sum_{k\in\mathcal{K}_m} \mathbf{w}^{\text{H}}_{m,k}\mathbf{F}^{\text{H}}_m\mathbf{F}_m\mathbf{w}_{m,k}, \leq p^{\max} \quad \forall m \in \mathcal{M}. \tag{4.17c}$$

Notice that the problem is still non-convex due to the QoS constraint (4.17b). However, we can find sub-optimal solutions using SDR. Towards this end, let us replace the digital precoder vector variable $\mathbf{w}_k$ by a matrix defined as $\left\{\mathbf{W}_k = \mathbf{w}_k\mathbf{w}^{\text{H}}_k\right\}_{k=1}^{K}$. Note that we can find an optimal precoder vector $\mathbf{w}_k$ from $\mathbf{W}_k$ if and only if $\mathbf{W}_k \succeq 0$ and $\text{rank}\left(\mathbf{W}_k\right) = 1$. Similarly, let us consider the equivalent channel as a matrix defined as $\mathbf{H}^{\text{eq}}_{k,b} = \left(\mathbf{h}^{\text{eq}}_{k,b}\right)^{\text{H}}\mathbf{h}^{\text{eq}}_{k,b}$. Considering trace properties, we can define the signal power received at a UE k relative to the transmission intended to a UE b as

$$|\mathbf{h}^{\text{eq}}_{k,b}\mathbf{w}_b|^2 = \text{tr}\left(\mathbf{w}^{\text{H}}_b\left(\mathbf{h}^{\text{eq}}_{k,b}\right)^{\text{H}}\mathbf{h}^{\text{eq}}_{k,b}\mathbf{w}_b\right) = \text{tr}\left(\left(\mathbf{h}^{\text{eq}}_{k,b}\right)^{\text{H}}\mathbf{h}^{\text{eq}}_{k,b}\mathbf{w}_b\mathbf{w}^{\text{H}}_b\right) = \text{tr}\left(\mathbf{H}^{\text{eq}}_{k,b}\mathbf{W}_b\right). \tag{4.18}$$

Note that we need to isolate the BS digital precoder components in order to formulate the power constraint using the new variable $\mathbf{W}_k$. Therefore, let us define $\mathbf{W}_{m,k} = \mathbf{w}_{m,k}\mathbf{w}^{\text{H}}_{m,k}$. Note that matrix $\mathbf{W}_k$ contains the cross component $\mathbf{w}_{m,k}\mathbf{w}^{\text{H}}_{p,k}$ where $m, p \in \mathcal{M}_k$ and the complete matrix is given by

$$\mathbf{W}_k = \begin{bmatrix} \mathbf{W}_{[\mathbf{m}]_1,k} & \cdots & \mathbf{w}_{[\mathbf{m}]_1,k}\mathbf{w}^{\text{H}}_{[\mathbf{m}]_{M_k},k} \\ \mathbf{w}_{[\mathbf{m}]_2,k}\mathbf{w}^{\text{H}}_{[\mathbf{m}]_1,k} & \cdots & \mathbf{w}_{[\mathbf{m}]_2,k}\mathbf{w}^{\text{H}}_{[\mathbf{m}]_{M_k},k} \\ \vdots & \ddots & \vdots \\ \mathbf{w}_{[\mathbf{m}]_{M_k},k}\mathbf{w}^{\text{H}}_{[\mathbf{m}]_1,k} & \cdots & \mathbf{W}_{[\mathbf{m}]_{M_k},k} \end{bmatrix}_{\mathbf{m}=(\mathcal{M}_k)^+}. \tag{4.19}$$

The matrices $\mathbf{W}_{m,k}$ are blocks placed in the diagonal of block matrix $\mathbf{W}_k$. From $\mathbf{B}_{m,k} \in \mathbb{B}^{(\sum_{p\in\mathcal{M}_k}|\mathcal{K}_p|)\times|\mathcal{K}_m|}$, where we can isolate the block of BS m by $\mathbf{B}_{m,k} = \mathbf{B}^{\text{H}}_{m,k}\mathbf{W}_k\mathbf{B}_{m,k}$. If a

UE k is associated with a given BS m, the matrix $\mathbf{B}_{m,k}$ is defined as

$$\mathbf{B}_{m,k} = \begin{bmatrix} \mathbf{0}_{|\mathcal{K}_{[\mathbf{m}]_1}|\times|\mathcal{K}_m|} \\ \vdots \\ \mathbf{0}_{|\mathcal{K}_{[\mathbf{m}]_{i-1}}|\times|\mathcal{K}_m|} \\ \mathbf{I}_{|\mathcal{K}_m|} \\ \mathbf{0}_{|\mathcal{K}_{[\mathbf{m}]_{i+1}}|\times|\mathcal{K}_m|} \\ \vdots \\ \mathbf{0}_{|\mathcal{K}_{[\mathbf{m}]_{M_k}}|\times|\mathcal{K}_m|} \end{bmatrix}_{\mathbf{m}=(\mathcal{M}_k)^+,\, [\mathbf{m}]_i=m}, \tag{4.20}$$

where $\mathbf{I}_{|\mathcal{K}_m|}$ is an identity matrix, $\mathbf{0}$ is a matrix filled with zeros of appropriate dimensions and i is the index indicating the position of m within vector $\mathbf{m}$. If a UE k is not associated with a given BS m, then $\mathbf{B}_{m,k} = \mathbf{0}_{(\sum_{p\in\mathcal{M}_k}|\mathcal{K}_p|)\times|\mathcal{K}_m|}$.

Therefore, the SDP equivalent problem for (4.17) can be formulated as:

$$\min_{\mathcal{W}} \sum_{m\in\mathcal{M}}\sum_{k\in\mathcal{K}_m} \operatorname{tr}\left(\mathbf{B}_{m,k}\mathbf{F}_m^{\mathrm{H}}\mathbf{F}_m\mathbf{B}_{m,k}^{\mathrm{H}}\mathbf{W}_k\right), \tag{4.21a}$$

$$\text{s.t. } \operatorname{tr}\left(\mathbf{H}_{k,k}^{\mathrm{eq}}\mathbf{W}_k\right) \geq r_k \sum_{\substack{b\in\mathcal{K}\\ b\neq k}} \operatorname{tr}\left(\mathbf{H}_{k,b}^{\mathrm{eq}}\mathbf{W}_b\right) + r_k\sigma^2, \quad \forall k\in\mathcal{K}, \tag{4.21b}$$

$$\sum_{k\in\mathcal{K}_m} \operatorname{tr}\left(\mathbf{B}_{m,k}\mathbf{F}_m^{\mathrm{H}}\mathbf{F}_m\mathbf{B}_{m,k}^{\mathrm{H}}\mathbf{W}_k\right) \leq p^{\max}, \quad \forall m\in\mathcal{M}, \tag{4.21c}$$

$$\operatorname{rank}(\mathbf{W}_k) = 1, \quad \forall k\in\mathcal{K}. \tag{4.21d}$$

The problems (4.17) and (4.21) are equivalent, with problem (4.21) also being difficult to solve, due to the non-convex rank constraint (4.21d).

By dropping the rank constraint (4.21d) we obtain an SDR of problem (4.17) formulated as:

$$\min_{\mathcal{W}} \sum_{m\in\mathcal{M}}\sum_{k\in\mathcal{K}_m} \operatorname{tr}\left(\mathbf{B}_{m,k}\mathbf{F}_m^{\mathrm{H}}\mathbf{F}_m\mathbf{B}_{m,k}^{\mathrm{H}}\mathbf{W}_k\right), \tag{4.22a}$$

$$\text{s.t. } \operatorname{tr}\left(\mathbf{H}_{k,k}^{\mathrm{eq}}\mathbf{W}_k\right) \geq r_k \sum_{\substack{b\in\mathcal{K}\\ b\neq k}} \operatorname{tr}\left(\mathbf{H}_{k,b}^{\mathrm{eq}}\mathbf{W}_b\right) + r_k\sigma^2, \quad \forall k\in\mathcal{K}, \tag{4.22b}$$

$$\sum_{k\in\mathcal{K}_m} \operatorname{tr}\left(\mathbf{B}_{m,k}\mathbf{F}_m^{\mathrm{H}}\mathbf{F}_m\mathbf{B}_{m,k}^{\mathrm{H}}\mathbf{W}_k\right) \leq p^{\max}, \quad \forall m\in\mathcal{M}. \tag{4.22c}$$

Note that problem (4.22) is a standard SDP, which can be solved using interior point methods [76]. However, due to relaxation, the solution of problem (4.22) might not have rank-1 matrices, and thus might not represent a feasible solution for problem (4.21). We prove in Appendix A that for the particular case in which $r_k > 0\ \forall k$ and $M \leq 2$, there is always a rank-1 solution for (4.22).

For scenarios where a rank-1 solution cannot be found, a rank-1 approximation can be determined using a randomization method, as demonstrated in [77]. In this method, sets of digital precoder candidates $\mathbf{W}_k$ are generated from the optimal solution matrices. For problem (4.22), we present the Gaussian randomization method described in Appendix B. This method can be applied to any scenario where a rank-1 solution cannot be found.

4.5 Numerical results

We assume a square environment with 4 BSs at each corner equipped with a 16×16 UPA with the center of the array pointing towards the center of the square. In this way, the square will be covered by a 90° sector of each antenna array. The minimum inter site distance between BSs is 200 meters, as illustrated in Figure 4.3. The antennas of the BS array are separated by half-wavelength, both horizontally and vertically, considering a system carrier frequency of 60 GHz. The channels were generated using the quasi deterministic radio channel generator (QuaDRiGA) model for the urban micro (UMi) LOS scenario [69].

We assume that the UEs are placed in hotspots inside of the square region. Each hotspot has 2 UEs randomly positioned considering a uniform distribution in a circle with 6 meters of radius. Note that the maximum distance among UEs in a hotspot is 12 meters, which is the correlation distance for cluster and ray-specific random variables in the 3GPP Urban Micro-Cell LOS channel model [78]. The position of each hotspot was uniformly generated inside a square without overlap between two hotspots. In the K-means algorithm, we consider the number of required clusters equal to the number of hotspots, which is an approximation of the optimal number of clusters. The covariance matrix from (4.9) was estimated considering 25 sequential channel samples, as considered in [73]. Each channel sample was estimated considering an interval of 0.25 ms, which is a reasonable transmit time interval (TTI) considering the 5G standard in 60 GHz [79]. The main parameters used in the simulations are specified in Table 4.1.

For the power consumption model, we assume $p^{\text{RF}} = 2p^{\text{ref}}$ and $p^{\text{PS}} = 1.5p^{\text{ref}}$, where $p^{\text{ref}} = 20$ mW is the reference power considering that the phase-shifter has a resolution of 4 bits [80].

Let us refer to the proposed framework described in Section 4.4 as clustering based (CB). For the purpose of providing a qualitative parameter to evaluate our framework solution, let us consider two baselines for UE-BS association methods:

1. **Full joint transmission (FJT)**: In this association method, we consider all UEs associated with all BSs, i.e., the message sent to each UE will be jointly precoded by the complete network.

2. **Mean channel power (MCP)**: In this method we associate each UE k with the BS that achieves $m^* = \arg\max_{m \in \mathcal{M}} \operatorname{tr}\left(\tilde{\mathbf{R}}_{m,k}\right)$. Notice that the trace of the estimated covariance

Figure 4.3 – Simulated environment with 4 UEs in the system.

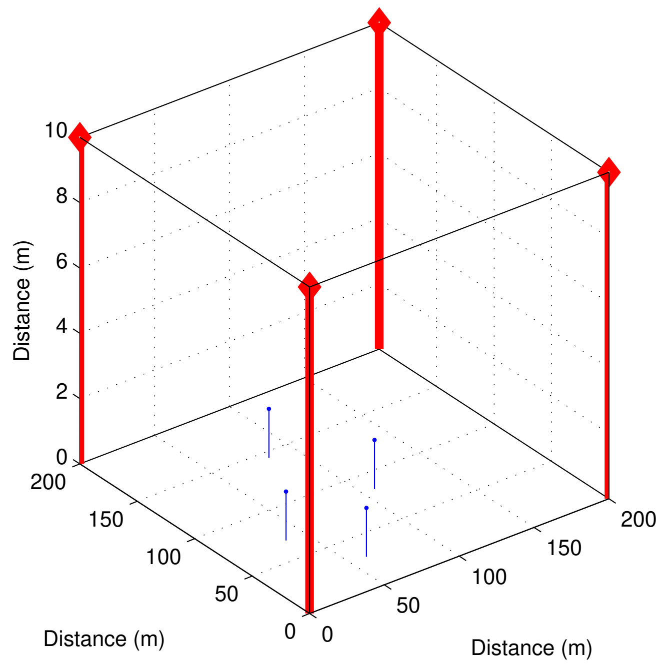

Source: Created by the author.

Table 4.1 – Simulation parameters for the analysis of spatial compatibility for UE-BS association.

Num. of BSs	4
Num. of hotspots	1 to 10
Num. of UEs per hotspot	2
Hotspot radius	6 m
Num. of BS antennas	256 (16×16 UPA)
Num. of UE antennas	1 (Omni-directional)
BS height	10 m
UE height	1.5 m
Distance between neighbor BSs	200 m
Maximum transmit power	30 dBm
Noise density	-174 dBm/Hz
Monte Carlo samples	250
Channel model	QuaDRiGA [69]
Scenario	3GPP 3D Urban Micro-Cell LOS

Source: Created by the author.

from (4.9) is equivalent to the sum of the mean channel power of each antenna in T channel samples. In this scenario each UE is associated with a single BS.

In Figure 4.4, the mean number of transmitting BSs, number of UEs served by multiple BSs and circuit power for all simulated methods are presented. These results do not necessarily represent gains or losses, but they contribute to the understanding of upcoming results.

In Figure 4.4a, the mean number of transmitting BSs in each UE-BS association method is shown. In the FJT method all BSs cooperate to transmit signals to each UE in the

Figure 4.4 – Mean number of active BSs, cooperative UEs and circuit power.

(a) Average number of active BSs.

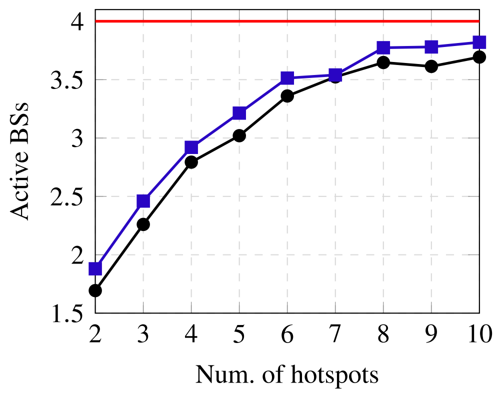

(b) Mean num. of cooperative UEs.

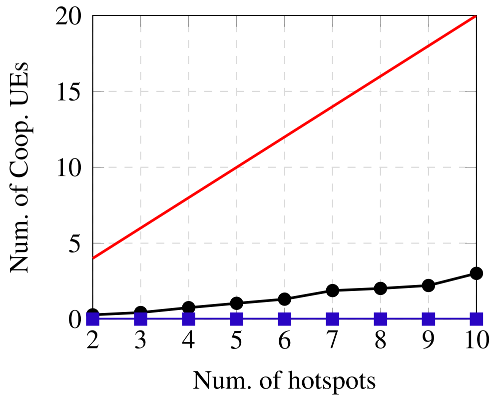

(c) Overall network circuit power.

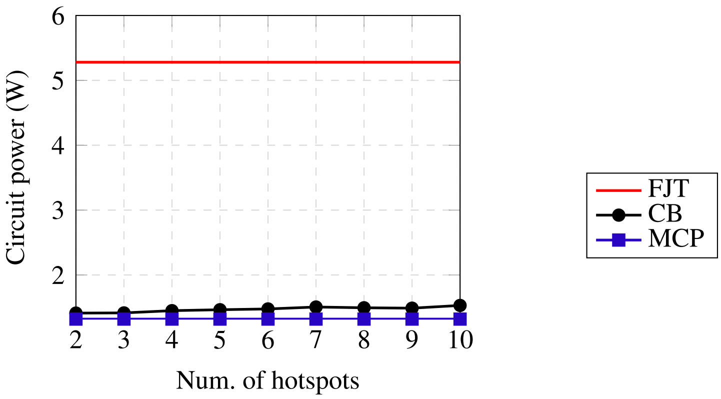

Source: Created by the author.

system, hence the number of BSs is fixed at the total. When we compare the MCP and the CB solutions, we can note that the CB achieves slightly less active BSs. The reason is the constraint in our proposal of only associating a cluster of UEs with a given BS, instead of UEs directly. This assumption reduces the granularity of UE-BS associations.

Figure 4.4b shows the mean number of UEs served by multiple BSs, which increases with the number of hotspots in the CB scenario, achieving 3 UEs in the case with 10 hotspots. This shows that the cluster solutions found by different BSs can vary due to the antenna array position. Also, as expected, the number of UEs served by multiple BSs increases linearly in the FJT method, since each UE is served by all BSs. Note that in the case of MCP all UEs are served by one BS and hence there are no cooperative UEs.

Let us consider as circuit power the power consumed by active RF chains and phase-shift circuits from (4.6), excluding the transmission power. As previously mentioned, the circuit power depends only on the UE-BS strategies, and not on the digital precoder design. Figure 4.4c illustrates the energy performance of each UE-BS association method. Note that in the FJT method, each BS has one active RF chain and one phase-shift circuit per UE, whereas in the MCP method, there is one active RF chain per UE in the entire network. Therefore, we can see that the FJT and MCP methods correspond, respectively, to examples of high and low circuit power consumption. The proposed CB association has performance between the FJT and MCP methods, due to the existence of cooperative UEs. We can note that for the simulated number of clusters, the circuit power consumption reaches a performance closer to that of MCP than to FJT. In the case with 10 clusters, the MCP achieves 1.32 W of circuit consumption, the proposed CB achieves 1.53 W and FJT reached 5.28 W. Hence, our proposal has an energy consumption 16% higher than the lowest value, whereas FJT requires 300% more energy than the same lowest value, which indicates that the proposed algorithm is, in average, far from the worst case in terms of circuit power consumption.

4.5.1 Weighted sum capacity results

To evaluate the capacity performance of our proposal and the impact of cooperative UEs, let us consider the sub-optimal solution for the weighted sum capacity of (4.7) proposed in Section 4.4. For simplicity, let us consider $a_k = 1\ \forall k \in \mathcal{K}$, which represents the sum capacity without the influence of different user priorities. Figure 4.5 presents the overall system sum capacity from the objective function (4.7a) normalized by the number of UEs in the system for all simulated methods and analog beamforming. This normalization represents the mean UE capacity achieved at each Monte Carlo sample. The overall sum capacity increases when more UEs are placed in the system, however, it can be seen that the mean UE capacity is reduced. The reasons are the reduction of the available transmission power per UE and the increased interference.

It can be seen that the FJT solution achieved the best capacity in comparison with the proposed CB association and MCP. The main reason is that FJT has the highest degrees of freedom, due to the considerable amount of active RF chains in the network. Another reason is that FJT always uses all power resources available in the network.

We can note that the eigenvector approximation provides somes gains in comparison to the DFT codebook, but such gains are reduced when the number of UEs increases. The reason is the objective of the optimization problem, which is to increase the data rate. Therefore, all BSs will transmit with all power budgets available. When the number of UEs increases, the ratio between the transmit power and total system data rate is reduced. Moreover, in a scenario with 20 UEs (10 hotspots) and considering the DFT approach, MCP achieves 3.57 bps/Hz, while CB reaches 4.45 bps/Hz, which corresponds to a gain of approximately 24%. We can see gains for all different loads of UEs, indicating that the separation of correlated channels in the CB UE-BS association provides enough gains to compensate for the reduction in transmission power (less active BSs) illustrated in Figure 4.4a.

In terms of sum capacity, FJT is clearly the best solution, but, as previously shown, it requires a large amount of circuit power. The trade-off between capacity and power consumption is better evaluated in terms of the energy efficiency of the network, which can be expressed as $\frac{\sum_{k\in\mathcal{K}} \log_2(1+\gamma_k)}{p^{\text{tot}}}$, [81] where γ_k is the SINR from (4.4) and p^{tot} is the total power of the system from (4.6). Figure 4.6 shows the energy efficiency for the weighted sum capacity problem.

Figure 4.5 – Average UE data rate for the weighted sum capacity problem.

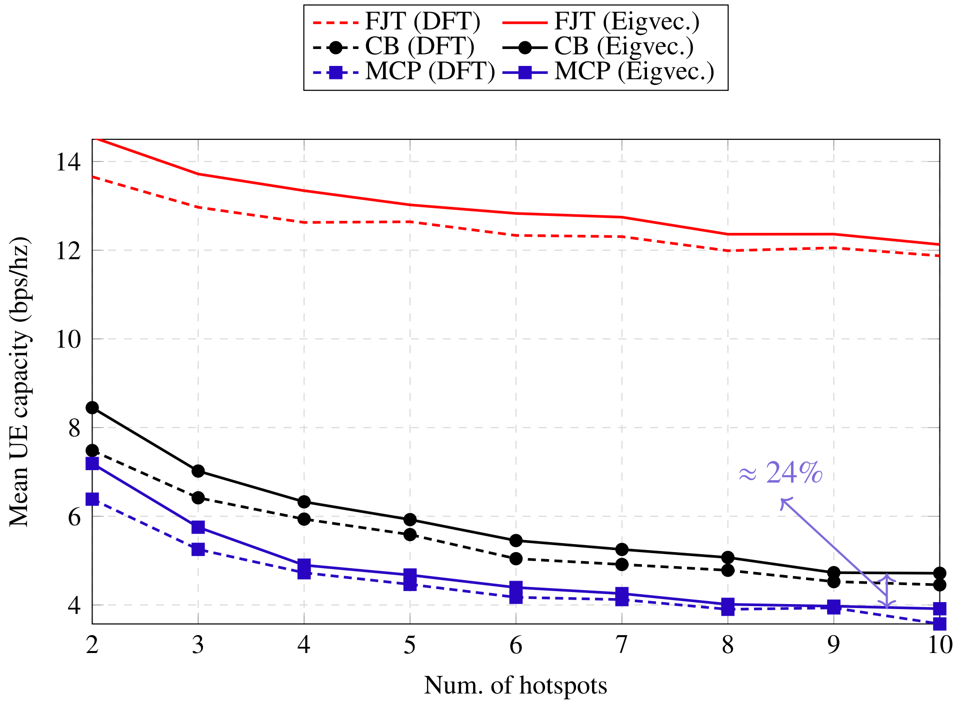

Source: Created by the author.

Figure 4.6 – Energy efficiency for the weighted sum capacity problem.

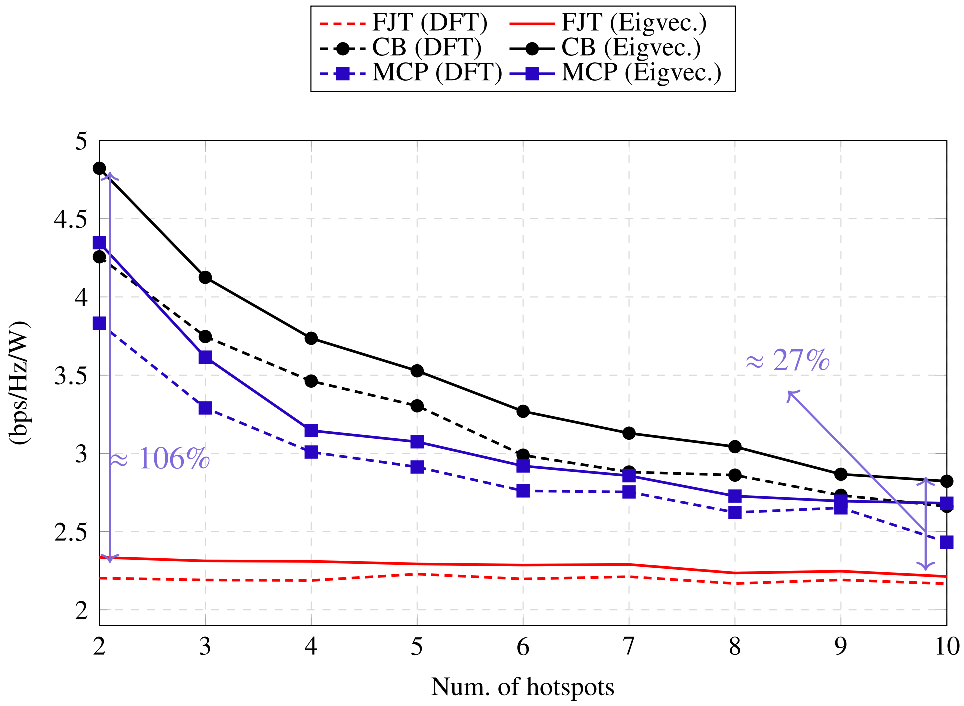

Source: Created by the author.

Although FJT presents the best system capacity performance, this solution has the worst performance in terms of energy efficiency. The reason is the high circuit energy consumption due to the large amount of RF chains in the network, as shown in Figure 4.4c. Comparing CB and MCP, we can observe that the former achieved an overall better energy

Figure 4.7 – Outage results for DFT codebook analog beamforming when varying the required SINR from 1 to 5 dB.

(a) 2 clusters. (b) 4 clusters. (c) 6 clusters.

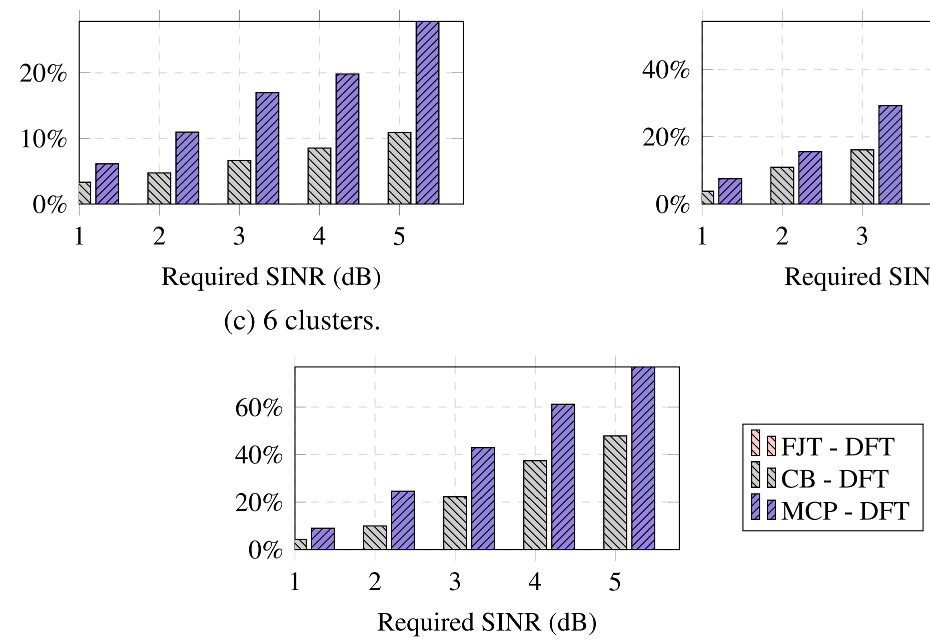

Source: Created by the author.

efficiency, with higher gains perceivable for small numbers of UEs. Therefore, the proposed framework represents the best trade-off between capacity and energy consumption.

4.5.2 *Power minimization with minimum SINR results*

The weighted sum capacity maximization problem is always feasible and the goal of the proposed successive convex approximation approach is to get as close to the optimal point as possible. The power minimization problem with minimum SINR constraints, on the other hand, could be infeasible. The main limiting factor is the power constraint, which may not be enough to reach the required SINR. Therefore, let us define the outage as the event in which the algorithm cannot find a feasible solution. Note that there are no outage events in the weighted sum-capacity problem, and thus we evaluate this metric only for the power minimization problem.

Regarding problem (4.22), it should be mentioned that an interior point method[1] was used to solve the relaxed SDP and, for the considered simulated scenario, all obtained solutions had rank 1.

In Figure 4.7, the percentage of outage events in the Monte Carlo samples is shown, considering a DFT-codebook for 2, 4 and 6 clusters. In a practical system, if a method does not find a feasible solution, the digital precoder problem may be solved again, considering a lower SINR requirement. However, in this chapter, we evaluate the capability of different methods to find a feasible solution, and we do not consider any SINR target search algorithm.

[1] To solve problem (4.22) we used CVX, a package for specifying and solving convex programs [82, 83].

Figure 4.8 – Outage results for Eigenvector Approximation analog beamforming when varying the required SINR from 1 to 5 dB.

(a) 2 clusters.

(b) 4 clusters.

(c) 6 clusters.

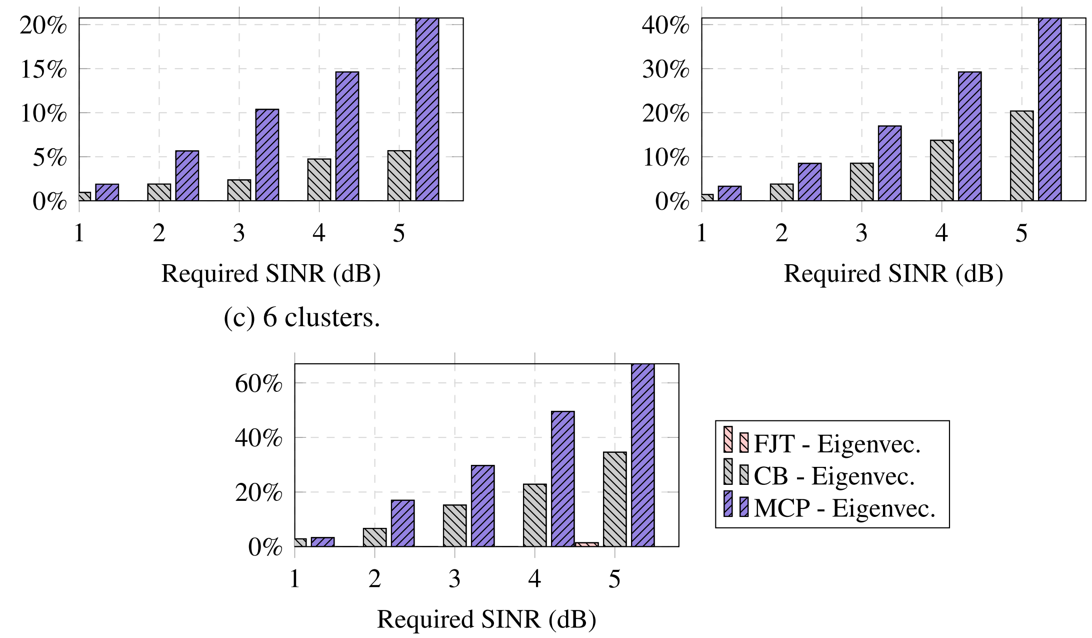

Source: Created by the author.

We can note that the FJT solution has zero outage in all simulated scenarios. The reason is the high degrees of freedom created by the large amount of RF chains in the network. As expected for the other methods, the outage increases when the required SINR and/or the number of clusters increase, due to the limitation of power and spatial resources. However, the outage of MCP increases in a higher rate in comparison with CB. In the scenario from Figure 4.7c, with 6 clusters and a required SINR of 5 dB, the MCP reaches more than 77% of outage, whereas the CB solution reaches only 48%. This represents 29% less outage by using the CB method in the worst considered scenario.

In Figure 4.8, the outage is presented for the same scenarios as in Figure 4.7, but considering the eigenvector approximation as the analog beamforming method. In general, the observed behavior is the same as the one from Figure 4.7. The main difference is the reduction of outage events. Even though the eigenvector approximation has the same phase-shift constraint as the DFT-codebook, in the eigenvector approach the phase shifts are selected independently by each antenna. Therefore, the equivalent channel created by the analog beamforming is more suitable in this case. From Figure 4.8c we can notice that MCP reached 67% of outage in the scenario with 6 clusters and 5 dB of required SINR, which represents 10% of outage reduction in comparison to Figure 4.7c. Similarly, the CB method reached 35%, representing a reduction of 13% compared to its performance in Figure 4.7c.

Figures 4.9a and 4.9b present the energy efficiency for the power minimization problem when varying the number of hotspots and required SINR, considering a DFT codebook[2].

[2] The results obtained with the eigenvector approximation are quite similar to those of the DFT codebook and for

Figure 4.9 – Energy efficiency (bps/Hz/W) of power minimization problem using DFT codebook.

(a) Scenario with 5 dB required SINR and varying number of hotspots (2 to 6).

(b) Scenario with 4 clusters and varying the minimum required SINR (2 to 5 dB).

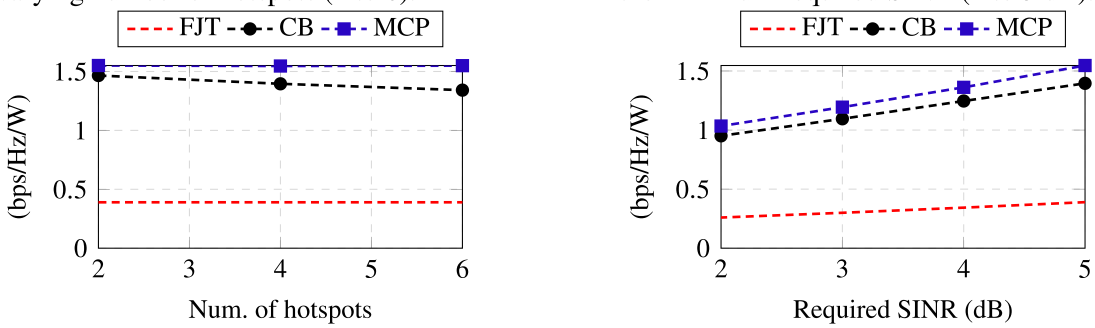

Source: Created by the author.

For these results, we only consider the Monte Carlo samples where a feasible solution has been found.

Due to constraint (4.8c) and minimization of power as objective, the SINR actually reached by UEs in the case of feasible solutions is in general the minimum required. The consequence is that the system capacity is equal for all simulated algorithms. The difference in terms of energy efficiency is due to the circuit and transmission power reached by each method. As previously mentioned, the circuit power consumption is higher for FJT, which results in the poor energy efficiency shown in Figures 4.9a and 4.9b.

The main difference in terms of energy efficiency when comparing the results in Figure 4.9a (power minimization) with those in Figure 4.6 (weighted sum capacity) is the worst performance of CB in relation to MCP. The reason is that the feasible solutions found by MCP always have one active RF chain in the network for each UE, whereas for CB there are some cooperative UEs using more than one RF chain. Despite different numbers of active RF chains, the capacity is equal for all simulated methods, indicating that for feasible samples the CB method tends to use more circuit power than MCP.

We can conclude that for the power minimization problem the algorithms present a trade-off between power consumption and feasibility. In that respect, the proposed CB approach presents a reasonable trade-off, achieving a significantly lower outage than MCP, at the cost of a slightly lower energy efficiency.

4.6 Conclusions

In this chapter, we proposed a framework for solving problems related to user clustering, UE-BS association and HBF in multi-cell networks, where one UE might receive its signal from one or multiple BSs. The considered problems are the weighted sum capacity maximization and the power consumption minimization with minimum SINR constraints. The formulated problems are non-convex and require a large amount of ICSI, which could be

this reason are not shown.

impractical in a massive MIMO C-RAN network. Due to those issues, we have presented a low-complexity solution using a reduced amount of ICSI.

In the proposed solution framework, the UE-BS associations and analog beamforming are determined considering second-order statistics, thus reducing the amount of ICSI required for the digital precoder. For the UE-BS association, we consider a new method based on UE clustering solutions found by each BS, which avoids high correlation among interfering and intended channels. After the UE-BS associations and analog beamforming are solved, the overall optimization problems are limited to the design of the digital precoders, which are in this case non-convex problems. We have proposed a different strategy for each optimization objective: an SCA method for the weighted sum capacity and a combination of SDR and Gaussian randomization approach for the power minimization with minimum SINR constraints. Specifically for the power minimization problem, we have proven that the optimal solution is guaranteed for a scenario with two BSs, however, our framework was also able to find good solutions with more BSs.

Numerical simulations were presented for both optimization criteria. In the case of the weighted sum capacity problem, the proposed CB solution achieved the best energy efficiency in comparison to the baseline cases MCP (each UE is served by only one BS) and FJT (all UEs are served by all BSs). Considering the power minimization problem, our framework was capable of finding more feasible solutions than Mean Channel Power, while achieving a higher energy efficiency than FJT.

The contents of this chapter can be extended in some directions. In the following, some of the possible future works are pointed out

- Although in the scenario studied in this chapter only a subset of BSs perform JT-CoMP, the presented optimization problems are centralized. In the proposal, ICSI requirements at the cloud have been significantly reduced by the analog beamforming step. However, in some dense scenarios, a large amount of ICSI must be reported to the cloud through the fronthaul. One possible direction to tackle this issue is the use of distributed solutions, where only a subset of BSs can cooperate to design their digital precoders locally with reduced signaling.

- Verify the validity of the proposed framework in sub-THz band frequencies. It is expected that bands above 100 GHz play an essential role in future sixth-generation. Due to the shorter wavelengths, the signals are less susceptible to free-space diffraction and suffer more significant pathloss than mmWave. A corresponding increase in the number of antennas is expected to mitigate such propagation effects. The evaluation of the proposal of this chapter in such frequencies is one possible direction to be investigated.

5 CONCLUSIONS

As presented in Chapter 1, the main purpose of this thesis was to study solutions based on spatial compatibility metrics to address problems of 5G networks. In the review presented in Chapter 1, some prominent solutions pointed by the research community and industry to meet the main requirements of 5G and B5G were identified. The review also demonstrated how those three methods are complementary in many aspects. In summary, network densification can increase the network capacity by increasing the radio resource reuse, however, the inter-cell interference becomes an issue. Another direction was to explore mmWave frequencies, which provide large amounts of bandwidth at the cost of severe propagation issues. Finally, massive MIMO was also mentioned as a promising direction, providing large antenna gains and directive beams.

The short-range of mmWave naturally leads to network densification, while massive MIMO can improve the range communication in mmWave frequencies at the same time that directive beams can also isolate the inter-cell interference. Besides, the mmWave propagation issues also avoid interference leakage among neighbor cells.

Despite many compatible characteristics of network densification, mmWave and massive MIMO, some other issues emerge during the practical implementation of those methods. Specifically regarding network densification, the traffic requirements of uplink and downlink became heterogeneous and with fast fluctuation due to the small number of UEs served by each small-cell. DTDD allows each cell to operate in an independent direction, which creates cross interference between BSs and UEs.

In Chapter 2, we proposed an SDMA grouping method for DTDD networks based on a spatial compatibility metric that combines channel attenuation and channel correlation, including the cross interfering channels. The proposed metric has two parameters that control the trade-off between intended channel attenuation, cross-interference correlation and co-interference correlation. The optimal solution of the formulated problem has exponential computational complexity. For this reason we also proposed two greedy sub-optimal solutions. The numerical results demonstrated that the trade-off regarding the adjustment of parameters has a different impact on UE capacity, indicating that the best multi-cell scheduling in those scenarios must consider channel quality and spatial compatibility in some proportions. The best set of parameters for the simulated network has been identified for the considered scenarios.

Due to the high cost and elevated energy consumption of RF chains in mmWave frequencies, the use of one RF chain per antenna can be a prohibitive requirement for massive MIMO. The research community and industry have adopted HBF as a practical solution for this issue, where a smaller number of RF chains are linked with a larger number of antennas.

In Chapters 3 and 4, we studied spatial compatibility for multi-cell HBF networks. Specifically in Chapter 3 we proposed an analog beam allocation method in a JT-CoMP scenario.

Despite cooperation of all BSs to transmit a message to all UEs, the amount of beams to be allocated is limited in the evaluated scenario. The proposal is a greedy beam association based on a spatial compatibility metric. The presented numerical results indicate that creating uncorrelated equivalent channels by analog beams allocation can improve the data rate capacity of the network.

Finally in Chapter 4, we proposed a solution for UE-BS association and HBF. Differently from Chapter 3, in the considered scenario some UEs can be served by one or multiple BSs. The proposal is to identify the set of UEs with correlated channels and associated with the same BS in order to avoid inter-cell interference. However, in some situations we identified that it could be impractical to find solutions where UEs with correlated channels are served by only one BS. In those situations we associate some UEs with multiple BSs and thus reduce inter-cell interference. In Chapter 4, two optimization problems were evaluated, sum capacity maximization and power minimization with minimum SINR requirements.

The numerical results demonstrated that, in terms of sum-capacity, the proposal has gains when compared with the baseline, where each UE is associated with only one BS. At the same time, there is a performance loss for the scenario where all BSs are serving all UEs. However, it could be concluded that when the circuit energy consumption is considered, our proposal achieves the best EE.

Regarding the numerical results of the power minimization problem, the proposal was capable of finding more feasible solutions in all simulated scenarios, when compared with one BS association case, and also achieve better EE when compared with the case that all BSs are serving all UEs. In this case, it was concluded that the proposal reaches a reasonable trade-off between EE and feasibility.

REFERENCES

1 3GPP. **3GPP Release 15**. July 2018. Available from: <http://www.3gpp.org/release-15>. Visited on: 18 Oct. 2018.

2 ITU-R. **IMT vision – Framework and Overall Objectives of the Future Development of IMT for 2020 and Beyond**. [S.l.], Sept. 2015. Available from: <https://www.itu.int/rec/R-REC-M.2083>. Visited on: 19 Oct. 2018.

3 BUSARI, S. A. et al. Millimeter-Wave Massive MIMO Communication for Future Wireless Systems: A Survey. **IEEE Communications Surveys and Tutorials**, v. 20, n. 2, p. 836–869, 2018.

4 HEMADEH, I. A. et al. Millimeter-Wave Communications: Physical Channel Models, Design Considerations, Antenna Constructions, and Link-Budget. **IEEE Communications Surveys and Tutorials**, v. 20, n. 2, p. 870–913, 2018.

5 RAPPAPORT, T. S. et al. **Millimeter wave wireless communications**. [S.l.]: Prentice Hall, 2015. ISBN 9780132172288.

6 AKDENIZ, M. R. et al. Millimeter Wave Channel Modeling and Cellular Capacity Evaluation. **IEEE Journal on Selected Areas in Communications**, v. 32, n. 6, p. 1164–1179, 2014.

7 PI, Z.; KHAN, F. An introduction to millimeter-wave mobile broadband systems. **IEEE Communications Magazine**, v. 49, n. 6, p. 101–107, 2011.

8 BJÖRNSON, E.; LARSSON, E. G.; MARZETTA, T. L. Massive MIMO: ten myths and one critical question. **IEEE Communications Magazine**, v. 54, n. 2, p. 114–123, 2016.

9 KIM, H.; KIM, J.; HONG, D. Dynamic TDD Systems for 5G and Beyond: A Survey of Cross-link Interference Mitigation. **IEEE Communications Surveys and Tutorials**, p. 1–1, 2020. Early Access. DOI: 10.1109/COMST.2020.3008765.

10 3GPP. **Evolved Universal Terrestrial Radio Access (E-UTRA)**: Physical Channels and Modulation. [S.l.], Dec. 2012. (Release 11, TR 36.211). Available from: <http://www.3gpp.org/dynareport/36211.htm>.

11 JI, H. et al. **Dynamic resource adaptation in beyond LTE-A TDD heterogeneous networks**. In: PROCEEDINGS of the IEEE International Conference on Communications (ICC). [S.l.: s.n.], 2013. P. 133–137.

12 ZHU, D.; MING LEI; GOLDSMITH, A. **Coordinated resource allocation in centralized radio access networks with dynamic downlink/uplink reconfiguration**. In: PROCEEDINGS of the IEEE Global Telecommunications Conference (GLOBECOM). [S.l.: s.n.], 2013. P. 3625–3630.

13 CHAO, C. et al. **Distributed dynamic-TDD resource allocation in femtocell networks using evolutionary game**. In: PROCEEDINGS of the IEEE Personal, Indoor and Mobile Radio Communications (PIMRC). [S.l.: s.n.], 2015. P. 1157–1162.

14 ZHU, D.; LEI, M. **Cluster-Based Dynamic DL/UL Reconfiguration Method in Centralized RAN TDD with Dense Deployment of Remote Radio Units**. In: PROCEEDINGS of the IEEE Vehicular Technology Conference (VTC). [S.l.: s.n.], 2013. P. 1–5.

15 SUN, F.; ZHAO, Y.; SUN, H. **Centralized Cell Cluster Interference Mitigation for Dynamic TDD DL/UL Configuration with Traffic Adaptation for HTN Networks**. In: PROCEEDINGS of the IEEE Vehicular Technology Conference (VTC2015-Fall). [S.l.: s.n.], 2015. P. 1–5.

16 SUN, F.; ZHAO, Y. **Cell cluster-based dynamic TDD DL/UL reconfiguration in TD-LTE systems**. In: PROCEEDINGS of the IEEE Wireless Communications and Networking Conference. [S.l.: s.n.], 2016. P. 1–5.

17 DING, M. et al. **Small cell dynamic TDD transmissions in heterogeneous networks**. In: PROCEEDINGS of the IEEE International Conference on Communications (ICC). [S.l.: s.n.], 2014. P. 4881–4887.

18 LAGEN, S.; AGUSTIN, A.; VIDAL, J. Joint User Scheduling, Precoder Design, and Transmit Direction Selection in MIMO TDD Small Cell Networks. **IEEE Transactions on Wireless Communications**, v. 16, n. 4, p. 2434–2449, 2017.

19 HUO, Z.; MA, N.; LIU, B. **Joint user scheduling and transceiver design for cross-link interference suppression in MU-MIMO dynamic TDD systems**. In: PROCEEDINGS of the IEEE International Conference on Computer and Communications (ICCC). [S.l.: s.n.], 2017. P. 962–967.

20 TENG, Y. et al. Traffic-aware resource allocation scheme for mMTC in dynamic TDD systems. **IET Communications**, v. 12, n. 15, p. 1910–1918, 2018.

21 ARDAH, K. et al. A Novel Cell Reconfiguration Technique for Dynamic TDD Wireless Networks. **IEEE Communications Letters**, v. 7, n. 3, p. 320–323, 2018.

22 HOCHWALD, B.; MARZETTA, T.; TAROKH, V. Multiple-antenna channel hardening and its implications for rate feedback and scheduling. **IEEE Transactions on Information Theory**, v. 50, n. 9, p. 1893–1909, 2004. DOI: `10.1109/TIT.2004.833345`.

23 RIHAN, M. et al. Taxonomy and Performance Evaluation of Hybrid Beamforming for 5G and Beyond Systems. v. 8, p. 74605–74626, 2020.

24 ALIMI, I. A.; TEIXEIRA, A. L.; MONTEIRO, P. P. Toward an Efficient C-RAN Optical Fronthaul for the Future Networks: A Tutorial on Technologies, Requirements, Challenges, and Solutions. **IEEE Communications Surveys and Tutorials**, v. 20, n. 1, p. 708–769, 2018.

25 CHINA MOBILE RESEARCH INSTITUTE. **C-RAN: The Road Towards Green RAN**. [S.l.], Dec. 2013.

26 HABIBI, M. A. et al. A Comprehensive Survey of RAN Architectures Toward 5G Mobile Communication System. **IEEE Access**, v. 7, p. 70371–70421, 2019. DOI: `10.1109/ACCESS.2019.2919657`.

27 RAO, X.; LAU, V. K. N. Distributed Fronthaul Compression and Joint Signal Recovery in Cloud-RAN. **IEEE Transactions on Signal Processing**, v. 63, n. 4, p. 1056–1065, 2015.

28 DOTTLING, M. et al. **Integration of Spatial Processing in the WINNER B3G Air Interface Design**. In: PROCEEDINGS of the IEEE Vehicular Technology Conference (VTC). [S.l.: s.n.], May 2006. v. 1, p. 246–250. DOI: `10.1109/VETECS.2006.1682813`.

29 LETAIEF, K. B.; ZHANG, Y. J. Dynamic multiuser resource allocation and adaptation for wireless systems. **IEEE Transactions on Wireless Communications**, v. 13, n. 4, p. 38–47, Aug. 2006. ISSN 1536-1284. DOI: `10.1109/MWC.2006.1678164`.

30 MACIEL, T. F.; KLEIN, A. **A Convex Quadratic SDMA Grouping Algorithm Based on Spatial Correlation**. In: PROCEEDINGS of the IEEE International Conference on Communications (ICC). [S.l.: s.n.], June 2007. P. 5342–5347. DOI: `10.1109/ICC.2007.884`.

31 ________. On the Performance, Complexity, and Fairness of Suboptimal Resource Allocation for Multiuser MIMO-OFDMA Systems. **IEEE Transactions on Vehicular Technology**, v. 59, n. 1, p. 406–419, Jan. 2010. ISSN 0018-9545. DOI: `10.1109/TVT.2009.2029438`.

32 LIMA, F. R. M. et al. Improved Spectral Efficiency With Acceptable Service Provision in Multiuser MIMO Scenarios. **IEEE Transactions on Vehicular Technology**, v. 63, n. 6, p. 2697–2711, July 2014. ISSN 0018-9545. DOI: `10.1109/TVT.2013.2293333`.

33 MAJIDZADEH, M.; ESLAMI, M. **A novel suboptimal SDMA grouping algorithm for multiuser MIMO-OFDMA systems**. In: PROC. Iranian Conference on Electrical Engineering (ICEE). [S.l.: s.n.], May 2014. P. 1805–1810. DOI: `10.1109/IranianCEE.2014.6999832`.

34 CASTANEDA, E. et al. An Overview on Resource Allocation Techniques for Multi-User MIMO Systems. **IEEE Communications Surveys and Tutorials**, v. 19, n. 1, p. 239–284, Firstquarter 2017. DOI: `10.1109/COMST.2016.2618870`.

35 VENKATASUBRAMANIAN, V. et al. **On the performance gain of flexible UL/DL TDD with centralized and decentralized resource allocation in dense 5G deployments**. In: PROCEEDINGS of the IEEE Personal, Indoor and Mobile Radio Communications (PIMRC). [S.l.: s.n.], 2014. P. 1840–1845.

36 VENKATASUBRAMANIAN, V.; MOYA, F. S.; PAWLAK, K. **Centralized and decentralized multi-cell D2D resource allocation using flexible UL/DL TDD**. In: PROCEEDINGS of the IEEE Wireless Communications and Networking Conference Workshops (WCNCW). [S.l.: s.n.], 2015. P. 305–310.

37 SANCHEZ MOYA, F. et al. **D2D mode selection and resource allocation with flexible UL/DL TDD for 5G deployments**. In: PROCEEDINGS of the IEEE International Conference on Communication Workshop (ICCW). [S.l.: s.n.], June 2015. P. 657–663. DOI: `10.1109/ICCW.2015.7247256`.

38 PATEROMICHELAKIS, E.; SAMDANIS, K. **A Graph Coloring Based Inter-Slice Resource Management for 5G Dynamic TDD RANs**. In: PROCEEDINGS of the IEEE International Conference on Communications (ICC). [S.l.: s.n.], 2018. P. 1–6.

39 CELIK, H.; SUNG, K. W. **Scalable resource allocation for dynamic TDD with traffic and propagation awareness**. In: PROCEEDINGS of the IEEE Wireless Communications and Networking Conference (WCNC). [S.l.: s.n.], 2018. P. 1–6.

40 RAMAMOORTHI, Y.; KUMAR, A. **Energy Efficiency in Millimeter Wave based Cellular Networks with DUDe and Dynamic TDD**. In: 2020 International Conference on COMmunication Systems NETworkS (COMSNETS). [S.l.: s.n.], 2020. P. 670–673.

41 YU, Z. et al. Dynamic resource allocation in TDD-based heterogeneous cloud radio access networks. **China Communications**, v. 13, n. 6, p. 1–11, 2016.

42 ARVOLA, A.; JOSHI, S.; TÖLLI, A. **Dynamic UL/DL Mode Selection and Resource Allocation in Multi-Cell MIMO TDD Systems**. In: 2019 53rd Asilomar Conference on Signals, Systems, and Computers. [S.l.: s.n.], 2019. P. 1936–1940.

43 COSTA, L. R. et al. **User Grouping Based on Spatial Compatibility for Dynamic-TDD Cooperative Networks**. In: PROCEEDINGS of the IEEE Global Telecommunications Conference (GLOBECOM). [S.l.: s.n.], 2018. P. 1–6.

44 YOON, C.; CHO, D. Energy Efficient Beamforming and Power Allocation in Dynamic TDD Based C-RAN System. **IEEE Communications Letters**, v. 19, n. 10, p. 1806–1809, 2015.

45 MICHALOLIAKOS, A.; AO, W. C.; PSOUNIS, K. **Joint user-beam selection for hybrid beamforming in asynchronously coordinated multi-cell networks**. In: PROC. Information Theory and Applications Workshop (ITA). [S.l.: s.n.], 2016. P. 1–10. DOI: `10.1109/ITA.2016.7888166`.

46 HOU, Q. et al. **Joint user scheduling and hybrid precoding design for MIMO C-RAN**. In: PROC. International Conference on Wireless Communications and Signal Processing (WCSP). [S.l.: s.n.], Oct. 2017. P. 1–6. DOI: `10.1109/WCSP.2017.8170974`.

47 COSTA, L. R. et al. **Beam Allocation based on Spatial Compatibility for Hybrid Beamforming C-RAN Networks**. In: PROCEEDINGS of the IEEE Workshop on Smart Antennas. [S.l.: s.n.], 2019. P. 1–6.

48 KIM, J. et al. **Joint design of digital and analog processing for downlink C-RAN with large-scale antenna arrays**. In: PROCEEDINGS of the IEEE Workshop on Signal Processing Advances in Wireless Communications (SPAWC). [S.l.: s.n.], July 2017. P. 1–5. DOI: `10.1109/SPAWC.2017.8227789`.

49 KIM, J. et al. Joint Design of Fronthauling and Hybrid Beamforming for Downlink C-RAN Systems. **IEEE Transactions on Communications**, v. 67, n. 6, p. 4423–4434, June 2019. ISSN 1558-0857. DOI: `10.1109/TCOMM.2019.2903142`.

50 TOLLI, A.; CODREANU, M.; JUNTTI, M. Cooperative MIMO-OFDM Cellular System with Soft Handover Between Distributed Base Station Antennas. **IEEE Transactions on Wireless Communications**, v. 7, n. 4, p. 1428–1440, 2008. ISSN 1558-2248. DOI: `10.1109/TWC.2008.061124`.

51 GARCIA, I. D. et al. **Dynamic cooperation set clustering on base station cooperation cellular networks**. In: PROCEEDINGS of the IEEE Personal, Indoor and Mobile Radio Communications (PIMRC). [S.l.: s.n.], Sept. 2010. P. 2127–2132. DOI: `10.1109/PIMRC.2010.5671660`.

52 KAVIANI, S. et al. Linear Precoding and Equalization for Network MIMO With Partial Cooperation. **IEEE Transactions on Vehicular Communications**, v. 61, n. 5, p. 2083–2096, 2012. ISSN 1939-9359. DOI: `10.1109/TVT.2012.2187710`.

53 YUAN, J. et al. User-Centric Networking for Dense C-RANs: High-SNR Capacity Analysis and Antenna Selection. **IEEE Transactions on Communications**, v. 65, n. 11, p. 5067–5080, 2017. ISSN 1558-0857. DOI: `10.1109/TCOMM.2017.2738630`.

54 PAN, C. et al. User-Centric C-RAN Architecture for Ultra-Dense 5G Networks: Challenges and Methodologies. **IEEE Communications Magazine**, v. 56, n. 6, p. 14–20, 2018. ISSN 1558-1896. DOI: `10.1109/MCOM.2018.1700483`.

55 JUNGNICKEL, V. et al. The role of small cells, coordinated multipoint, and massive MIMO in 5G. **IEEE Communications Magazine**, v. 52, n. 5, p. 44–51, May 2014. ISSN 1558-1896. DOI: `10.1109/MCOM.2014.6815892`.

56 BJÖRNSON, E.; SANGUINETTI, L. Scalable Cell-Free Massive MIMO Systems. **IEEE Transactions on Communications**, v. 68, n. 7, p. 4247–4261, 2020.

57 ALONZO, M.; BUZZI, S. **Cell-free and user-centric massive MIMO at millimeter wave frequencies**. In: PROCEEDINGS of the IEEE Personal, Indoor and Mobile Radio Communications (PIMRC). [S.l.: s.n.], 2017. P. 1–5. DOI: `10.1109/PIMRC.2017.8292302`.

58 ALONZO, M. et al. Energy-Efficient Power Control in Cell-Free and User-Centric Massive MIMO at Millimeter Wave. **IEEE Transactions on Green Communications and Networking**, v. 3, n. 3, p. 651–663, 2019. ISSN 2473-2400. DOI: `10.1109/TGCN.2019.2908228`.

59 FEMENIAS, G.; RIERA-PALOU, F. **Reduced-complexity downlink cell-free mmWave Massive MIMO systems with fronthaul constraints**. In: PROCEEDINGS of the European Signal Processing Conference. [S.l.: s.n.], 2019. P. 1–5. DOI: `10.23919/EUSIPCO.2019.8902784`.

60 COSTA, L. R. et al. **Interference mitigation based on precoded SRS**. In: PROC. IEEE Sensor Array and Multichannel Signal Processing Workshop (SAM). [S.l.: s.n.], July 2016. P. 1–5. DOI: `10.1109/SAM.2016.7569712`.

61 LAND, A. H.; DOIG, A. G. An Automatic Method of Solving Discrete Programming. **Econometrica**, [Wiley, Econometric Society], v. 28, n. 3, p. 497–520, June 1960. Available from: <`http://www.jstor.org/stable/1910129`>.

62 CPLEX, I. I. V12. 1: User's Manual for CPLEX. **International Business Machines Corporation**, v. 46, n. 53, p. 157, 2009.

63 3GPP. **Evolved Universal Terrestrial Radio Access (E-UTRA): Further enhancements to LTE Time Division Duplex (TDD) for Downlink-Uplink (DL-UL) interference management and traffic adaptation**: Technical Specification Group Radio Access Network. [S.l.], June 2012. (Release 11, 36.828).

64 CAPOZZI, F. et al. Downlink Packet Scheduling in LTE Cellular Networks: Key Design Issues and a Survey. **IEEE Communications Surveys and Tutorials**, v. 15, n. 2, p. 678–700, May 2013. ISSN 1553-877X. DOI: `10.1109/SURV.2012.060912.00100`.

65 NGUYEN, V. K.; EVANS, J. S. **Multiuser Transmit Beamforming via Regularized Channel Inversion: A Large System Analysis**. In: PROCEEDINGS of the IEEE Global Telecommunications Conference (GLOBECOM). [S.l.: s.n.], Nov. 2008. P. 1–4. DOI: `10.1109/GLOCOM.2008.ECP.176`.

66 MUHARAR, R.; EVANS, J. **Downlink Beamforming with Transmit-Side Channel Correlation: A Large System Analysis**. In: PROCEEDINGS of the IEEE International Conference on Communications (ICC). [S.l.: s.n.], June 2011. P. 1–5. DOI: `10.1109/icc.2011.5962672`.

67 ZHANG, H.; DAI, H. Cochannel interference mitigation and cooperative processing in downlink multicell multiuser MIMO networks. **EURASIP Journal on Wireless Communications and Networking**, v. 2004, n. 2, p. 222–235, Dec. 2004. ISSN 1687-1499. DOI: `10.1155/S1687147204406148`.

68 MARSCH, P.; FETTWEIS, G. P. (Eds.). **Coordinated multi-point in mobile communications - From theory to practice**. [S.l.]: Cambridge University Press, 2011. ISBN 9780511783029.

69 JAECKEL, S. et al. QuaDRiGa: A 3-D Multicell Channel Model with Time Evolution for Enabling Virtual Field Trials. **IEEE Transactions on Antennas and Propagation**, v. 62, n. 6, p. 3242–3256, June 2014. ISSN 0018-926X. DOI: `10.1109/TAP.2014.2310220`.

70 KIM, J. et al. **Joint design of digital and analog processing for downlink C-RAN with large-scale antenna arrays**. In: PROCEEDINGS of the IEEE Workshop on Signal Processing Advances in Wireless Communications (SPAWC). [S.l.: s.n.], July 2017. P. 1–5. DOI: `10.1109/SPAWC.2017.8227789`.

71 ARDAH, K. et al. A Unifying Design of Hybrid Beamforming Architectures Employing Phase Shifters or Switches. **IEEE Transactions on Vehicular Technology**, v. 67, n. 11, p. 11243–11247, Nov. 2018. ISSN 0018-9545. DOI: `10.1109/TVT.2018.2865705`.

72 NAM, J. et al. Joint Spatial Division and Multiplexing: Opportunistic Beamforming, User Grouping and Simplified Downlink Scheduling. **IEEE Journal of Selected Topics in Signal Processing**, v. 8, n. 5, p. 876–890, Oct. 2014. DOI: `10.1109/JSTSP.2014.2313808`.

73 MAURICIO, W. V. F. et al. **A Low Complexity Solution for Resource Allocation and SDMA Grouping in Massive MIMO Systems**. In: PROCEEDINGS of the IEEE International Symposium on Wireless Communications Systems (ISWCS). [S.l.: s.n.], Aug. 2018. P. 1–6. DOI: `10.1109/ISWCS.2018.8491076`.

74 LEE, C.; CHUNG, W. Hybrid RF-Baseband Precoding for Cooperative Multiuser Massive MIMO Systems With Limited RF Chains. **IEEE Transactions on Communications**, v. 65, n. 4, p. 1575–1589, Apr. 2017. ISSN 0090-6778. DOI: `10.1109/TCOMM.2016.2646359`.

75 ZHOU, Y.; YU, W. Fronthaul Compression and Transmit Beamforming Optimization for Multi-Antenna Uplink C-RAN. **IEEE Transactions on Signal Processing**, v. 64, n. 16, p. 4138–4151, 2016.

76 POTRA, F. A.; WRIGHT, S. J. Interior-point methods. **Journal of Computational and Applied Mathematics**, v. 12, n. 1, p. 281–302, 2000. ISSN 0377-0427. DOI: `https://doi.org/10.1016/S0377-0427(00)00433-7`.

77 KARIPIDIS, E.; SIDIROPOULOS, N. D.; LUO, Z. Quality of Service and Max-Min Fair Transmit Beamforming to Multiple Cochannel Multicast Groups. **IEEE Transactions on Signal Processing**, v. 56, n. 3, p. 1268–1279, Mar. 2008.

78 3GPP. **Study on channel model for frequencies from 0.5 to 100 GHz**. [S.l.], May 2017. (Release 14, TR 38.901). Available from: <`http://www.3gpp.org/dynareport/36211.htm`>.

79 ZAIDI, A. A. et al. OFDM Numerology Design for 5G New Radio to Support IoT, eMBB, and MBSFN. **IEEE Communications Standards Magazine**, v. 2, n. 2, p. 78–83, June 2018. DOI: 10.1109/MCOMSTD.2018.1700021.

80 MÉNDEZ-RIAL, R. et al. Hybrid MIMO Architectures for Millimeter Wave Communications: Phase Shifters or Switches? **IEEE Access**, v. 4, p. 247–267, 2016. ISSN 2169-3536. DOI: 10.1109/ACCESS.2015.2514261.

81 ARDAH, K. et al. Hybrid Analog-Digital Beamforming Design for SE and EE Maximization in Massive MIMO Networks. **IEEE Transactions on Vehicular Technology**, v. 69, n. 1, p. 377–389, 2020. DOI: 10.1109/TVT.2019.2933305.

82 GRANT, M.; BOYD, S. **CVX: Matlab Software for Disciplined Convex Programming, version 2.1**. [S.l.: s.n.], Mar. 2014. http://cvxr.com/cvx.

83 ________. Graph implementations for nonsmooth convex programs. In: BLONDEL, V.; BOYD, S.; KIMURA, H. (Eds.). **Recent Advances in Learning and Control**. [S.l.]: Springer-Verlag Limited, 2008. (Lecture Notes in Control and Information Sciences). http://stanford.edu/~boyd/graph_dcp.html. P. 95–110.

84 HUANG, Y.; PALOMAR, D. P. Rank-Constrained Separable Semidefinite Programming With Applications to Optimal Beamforming. **IEEE Transactions on Signal Processing**, v. 58, n. 2, p. 664–678, Feb. 2010. ISSN 1053-587X. DOI: 10.1109/TSP.2009.2031732.

85 YINYU, Y. **Interior Point Algorithms: Theory and Analysis**. USA: John Wiley and Sons, Inc., 1997. ISBN 0471174203.

A CONDITIONS FOR OPTIMAL RANK ONE SOLUTION OF POWER MINIMIZATION PROBLEM

In this appendix, we prove that the solution for the power minimization problem using the proposed SDR presented in Section 4.4.4 is optimal for scenarios with two BSs.

For simplicity, let us define the matrices $\mathbf{T}_{m,k} = \mathbf{B}_{m,k}\mathbf{F}_m^H\mathbf{F}_m\mathbf{B}_{m,k}^H$, $\mathbf{T}_k = \sum_{m\in\mathcal{M}}\mathbf{T}_{m,k}$ and

$$\mathbf{A}_{k,b} = \begin{cases} \mathbf{H}_{k,k}^{\text{eq}} & k = b, \\ -r_k\mathbf{H}_{k,b}^{\text{eq}} & k \neq b. \end{cases} \tag{A.1}$$

As both matrices $\mathbf{T}_{m,k}$ and $\mathbf{W}_k$ are square for all m and k values, we can apply the relation $\operatorname{tr}(\mathbf{A}+\mathbf{B}) = \operatorname{tr}(\mathbf{A}) + \operatorname{tr}(\mathbf{B})$ that holds for any square matrices A and B. The objective function in (4.22a) can be reformulated as:

$$\sum_{m\in\mathcal{M}} \operatorname{tr}\left(\mathbf{T}_{m,k}\mathbf{W}_k\right) = \operatorname{tr}\left(\sum_{m\in\mathcal{M}} \mathbf{T}_{m,k}\mathbf{W}_k\right) = \operatorname{tr}\left(\left(\sum_{m\in\mathcal{M}} \mathbf{T}_{m,k}\right)\mathbf{W}_k\right) = \operatorname{tr}\left(\mathbf{T}_k\mathbf{W}_k\right). \tag{A.2}$$

Note that if $k \notin \mathcal{K}_m$, by definition, the matrix $\mathbf{B}_{k,m}$ will have all elements equal to zero, and as a consequence the matrix $\mathbf{C}_{m,k}$ will also be a zero matrix. Without loss of generality, we can say that $\sum_{k\in\mathcal{K}_m}\operatorname{tr}\left(\mathbf{T}_{m,k}\mathbf{W}_k\right)$ is equivalent to $\sum_{k\in\mathcal{K}}\operatorname{tr}\left(\mathbf{T}_{m,k}\mathbf{W}_k\right)$. Therefore, the optimization problem (4.22) can be rearranged as

$$\underset{\mathbf{W}}{\text{minimize}} \sum_{k\in\mathcal{K}} \operatorname{tr}\left(\mathbf{T}_k\mathbf{W}_k\right) \tag{A.3a}$$

$$\text{s.t.} \quad \sum_{b\in\mathcal{K}} \operatorname{tr}\left(\mathbf{A}_{k,b}\mathbf{W}_k\right) \geq r_k\sigma^2 \quad \forall k \in \mathcal{K}, \tag{A.3b}$$

$$\sum_{k\in\mathcal{K}} \operatorname{tr}\left(\mathbf{T}_{m,k}\mathbf{W}_k\right) \leq p^{\max} \quad \forall m \in \mathcal{M}. \tag{A.3c}$$

Problem (A.3) is a separable SDP. The authors in [84] demonstrated the condition for the existence of reduced rank solution for problems defined as:

$$\underset{\mathbf{X}}{\text{minimize}} \sum_{l=1}^{L} \operatorname{tr}\left(\mathbf{O}_l\mathbf{X}_l\right) \tag{A.4a}$$

$$\text{s.t.} \quad \sum_{l=1}^{L} \operatorname{tr}\left(\mathbf{G}_{g,l}\mathbf{X}_l\right) \trianglerighteq b_m \quad g = 1, \cdots, G \tag{A.4b}$$

$$\mathbf{X}_l \succeq 0 \quad l = 1, \cdots, L, \tag{A.4c}$$

where $\trianglerighteq \in \{\geq, =, \leq\}$, G is the number of constraints and L is the number of semidefinite variable matrices. The $\mathbf{G}_{g,l}$ are Hermitian matrices, not necessarily positive semidefinite. The authors of [84] proved the theorem below.

Theorem 1 (Theorem 3.1 [84]) *Suppose that the separable SDP in* (A.4) *and its dual problem are solvable. Then, problem* (A.4) *has always an optimal solution such that* $\sum_{l=1}^{L}\operatorname{rank}^2\left(\mathbf{X}_l\right) \leq G$.

It is straightforward to see that problem (A.3) is equivalent to problem (A.4), with $K+M$ constraints.

Proposition 1 *Suppose that the primal and dual problem of* (A.3) *are feasible and* $r_k > 0\ \forall k \in \mathcal{K}$*, then the optimal solution of problem* (A.3) *has non zero matrix* $\mathbf{W}_k\ \forall k \in \mathcal{K}$.

Proof. The constraint (A.3b) is equivalent to constraint (4.21b). For all $k \in \mathcal{K}$, if $r_k > 0$ it implies that

$$\operatorname{tr}\left(\mathbf{H}^{\text{eq}}_{k,k}\mathbf{W}_k\right) - r_k \sum_{\substack{b\in\mathcal{K}\\ b\neq k}} \operatorname{tr}\left(\mathbf{H}^{\text{eq}}_{k,b}\mathbf{W}_b\right) \geq r_k\sigma^2. \tag{A.5}$$

Note that the interference from other UEs and the noise power are always larger than or equal to zero, i.e., $r_k \sum_{\substack{b\in\mathcal{K}\\ b\neq k}} \operatorname{tr}\left(\mathbf{H}^{\text{eq}}_{k,b}\mathbf{W}_b\right) \geq 0$ and $\sigma^2 > 0$. Therefore, condition (A.5) can only be fulfilled if $\mathbf{W}_k$ is a non zero matrix. ■

Proposition 1 is the condition to show the cases in which the rank-1 solution is the optimal solution of problem (4.21), presented below.

Proposition 2 *Suppose that the primal and dual problem of* (A.3) *are feasible and* $r_k > 0\ \forall k \in \mathcal{K}$*, then there is a rank-1 optimal solution of problem* (A.3) *if* $M \leq 2$.

Proof. From Proposition 1, $\mathbf{W}_k$ are non zero matrices, thereby, $\operatorname{rank}(\mathbf{W}_k) \neq 0\ \forall k$. From Theorem 1, optimal solutions can only be guaranteed if $\sum_{k\in\mathcal{K}} \operatorname{rank}^2(\mathbf{W}_k) \leq K+M$ holds. Therefore, optimal rank-1 solutions are guaranteed for $M \leq 2$. If $M = 3$, the optimal solution can have W_k with $\operatorname{rank}(\mathbf{W}_k) = 2$ for a given k, which is valid only for $M \leq 2$. ■

B GAUSSIAN RANDOMIZATION FOR SDR OF POWER MINIMIZATION PROBLEM

In this appendix, we present a Gaussian randomization method for problem (4.22) in order to find candidates for digital precoders. Firstly, let $\mathbf{W}_k^*$ be an optimal solution of problem (4.22) and the eigen-decomposion of each matrix be given as $\mathbf{W}_k^* = \mathbf{L}_k \mathbf{E}_k \mathbf{L}_k^{\mathrm{H}}$. The l-th digital precoder candidate for a given UE k can be calculated as $\mathbf{w}_k^l = \mathbf{L}_k \mathbf{E}_k^{1/2} \mathbf{l}_k^l$, where $\mathbf{l}_k^l \in \mathbb{C}^{\left(\sum_{m \in \mathcal{M}_k} |\mathcal{K}_m|\right) \times 1} \sim \mathcal{CN}(\mathbf{0}, \mathbf{I})$.

Note that we cannot guarantee that a given sample l of candidates will satisfy the SINR and power constraints of problem (4.22), so a power allocation method must be applied. Due to the interference scenario, we cannot apply a power allocation by scaling up the digital precoder candidates. Let $\mathbf{W}_k^l = \mathbf{w}_k^l {\mathbf{w}_k^l}^{\mathrm{H}}$ be a rank-1 matrix calculated from the digital precoder candidate. We can define the power received by a UE k from the signal sent to a UE b as $z_{k,b,l} = \operatorname{tr}\left(\mathbf{H}_{k,b}^{\mathrm{eq}} \mathbf{W}_b^l\right)$ and the transmission power of a BS m to a UE k as $g_{k,m,l} = \operatorname{tr}\left(\mathbf{B}_{m,k} \mathbf{F}_m^{\mathrm{H}} \mathbf{F}_m \mathbf{B}_{m,k}^{\mathrm{H}} \mathbf{W}_k^l\right)$.

The power allocation problem for the l-th digital precoder candidates can be formulated as

$$\min_{p_k \forall k} \sum_{k \in \mathcal{K}} p_k \tag{B.1a}$$

$$\text{s.t.} \quad z_{k,k,l} p_k - r_k \sum_{\substack{b \in \mathcal{K} \\ b \neq k}} z_{k,b,l} p_b + r_k \sigma^2 \geq 0 \quad \forall k \in \mathcal{K}, \tag{B.1b}$$

$$\sum_{k \in \mathcal{K}} g_{k,m,l} p_k \leq p^{\max} \quad \forall m \in \mathcal{M}, \tag{B.1c}$$

where p_k is the factor to scale the digital vector of a UE k. The constraints (B.1b) and (B.1c) ensure that the minimum SINR and the power constraint from the original problem will be fulfilled. Note that problem (B.1) is a linear problem and can be efficiently solved by an interior point method [85].

The Gaussian randomization method consists of randomly generating digital precoder candidates $\mathbf{w}_k^l$ and solving the power allocation problem (B.1) to find a feasible rank-1 solution of (4.22).